UNIVERSITY OF OKLAHOMA

GRADUATE COLLEGE

REFRACTION-SEISMIC-CONSTRAINED SEISMIC STRATIGRAPHY OF THE SOUTHWESTERN RED SEA (OFFSHORE ERITREA) AND TECTONIC IMPLICATIONS

A THESIS

SUBMITTED TO THE GRADUATE FACULTY
in partial fulfillment of the requirements for the

degree of

MASTER OF SCIENCE

BY
ESHETU GEBRETSADIK
Norman, Oklahoma

1997

Downloaded from SHAREOK. Persistent Handle URL: https://hdl.handle.net/11244/341170
UNIVERSITY OF OKLAHOMA LIBRARIES

OU
THESIS
GEB
cop. 2

REFRACTION-SEISMIC-CONSTRAINED SEISMIC STRATIGRAPHY OF THE SOUTHWESTERN RED SEA (OFFSHORE ERITREA) AND TECTONIC IMPLICATIONS

A THESIS APPROVED FOR
SCHOOL OF GEOLOGY AND GEOPHYSICS

BY

[redacted]

©Copyright by ESHETU
All Rights

©Copyright by ESHETU GEBRETSADIK 1997
All Right Reserved

ACKNOWLEDGMENTS

I would like to acknowledge the Ministry of Mines and Energy of Ethiopia and the Ministry of Mines and Water Resources of Eritrea for providing data for this study, a part of OU Red Sea Research Program.

I am greatly indebted to Dr. John D. Pigott, Chair of my thesis committee, for his unlimited assistance and patience. Dr. P you are not only an adviser but also a true friend. It is a challenge and a pleasure to work with you. I greatly appreciate the help of Dr. James M. Forgotson and Dr. Judson L. Ahern for their editorial assistance on this thesis. Dr. Roger Young I am obliged to you for your valuable comment on the final thesis draft. Donna simply thank you very much for every thing. I also would like to thank all my friends within the school and outside for the encouragement and assistance they have provided me.

Last, but not least, I express my gratitude to my fiancee Miss Abenet Demissie for her unreserved kind advise, especially during my difficult times.

I dedicate this thesis to my beloved mother the late Dessu Feissa, who was an inspiration and the North star in my life.

Above all thanks to the almighty God.

ABSTRACT

Red Sea Rifting models have been founded upon assumed structural styles of the basement which have been interpreted exclusively from either regional geophysical survey or poor-resolution single-channel reflection seismic profiles, seldom with the integration of multi-channel industry-acquired reflection seismic. The problem of imaging the basement and its associated structures with seismic reflection profiling has been compounded by significant wavelet attenuation and multiple generation contributed by the overlying evaporite section. Improved images of Late Cenozoic structure are obtained using 2000 kms (1250 miles) of 24-fold seismic sections of the southwestern Red Sea (offshore Eritrea) constrained by refraction velocities.

Integrated seismic stratigraphy (wide-angle refraction seismic, borehole seismology and reflection seismic) of the southwestern Red Sea reveals the following structural types: basinward dipping step fault systems, en echelon tilted block fault systems, high-angle symmetrical block fault systems, rift margin parallel step fault systems, counter regional dipping faults, basinward dipping listric faults, high-angle fault systems associated with halokinesis.

Differences in stretching occur in each of the four structural zones indicated below, from the axial trough outward.

1. stretching is infinite at the axial trough (Zone I).

2. stretching is major ($\beta = 1.25$) within the en echelon tilted block zone (Zone II).

3. Stretching is moderate ($\beta = 1.1$) in the symmetrical horst and grabens zone (Zone III).

4. Stretching is minimal ($\beta = 1.01$) at the downwarped rift flank (Zone IV).

Through time, stretching magnitude varies non-systematically within each episode. The first episode (25 ma) is predominantly pure shear (high-angle normal faulting), basement involved, and capped by a wide spread unconformity increasing in erosional magnitude towards the axial trough. The second rifting episode (14 ma) was accommodated by reactivation of older rift faults and creation of new ones. The third rifting episode (5 ma) was mainly pure shear and involved the modification of an existing evaporite blanket into swells in phase with underlying horsts and grabens. Halokinetic modification continued with evaporite withdrawal,

development of counter regional dipping faults and imbricate sediment rafts.

The southwestern Red Sea rifting appears to be described as a multi-phased crustal attenuation model, with structural features supportive of a pure shear (high-angled faulting) regional extension model with local transfer zones of simple shear. In addition, the episodicity of the rifting event changes the idea of one rifting event and opens up many new hydrocarbon play concepts.

TABLE OF CONTENTS

	Page
ACKNOWLEDGMENTS	iv
ABSTRACT	v
LIST OF TABLES	xi
LIST OF FIGURES	xiii
I. INTRODUCTION	1
I. 1. Definition of the Problem	1
I. 2. Strategy	3
II. BACKGROUND	6
II. 1. Location and Description of the Southwestern Red Sea	6
II. 2. Tectonic Setting and Principal Rifting Theories	7
II. 2. a. Tectonic Setting	7
II. 2. b. Principal Rifting Theories	11
II. 3. Previous Exploration Activity in the Area	18
III OBSERVATIONS	24
III.1. Geological and Geophysical Control	25
III. 1.a. Well Logs	25
III. 1.b. Synthetic Seismograms	33

III. 1.c. Refraction Seismic Profiles 36

III.1.d. Reflection Seismic Profiles 43

III.2. Stratigraphy 45

III.2.a. Undifferentiated Pre-Cambrian Metamorphic Rocks 47

III.2.b. Infra-evaporite Rocks 48

III.2.b.i. Infra-evaporite Paleozoic Sediments 48

III.2.b.ii. Infra-evaporite Mesozoic Sediments 50

III.2.b.iii Infra-evaporite Cenozoic Rocks 52

III.2.c. Intra-evaporite Rocks 52

III.2.d. Supra-evaporite Rocks 52

III.3. Seismic Stratigraphic Profile 54

III.4. Structure 60

III.4.a. Structural Styles from Seismic Sections 60

III.4.b. Subsurface Structure 64

III.5. Sequence Stratigraphy (Intra-evaporite Isochron) 72

IV. INTERPRETATION 75

IV.1. Tectonics 75

IV.2. Transfer Zones 77

IV.3 Fourier Division Wavelet Processing 78

IV.4. Seismic Attribute Analysis 84

IV.5. Crustal Stretching Analysis 90

IV.6. Petroleum System 92

IV.6.a. Potential Source Rocks 92

IV.6.b. Potential Reservoir Rocks 94

IV.6.c. Sealing Rocks 96

IV.6.d. Traps 97

V. SUMMARY 98

VI. CONCLUSIONS 100

REFERENCES 103

Appendix I 115

Appendix II 119

Appendix III 123

Appendix IV 125

LIST OF TABLES

Page

Table 1. Exploration activity before and During World War II (compiled from UNDP/World Bank, 1991) 19

Table 2a. General exploration activity in the Ethiopian Red Sea by year and company (compiled from UNDP/World Bank, 1991) 20

Table 2b. Wells drilled in the Ethiopian Red Sea (offshore) after World War II (compiled from UNDP/World Bank, 1991) 21

Table 2c. Geophysical exploration activity in the Ethiopian Red Sea (offshore) (compiled from UNDP/World Bank, 1991) 22

Table 2d. Reflection seismic exploration activity of the Ethiopian Red Sea (offshore) (compiled from UNDP/World Bank, 1991) 23

Table 3. Correlation for refraction profile depth vs reflection seismic 43

Table 4. Reflection seismic recording, processing and display parameters 44

Table 5a. Calculated (β) for southwestern Red Sea (offshore Eritrea Line 520) 91

Table 5b. Calculated average (β) for southwestern Red Sea (Line 520) at each rifting episode and within each zone. 91

LIST OF FIGURES

Page

Figure 1. Location of the Red Sea and Gulf of Aden Basins (Project Area indicated) 2

Figure 2. Location map of : wells, oil seeps and wells with oil shows in the Ethiopian Red Sea. (source UNDP/World Bank, 1991). 5

Figure 3. Schematic map of major structural elements of northern Ethiopia. (modified from Berhe, 1986; Makris and Rihm, 1991; Marl et al., 1979 and Sovoyat et al., 1989). 8

Figure 4. Generalized schematic diagram a) Simple pure shear (high-angle faulting) model of Lowell and Genik (1972); b) modified pure shear (Diffused shear and normal faulting) model (Martinez and Cochran, 1988). 13

Figure 5. Generalized schematic diagram a) Low-angle detachment simple shear model (Wernicke, 1985; Voggenrieter et al., 1988), and b) modified Low-angle detachment simple shear model (Bohannon, 1989). 14

Figure 6. Shear controlled pull apart basin development (Makris and Rihm, 1989). 15

Figure 7. Location map of previous acreage and company activity in the Ethiopian Red Sea . (source UNDP/World Bank, 1991). 24

Figure 8. Summary well-log for Secca Fawn-1 (source Robertson Group, 1991). 26

Figure 9. Summary well-log for Thio-1 Well (source Robertson Group, 1991). 27

Figure 10. Synthetic seismogram for Secca Fawn-1 well. 29

Figure 11. Synthetic seismogram for Thio-1 well. 30

Figure 12. Southwestern Red Sea (offshore Eritrea) Shotpoint location the Tectonic Provinces. 34

Figure 13. synthetic seismogram (top), observed seismic section bottom models for Profile IV (after Egloff et al., 1991). 38

Figure 14. Seismic section ray tracing model for Profile IV (after Egloff et al., 1991). 39

Figure 15. Crustal model, bathymetry and location for Profile IV (after Egloff et al., 1991). 40

Figure 16. Line 1140 (twt) depth correlated to refraction Profile VI 41

Figure 17. Line 1160 (twt) depth correlated to refraction Profile VI 42

Figure 18. Generalized stratigraphic column for northern Ethiopia. (modified from Sovoyat et al., 1989). 46

Figure 19. Generalized geologic map northern Ethiopia, with offshore evaporite distribution of southwestern Red Sea (modified from Hutchinson, 1972). 49

Figure 20. Measured Mesozoic sections from Danakil Area, North Ethiopia (see Figure 4 for location). (source IPL internal inter-office report, 1989 and Gulf Oil unpublished report). 51

Figure 21. Condensed borehole lithologic column for Ethiopian Red Sea (for location of wells see Figure 2.) (source UNDP/ World Bank, 1991). 53

Figure 22. Southern Red Sea Regional Seismic transect. (in back pocket) 56

Figure 23. Southwestern Red Sea (offshore Eritrea) twt Top Basement Structure. 66

Figure 24. Southwestern Red Sea (offshore Eritrea) twt Top Infra-evaporite Structure. 69

Figure 25. Southwestern Red Sea (offshore Eritrea) twt Top Intra-evaporite Structure 70

Figure 26. Southwestern Red Sea (offshore Eritrea) twt Intra-evaporite Isochron. 71

Figure 27 a) Unprocessed condensed reflection seismic section of Line 435E. b) Magnified part of 'a'. 74

Figure 28 a) Zero-phase wavelet extracted at from Line 435E at CDP 325. b) Forward fourier-division inverse wavelet of the Zero-phase wavelet in 'a'. 79

Figure 29 a) Forward fourier-division wavelet filtered condensed seismic section of Line 435E. b) Magnified part of 'a'. 80

Figure 30 a) Seismic attribute display: color coded display of Line 435E. b) Magnified part of 'a'. 84

Figure 31 a) Seismic attribute display: instantaneous phase display of Line 435E. b) Magnified part of 'a'. 85

Figure 32 a) Seismic attribute display: amplitude strength (envelop) display of Line 435E. b) Magnified part of 'a'. 86

Figure 33 a) Seismic attribute display: real polarity of Line display of Line 435E. b) Magnified part of 'a'. 87

I. INTRODUCTION

I. 1. Definition of the Problem

Answers to four questions are paramount to the successful understanding of the geology of the southwestern Red Sea (Figure 1): What is the style and timing of the southwestern (offshore Eritrea) Red Sea rifting? What is the relationship between the rifting and sedimentation? What factors affect our ability to seismically image beneath the evaporite and thus answer these questions? Can we mitigate or overcome these factors?

Infra-evaporite interpretation is key to understanding the basin development and basin sedimentation history. However, this interpretation is complicated by salt horizons that create ray bending problem and are also sources of significant multiple energy. The multiples generated off the top and base of salt layers add to the existing water bottom multiples (MacKay and Dragoset 1994). Thick evaporites containing salt deposits in the southwestern Red Sea generate multiples that pose a serious problem for imaging the underlying units and structures beneath the evaporite, obscuring true stratal reflections in some instances and creating stratal artifacts in others. In addition, the non-uniform nature of the evaporite

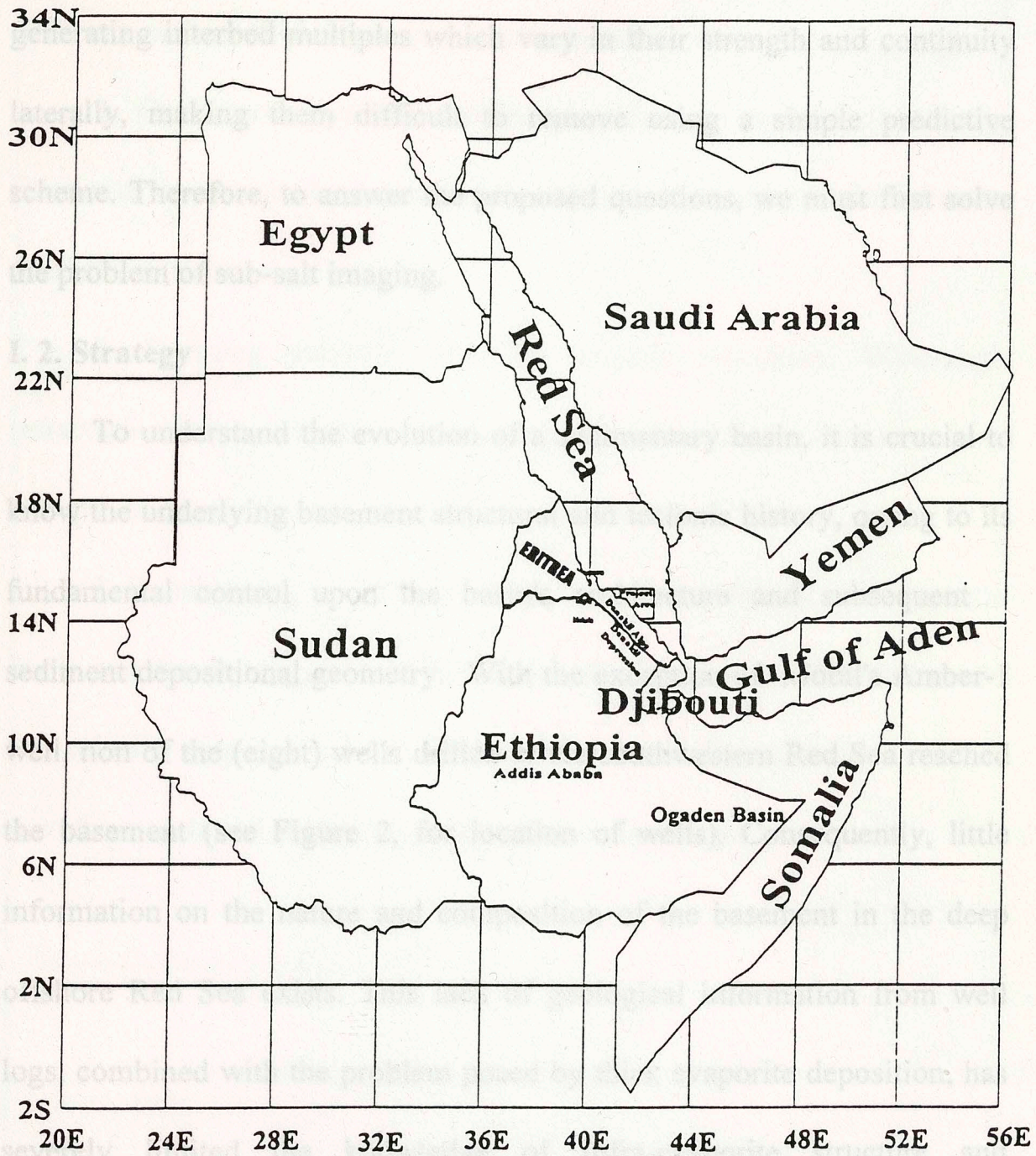

Figure 1. Location of the Red Sea and Gulf of Aden Basins (Project area indicated).

sequence in the region aggravates the Infra-evaporite unit mapping by generating interbed multiples which vary in their strength and continuity laterally, making them difficult to remove using a simple predictive scheme. Therefore, to answer the proposed questions, we must first solve the problem of sub-salt imaging.

I. 2. Strategy

To understand the evolution of a sedimentary basin, it is crucial to know the underlying basement structural and tectonic history, owing to its fundamental control upon the basin's architecture and subsequent sediment depositional geometry. With the exception of Mobil's Amber-1 well, non of the (eight) wells drilled in the southwestern Red Sea reached the basement (see Figure 2, for location of wells). Consequently, little information on the nature and composition of the basement in the deep offshore Red Sea exists. This lack of geological information from well logs, combined with the problem posed by thick evaporite deposition, has severely limited the knowledge of Infra-evaporite structure and stratigraphy. However, the number of hypotheses attempting to explain the Red Sea's evolutionary history are disproportionate to the amount of

constraining geological information available. Nevertheless, to tackle this difficulty, a three fold approach was attempted:

1. Optimization of sub-salt imaging through wavelet processing. Fourier division wavelet processing was applied to improve the reflection seismic section.

2. Defining sub-salt reflection seismic velocities. Wide-angle refraction seismic velocities from sonobuoy refraction surveys were used to depth constrain the reflection seismic horizons.

3. Constraining seismic interpretation using synthetic seismograms. Sonic and density logs of available boreholes were used to forward model the seismic response of a constrained reflectivity convolved with a waveform assumed analogous to the seismic lines input.

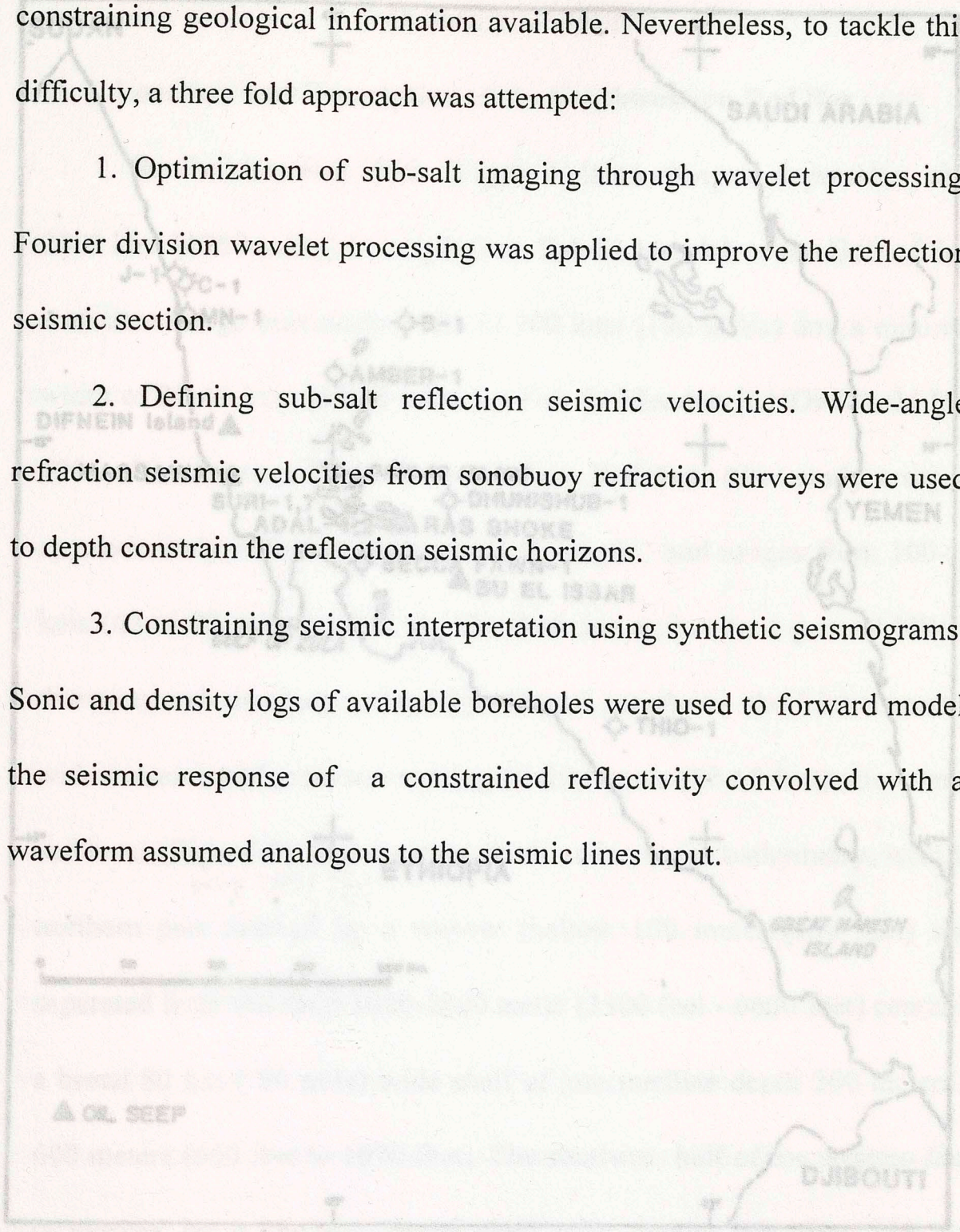

Figure 2. Location map of wells, oil seeps and wells with oil shows in the Ethiopian Red Sea (offshore). (source UNDP/World Bank report, 1991).

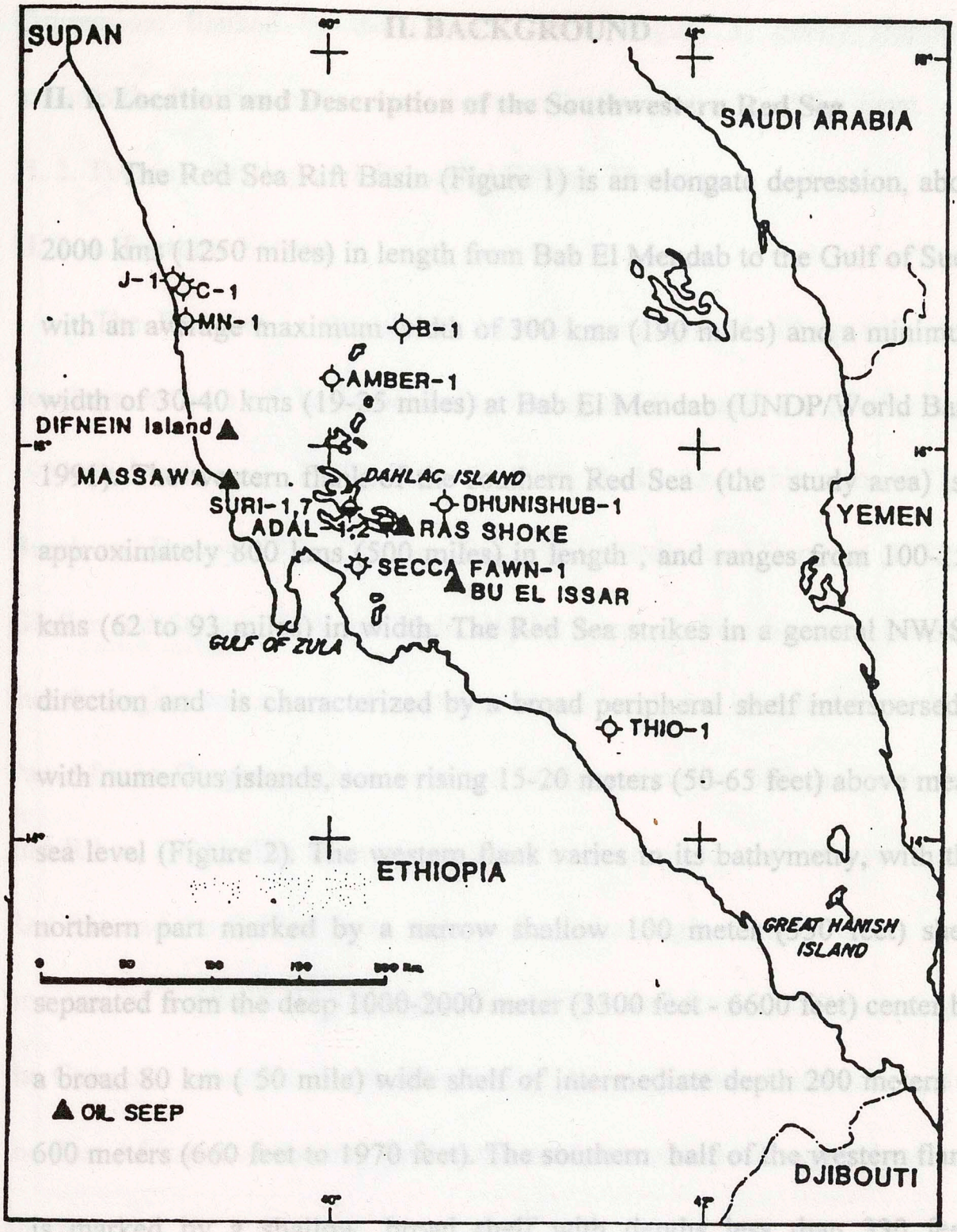

Figure 2. Location map of: wells, oil seeps and wells with oil shows in the Ethiopian Red Sea (offshore). (source UNDP/World Bank report, 1991).

II. BACKGROUND

II. 1. Location and Description of the Southwestern Red Sea

The Red Sea Rift Basin (Figure 1) is an elongate depression, about 2000 kms (1250 miles) in length from Bab El Mendab to the Gulf of Suez, with an average maximum width of 300 kms (190 miles) and a minimum width of 30-40 kms (19-25 miles) at Bab El Mendab (UNDP/World Bank 1991). The western flank of the southern Red Sea (the study area) is approximately 800 kms (500 miles) in length , and ranges from 100-150 kms (62 to 93 miles) in width. The Red Sea strikes in a general NW-SE direction and is characterized by a broad peripheral shelf interspersed with numerous islands, some rising 15-20 meters (50-65 feet) above mean sea level (Figure 2). The western flank varies in its bathymetry, with the northern part marked by a narrow shallow 100 meter (330 feet) shelf separated from the deep 1000-2000 meter (3300 feet - 6600 feet) center by a broad 80 km (50 mile) wide shelf of intermediate depth 200 meters to 600 meters (660 feet to 1970 feet). The southern half of the western flank is marked by a shallow, broad shelf with depths less than 330 feet. Onshore, the coastal plain area is a gently sloping undulating surface with few highs, separated from the highland by a steep escarpment. The Afar

Depression, flanked by the Danakil Horst (Figure 3) gently sloping towards the Red Sea coast occurs between the escarpment and the coast.

II. 2. Tectonic Setting and Principal Rifting Theories

II. 2. a. Tectonic Setting

The Red Sea is the classic tectonic paradigm of rifting with its development as a rift basin occurring during the Cenozoic era (Stefanini, 1933 (in Marla et al., 1979); Dainelli, 1943; Burke And Whiteman, 1973; Burek and Dewey, 1973; Girdler, 1958, 1964; Girdler and Darracot ,1972; Girdler and Styles, 1974 and Mohr, 1971). Some workers have suggested that the region was a zone of crustal structural weakness inherited from the Pan-African Orogeny, which occurred at approximately 600 ma (Makris and Rihm, 1991). The zone of weakness is believed to have allowed the Red Sea and the Gulf of Suez to have formed a single elongate basin, as one arm of a rift-rift-rift triple junction (Pilger and Rosler, 1976) during the Cenozoic extension event. The Gulf of Aden was the second arm, and the East African Rift System formed the third arm which subsequently was aborted.

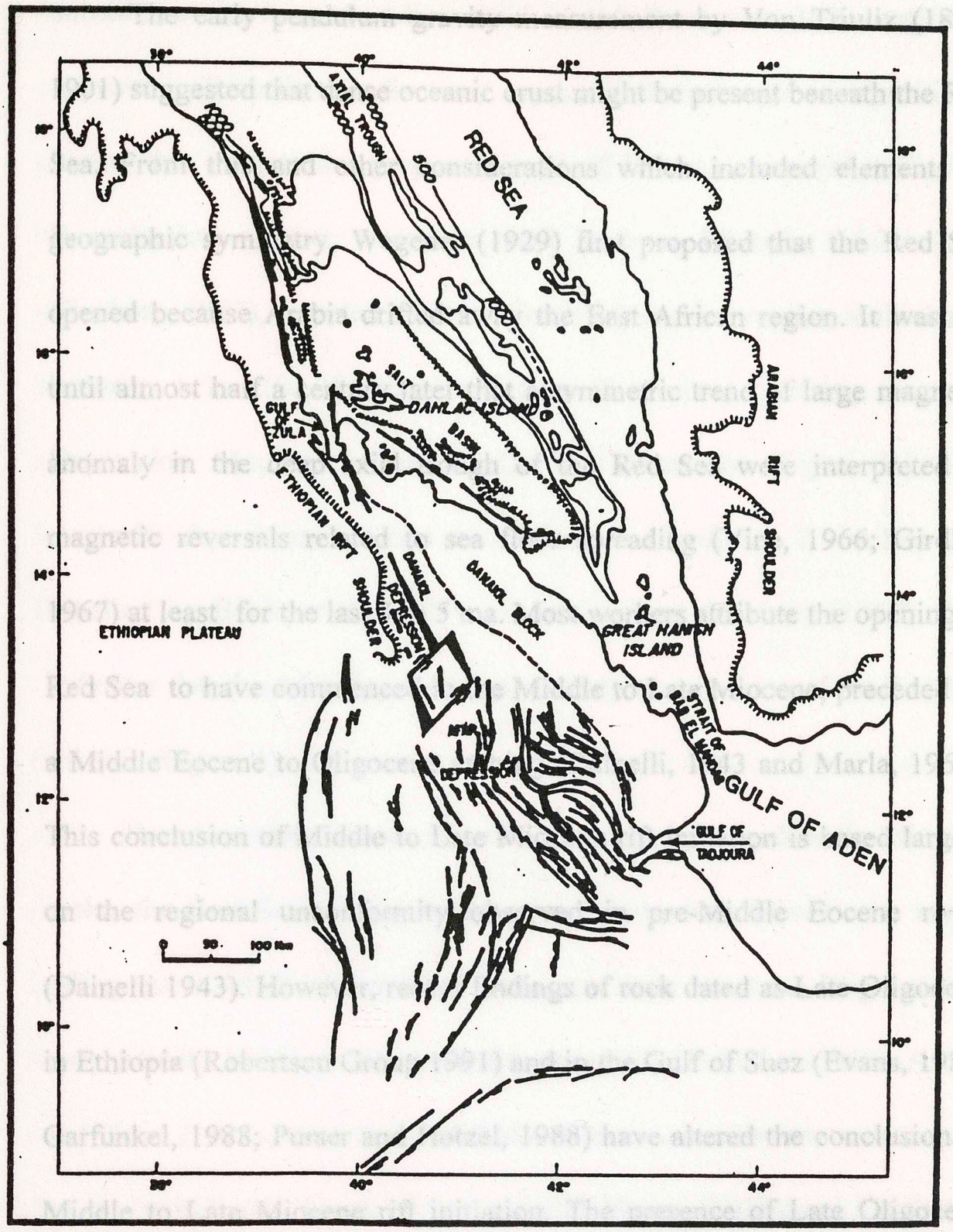

Figure 3. Schematic map of major structural elements of northern Ethiopia. (modified from Berhe, 1986; Makris and Rihm, 1991; Marla et al., 1979 and Sovoyat et al., 1989).

The early pendulum gravity measurement by Von Triuliz (1898, 1901) suggested that dense oceanic crust might be present beneath the Red Sea. From this and other considerations which included elements of geographic symmetry, Wegener (1929) first proposed that the Red Sea opened because Arabia drifted away the East African region. It was not until almost half a century later that a symmetric trend of large magnetic anomaly in the deep axial trough of the Red Sea were interpreted as magnetic reversals related to sea floor spreading (Vine, 1966; Girdler, 1967) at least for the last 3 to 5 ma. Most workers attribute the opening of Red Sea to have commenced in the Middle to Late Miocene, preceded by a Middle Eocene to Oligocene arching (Dainelli, 1943 and Marla, 1963). This conclusion of Middle to Late Miocene rift initiation is based largely on the regional unconformity observed in pre-Middle Eocene rocks (Dainelli 1943). However, recent findings of rock dated as Late Oligocene in Ethiopia (Robertson Group 1991) and in the Gulf of Suez (Evans, 1988; Garfunkel, 1988; Purser and Hotzel, 1988) have altered the conclusion of Middle to Late Miocene rift initiation. The presence of Late Oligocene rocks (Habab Formation) in the Thio-1 well (Robertson Group, 1991), and Early to Late Miocene rocks in the Gulf of Zula, Eritrea where a high

subsidence rate is marked by a thick Hababb Formation (Infra-evaporite) deposition (from Seismic Section), suggested the presence of depositional basins that predate the proposed onset of Late Miocene rift initiation. Reevaluation of their previous work onshore Ethiopia (Makris and Ginzberg, 1987), revealed a thick sedimentary section varying in thickness between 1 km (0.625 mile) to 5 kms (3.1 miles) covering the Afar Depression. Moreover within the Danakil Depression (Figure 3a) thick evaporite deposition 2.2 kms to 3.5 kms (1.4 miles to 2.2 miles) was reported by Behle et al. (1975) and Makris and Ginzberg (1987). This indicates that the Afar Depression is possibly an extension of the Red Sea rift axis (Figure 3).

Based on the presence of Late Oligocene to early Middle Miocene rocks, the Red Sea rift basin formation can be traced back to a major rifting event which commenced sometime from the Late Oligocene to early Middle Miocene. However, Evans (1988) Garfunkel (1988) Purser and Hotzl (1988), state the pre-Middle Eocene unconformity was caused by the world-wide lowstand in sea level. Evans (1988) and Garfunkel (1988) estimate lowering of sea level 600 to 1600 feet in the Gulf of Suez area. Berhe (1986) argues that there was no pre-rift uplift in the southern

Red Sea, which was formed as a result of the attenuation of the continental crust. Whereby the median region south of 16^0N is considered to be underlain by thinned continental crust which thickens farther toward the south, owing to the shifting of the Red Sea axis into the Danakil depression. The southwestern part of the Red Sea has a wide shallow shelf bordering the narrow deep axial trough. The presence of a narrow deep axial trough is supported by high heat flow values in central part of the Red Sea (Makris et al., 1991).

II. 2. b. Principal Rifting Theories

There is presently no consensus among workers on the style and timing for the evolution of the Red Sea. Some workers suggest that the entire Red Sea formed by pure shear and is floored by oceanic crust, (Brown and Girdler, 1982; Girdler and Style, 1974; Girdler and Underwood, 1983), while others (Makris and Rihm, 1991) have suggested the origin occurred by pull apart owing to regional simple shear of thinned continental crust that included pockets of oceanic crust.

Among the proposed mechanisms, the following are the main types: (1) Pure shear (high-angle faulting) (Lowell and Genik, 1972) or modified pure shear (Diffused shear and normal faulting) (Martinez and Cochran,

1988) (Figure 4a and b), (2) Low-angle detachment-simple shear (Wernicke, 1985) or modified low-angle detachment simple shear model (Bohannon, 1989) (Figure 5a and b), and (3) Shear controlled pull apart basin development (Makris and Rihm, 1991) (Figure 6).

Lowell and Genik (1972) proposed based on investigations onshore and adjacent to the southern Red Sea a simple pure shear (high-angle faulting) model which includes mafic dike injections into the thinned continental crust to accommodate the stretching. They suggested the Red Sea developed in its earlier stage as a continental rift with numerous asymmetric half grabens separated by zones of transform faults. The subsequent tectonic extension was accompanied by the intrusion of mafic dikes into the continental crust. The final stage of Red Sea development was the transformation of these half grabens into a symmetric rift with a deep central zone (Figure 4a).

Cochran and Martinez (1989) proposed a modified pure shear (diffused shear with normal faulting) model from their work in the northern Red Sea and Gulf of Suez (Figure 4b). They argued that the northern part of Red Sea represents thinned continental crust (Figure 4b), a

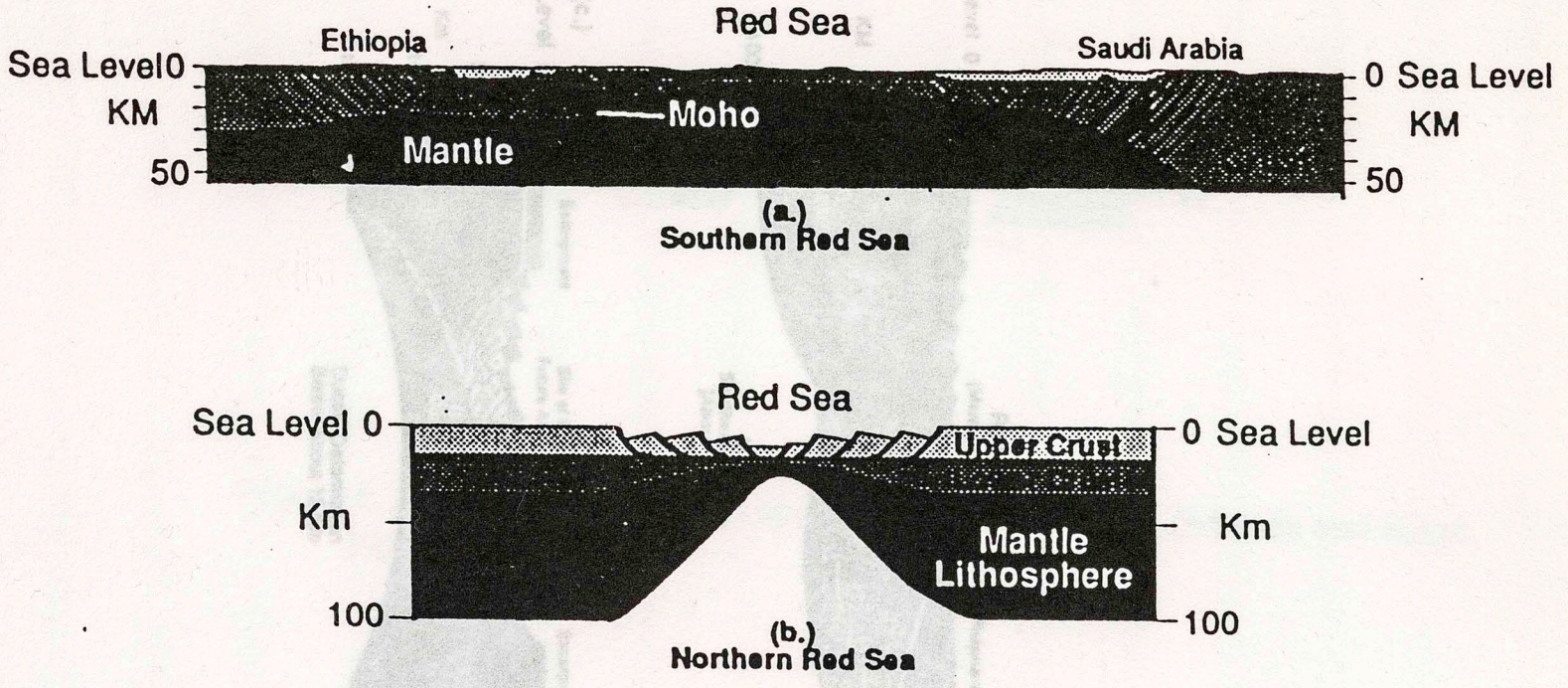

Figure 4. Generalized schematic diagram a) Simple pure shear (high-angle faulting) model of Lowell and Genik (1972); b) modified pure shear (Diffused shear and normal faulting) model (Martinez and Cochran, 1988).

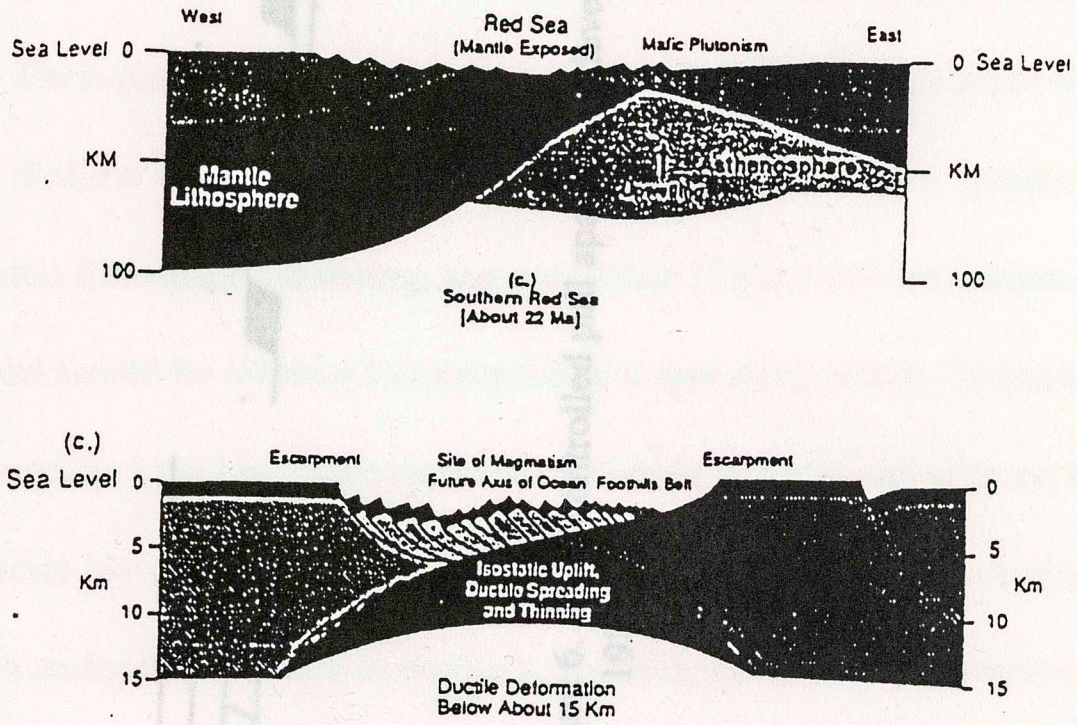

Figure 5. Generalized schematic diagram a) Low-angle detachment simple shear model (Wernicke, 1985; Veggenrieter et al., 1988), and b) modified Low-angle detachment simple shear model (Bohannon, 1989)

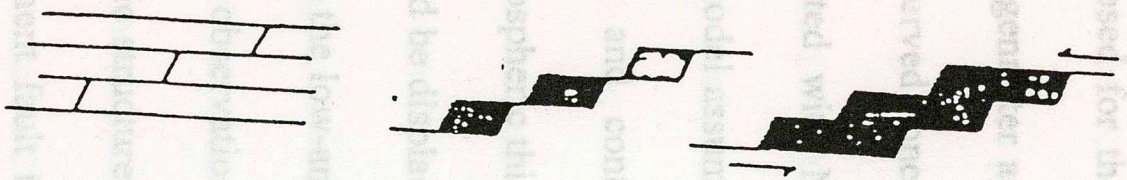

Figure 6. Shear controlled pull apart basin development (Makris and Rihm, 1989).

transition between continental rift and oceanic rift, with a faulted upper brittle crust and sheared lower ductile crust.

The low-angle detachment simple shear model of Wernicke (1985) originally proposed for the North American Basin and Range was later applied by Voggenrieter and Hotzl (1989) (Figure 5a) to the Red Sea to explain the observed none symmetric occurrence of Cenozoic mafic dike swarms associated with NW trending faults on the Arabian Red Sea margin. Their model assumes shearing along a detachment fault plane that begins shallow and continues into the lithosphere which produces asymmetric lithospheric thinning, and volcanism (Figure 5a). Volcanism in this model would be displaced eastward of the spreading center. Bohannon (1989) modified the low-angle detachment simple shear model (Figure 5b) to reconcile his observations of the mafic volcanic rocks on the Arabian side with tectonic structures in northern Somalia. He included a westward dipping detachment fault that meets the east dipping major detachment fault (Figure 5b). In this modified low-angle detachment simple shear model, the site of volcanism and spreading would be once again in the center of the axial trough.

Pull apart basins are pockets of rhombic basins produced by strike slip movement along a major strike slip fault system (Aydin and Nur, 1982). Makris and Rihm (1991) proposed a shear controlled pull-apart basin model for the Red Sea (Figure 6), having separate pockets of rhombic cells formed as pull apart basins owing to strike slip movement. In their mature stage these pull apart basins are floored by oceanic crust. Makris and Rihm (1991) suggested that wrench faulting played a major role in the early evolution of the Red Sea, by forming a steep western flank.

All of the numerous theories on the mechanical models for the development of the Red Sea accept that it is a rift basin, it formed sometime during the middle Cenozoic and that it represents one arm of triple rift-rift-rift junction within the Afar depression. The East African Rift System represents the abandoned arm and the Gulf of Aden represents the third arm (Burke And Whiteman, 1973; Burke and Dewey, 1973 and Cole 1939) (Figure 3). It should be emphasized that much of the evidence used by these workers came from independently sparsely collected outcrop geological data, some regional geophysical surveys and only limited use of multi-channel reflection seismic where available. This paper will attempt

to incorporate the previous observations with a new, refraction velocity constrained seismic stratigraphic analysis of the southwestern Red Sea.

II. 3. Previous Exploration Activity in the Area

Exploration in the southwestern Red Sea began in the nineteen twenties, when Italy militarily occupied this region. During this time, Italy drilled one shallow exploration well: Buel Issar (Table 1 and Figure 2). The borehole drilled was shallow: 160 meters (525 feet), and was located at $15^{0}20'30"$ latitude and $40^{0}06'48"$ longitude, based upon an indication of oil seeps around the Buel Issar island (see Figure 2). Later during World War II, Italy continued its oil exploration in the Ethiopian onshore, and drilled 11 more shallow wells around the Dahlak Island (Table 1), based upon oil seep occurrences. None of the wells drilled were economic. A second phase of exploration was after World War II during the reign of Emperor Haile Slassie I, (1958 to 1977) (Tables 2a through d). A five day gas blow out occurred in the Mobil C-1 well and a number of oil shows were encountered in a few of the other wells (Figure 2). No commercial discoveries were made. Owing to an unfavorable political situation exploration activity halted until the late 1980's.

The third phase of exploration commenced in late 1980's during the ruling of the socialist government, but was soon interrupted, by the political unrest in the area in 1990. The three companies that operated in the area were: British Petroleum, IPL and AMOCO.

The exploration activities summary is given in (tables 1 and 2a through d and Figure 7). Even though exploration in the region extends over a long time span, activity was sporadic and not continuous.

Well	Latitude	Longitude	Year	Company	Elevation (meters)	Tops (meters)			TD (meters
						Dhunishub	Desset	Amber	
Bu El Issar	15°20'19"	40°30'48"	1921	Societa Mineraria dell'Africa Orientale	?	Surface	150	----	160?
Dahlak-1	15°38'30"	40°06'20"	1936	Agip	24	Surface	116	---	170
Suri-1	15°40'57"	40°06'27"	1936-40	Agip	20	Surface	61	299	1700.5
Suri-2	15°41'02"	40°06'46"	1937-38	Agip	23	Surface	72	343	425
Suri-3	15°41'12"	40°07'29"	1937-38	Agip	19	Surface	92	267	668
Suri-4	15°40'29"	40°06'22"	1938	Agip	24	Surface	82	314	541
Suri-5	15°40'50"	40°05'32"	1937-38	Agip	27	Surface	40	195	312
Suri-6	15°41'19"	40°05'58"	1938	Agip	25	Surface	60	160	559
Suri-7	15°42'40"	40°03'33'	1939-40	Agip	25	Surface	56	285	2503
Adal-1	15°36'29"	40°18'50"	1939	Agip	15	Surface	115	367	804
Adal-2	15°37'07"	40°16'50	1936-40?	Agip	30?	Surface	200	730	2475
Ras Shoke-1	15°33'09"	40°25'20'	1936-40?	Agip	5.5	Surface	103	302	603

Table 1 Exploration activity before and during World War II. (compiled from UNDP/World Bank, 1991)

YEAR	ACTIVITIES
1920-1921	Sociate Mineraria dell'Africa Orientale drilled shallow well on Bu El Issar Island.
1935-1940	Shallow drilling by AGIP on Dahlak Islands (SURI 1-7, ADAL 1 and 2, DAHLAK-1, RAS SHOKE-1.
1958-1960	Geological, gravity and magnetic survey of coastal area by NAFTAPLIN of Yugoslavia.
1962	MOBIL acquired offshore acreage.
1964	MOBIL shot shallow penetration seismic survey, Gulf acquired offshore acreage.
1965	Dhunishub-1 drilled by GULF.
1966	Amber-1 drilled by MOBIL, ESSO farmed into MOBILE acreage.
1968	Secca Fawn-1 drilled by GULF, ETHIOPIAN OIL acquired offshore acreage.
1969	B-1, C-1 drilled by MOBIL.
1970	GULF and MOBIL relinquished.
1972	GAO farmed into ETHIOPIAN OIL acreage.
1973	J-1 and MN-1 drilled by GAO.
1974	ETHIOPIAN OIL relinquished.
1975	SHELL acquired offshore acreage, shot seismic survey.
1976	Thio-1 drilled by SHELL.
1977	SHELL relinquished

Table 2a. General exploration activity in the Ethiopian Red Sea by year and company (compiled from UNDP/World Bank, 1991)

Well	C-1	J-1	MN-1	Secca fawn	Thio-1
Location	16°49'24" 39°49'53"	16°50'48" 39°08'32"	16°39'00" 39°11'35"	15°23'24" 40°09'56"	14°34'14" 41°30'43"
Company	Mobil	GAO	GAO	Gulf	Shell
KB	35'	37'	37'	53'	45'
Spud date	Oct. 5, 1969	July 5, 1973	Aug. 27,1973	Nov. 16, 1968	Des 19, 1976
Complete date	Feb. 11, 1970	Aug. 26,1973	Oct. 6, 1973	Feb. 10, 1969	Feb. 23, 1977
W. depth	213'	95'	194	182'	166'
T. depth	9874'	10281'	9410	1592,	10233'
G.G. °F/100'	2.63	2.29	2.03	2.97	2.08
Dhunishub top	248'	-----	-----	182'	211'
Desset top	4300'	1000'	1250'	1150'	-----
Amber top	6060'	5938'	5423'	8127'	981'
U.Habab top	9865'	6920'	5963'	-----	4690'
M. Habab top	-----	-----	-----	-----	5650'
L. Habab top	-----	7450'	-----	-----	6075'

Table 2b. Wells drilled in the Ethiopian Red Sea (offshore) after World War II (compiled from UNDP/World Bank, 1991)

Company	Survey	Years	No. of stations or line-km
Gravity			
NAFTAPLIN	LAND	1958/1960	4,664 stations
MOBIL	Land	1965/1967	5,189 stations
SHELL	Marine	1974/1975	4,178 line-km
Magnetic			
NAFTAPLIN	Land	1958/1960	4,664 stations
MOBIL	Aeromagnetic	1963	8,267 line-km
GULF	Aeromagnetic	1964/1965	12,416 line-km
BARUCH FORTER	Aeromagnetic	1968	6,150
SHELL	Marine	1974/1975	4,082?
ETHIOPIAN OIL	Aeromagnetic	1969?	unknown

Table 2c. Geophysical exploration activity in the Ethiopian Red Sea (offshore) (compiled from UNDP/World Bank, 1991)

Company	Year	Reflection line-km		Reflection fold of coverage	Refraction line-km
		Analog	Digital		
MOBIL					
Mobil LoFes	1963/64	8048	---	Single	---
Ray Marine	1964/65	2998	---	Single	214
Ray Onshore	1964/65	80	---	Single	57
GSI Six-fold Marine	1966	---	298	Six	?
Ray Six-fold Marine	1966/67	---	1943	Six	---
Western Six-fold Marine	1968	---	892	Six	---
Total		11126	3133		271
SIGNAL					
Western 24-fold Marine	1972	---	461	24	---
MME					
Western 48-fold Marine	1984	---	945	48	---
GULF					
Marine Single-fold	1964	275	---	Single	---
GSI Marine Single-fold	1965	822	---	Single	---
Ray Dahlak Island	1965	47	---	Single	201
Ray Marine Single-fold	1965	265	---	Single	---
GSI Marine	1966	---	81	Six	---
Western Marine	1967	---	862	Six	---
Total		1409	943		201
SHELL					
Lady Glorita 1	1972	---	518	24	---
Lady Glorita 2	1972/73	---	1782	24	---
Three Part Recon.	1974/75	---	6183	24	---
Detail Survey	1975	---	507	48	---
Total					
BARUCH FOSTER					
Baruch Foster	1969	---	2250	?	---
Ethiopian Oil	1969	---	427	24	---
General American Oil	1974	---	23	24	---
Total		---	2700		---

Table 2d. Reflection seismic exploration activity of the Ethiopian Red Sea (offshore) (compiled from UNDP/World Bank, 1991)

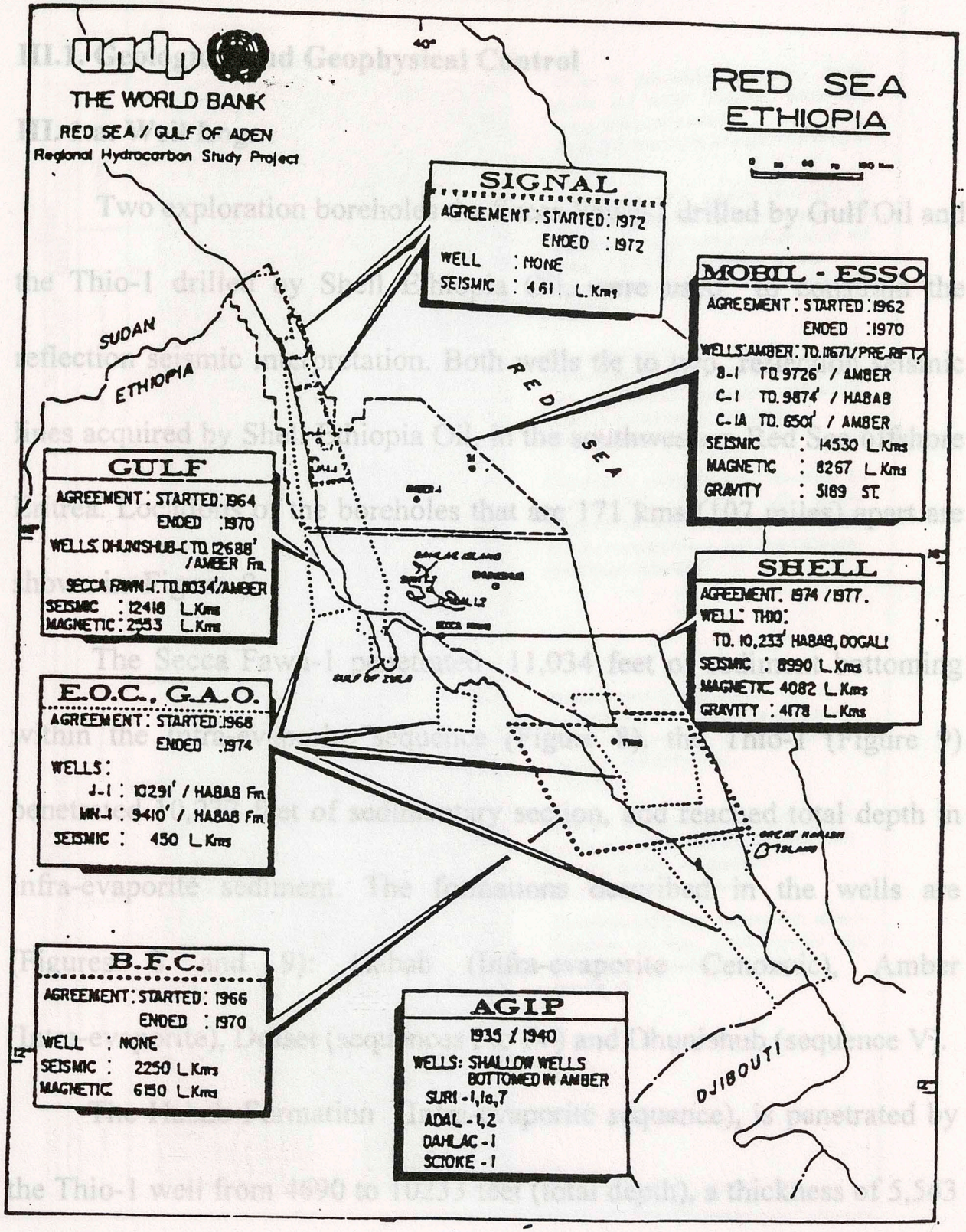

Figure 7. Location map of previous acreage and company activity in the Ethiopian Red Sea. (source UNDP/World Bank report, 1991).

III. OBSERVATIONS

III.1. Geological and Geophysical Control

III. 1.a. Well Logs

Two exploration boreholes the Secca Fawn-1 drilled by Gulf Oil and the Thio-1 drilled by Shell Ethiopia Oil, were used to constrain the reflection seismic interpretation. Both wells tie to two reflection seismic lines acquired by Shell Ethiopia Oil, in the southwestern Red Sea offshore Eritrea. Locations of the boreholes that are 171 kms (107 miles) apart are shown in Figure 2.

The Secca Fawn-1 penetrated 11,034 feet of sediment bottoming within the Intra-evaporite sequence (Figure 8). the Thio-1 (Figure 9) penetrated 10,233 feet of sedimentary section, and reached total depth in Infra-evaporite sediment. The formations described in the wells are (Figures 8 and 9): Habab (Infra-evaporite Cenozoic), Amber (Intra-evaporite), Desset (sequences I to IV) and Dhunishub (sequence V).

The Habab Formation (Infra-evaporite sequence), is penetrated by the Thio-1 well from 4690 to 10233 feet (total depth), a thickness of 5,543 feet. The Habab Formation age is Early to Middle Miocene (Robertson Group 1991). The sonic velocity of this formation ranges between 2.4 km

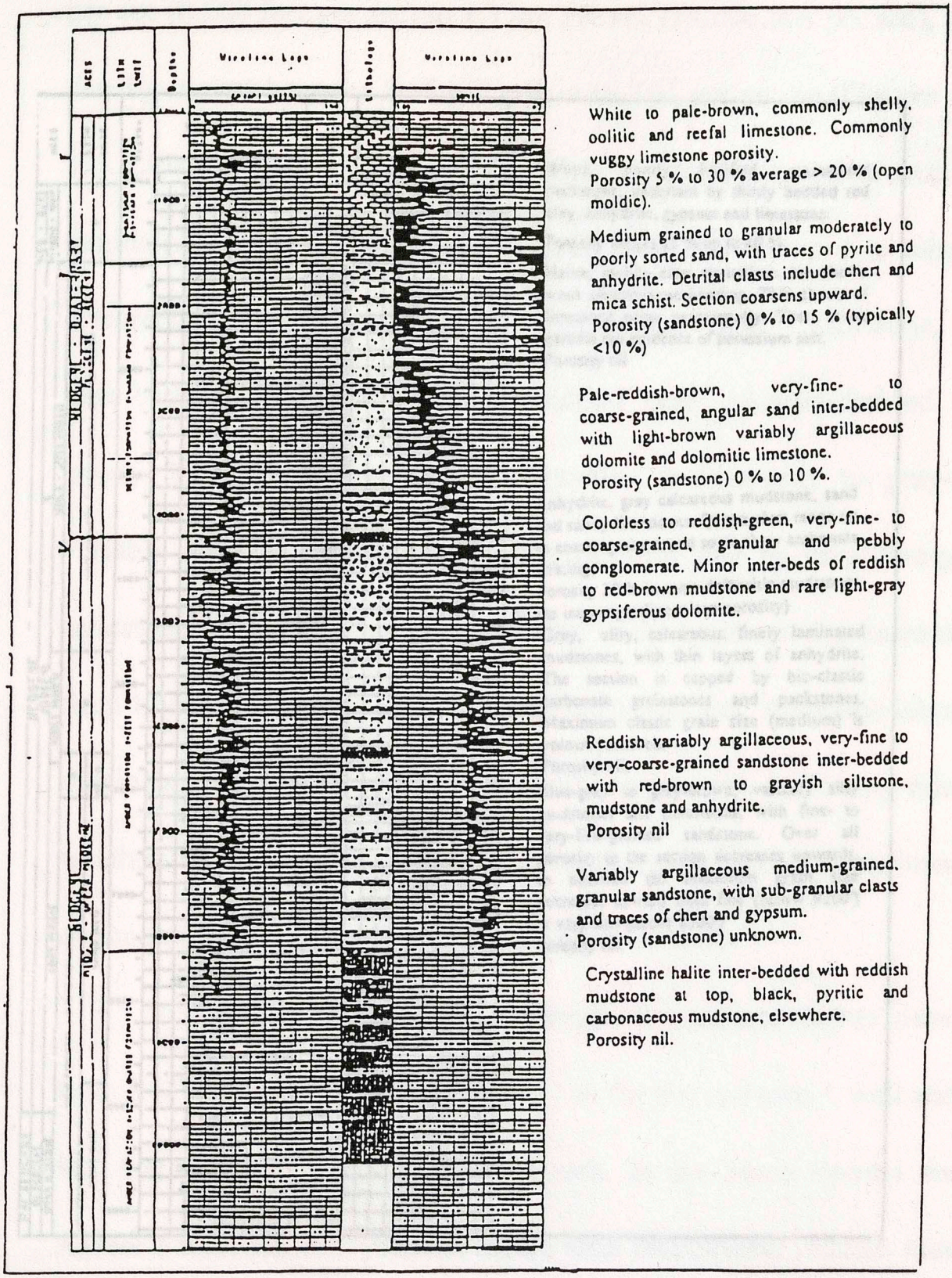

Figure 8. Summary well-log for Secca Fawn-1. (source Robertson group, 1991).

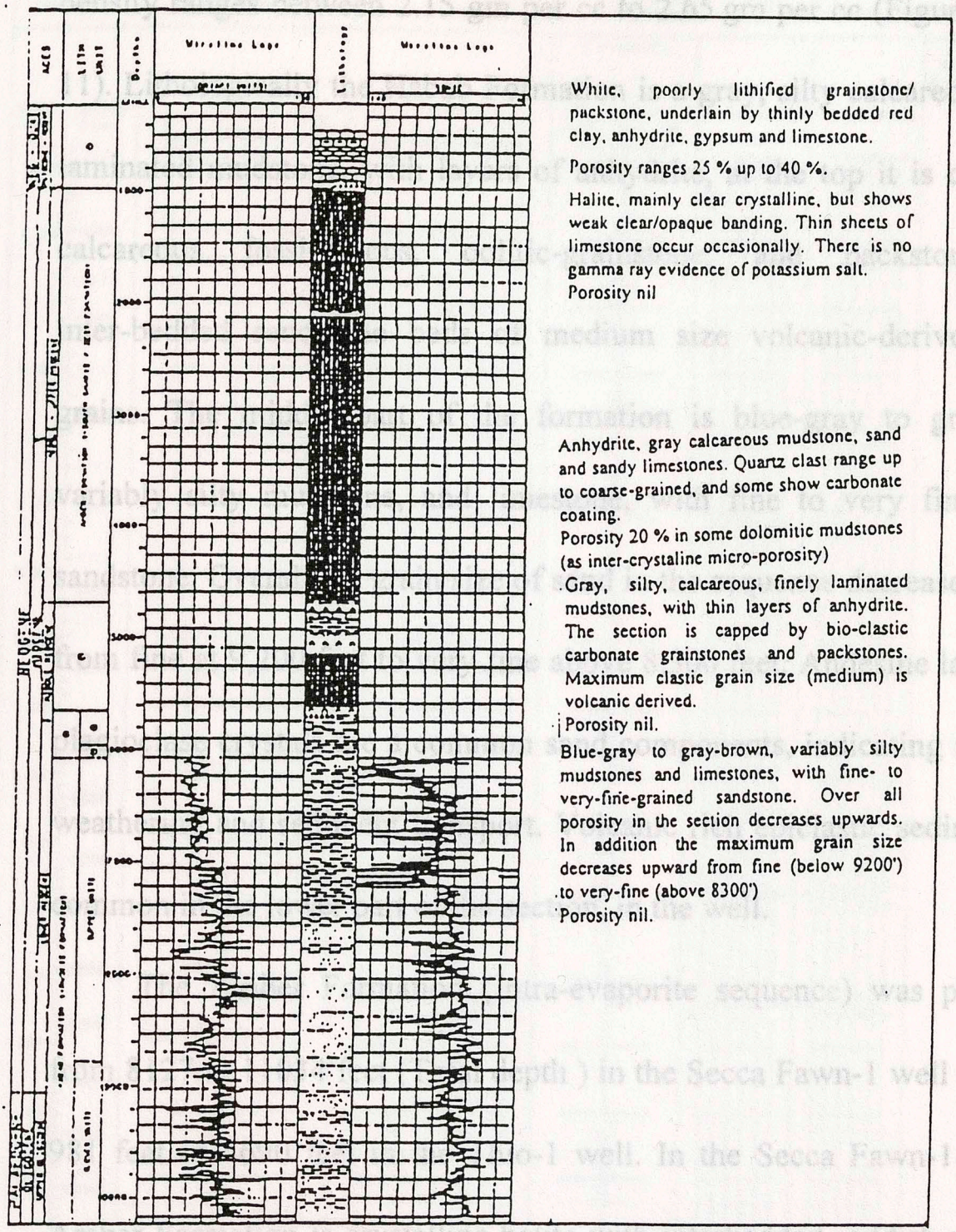

Figure 9. Summary well-log for Thio-1 well. (source Roberson Group, 1991).

per sec (8,000 feet per sec) to 4.3 km per sec (14,000 feet per sec), and the density ranges between 2.15 gm per cc to 2.65 gm per cc (Figures 10 and 11). Lithologically the Hababb Formation is a gray, silty calcareous, finely laminated mudstone, with layers of anhydrite, at the top it is capped by calcareous fossiliferous, oolitic-grainstone, and packstone, with inter-bedded sandstone beds of medium size volcanic-derived clastic grains. The middle part of the formation is blue-gray to gray-brown variably silty mudstone, and limestone, with fine to very fine-grained sandstone. Overall the grain size of sand in the sequence decreases upward from fine at 9,200 feet to very fine above 8,300 feet. Andesine labradorite plagioclase crystals are a common sand components, indicating minimum weathering and sediment transport. Volcanic rich epiclastic sediments are common in the lower part of the section, in the well.

The Amber Formation (Intra-evaporite sequence) was penetrated from 8127 to 11034 feet (Total depth) in the Secca Fawn-1 well and from 981 feet to 4690 feet in the Thio-1 well. In the Secca Fawn-1 well the Amber Formation is crystalline halite with interbedded reddish mudstone at the top and black pyritic carbonaceous mudstones with thin beds of crystalline anhydrite elsewhere. The sonic velocity of evaporite (salt) in

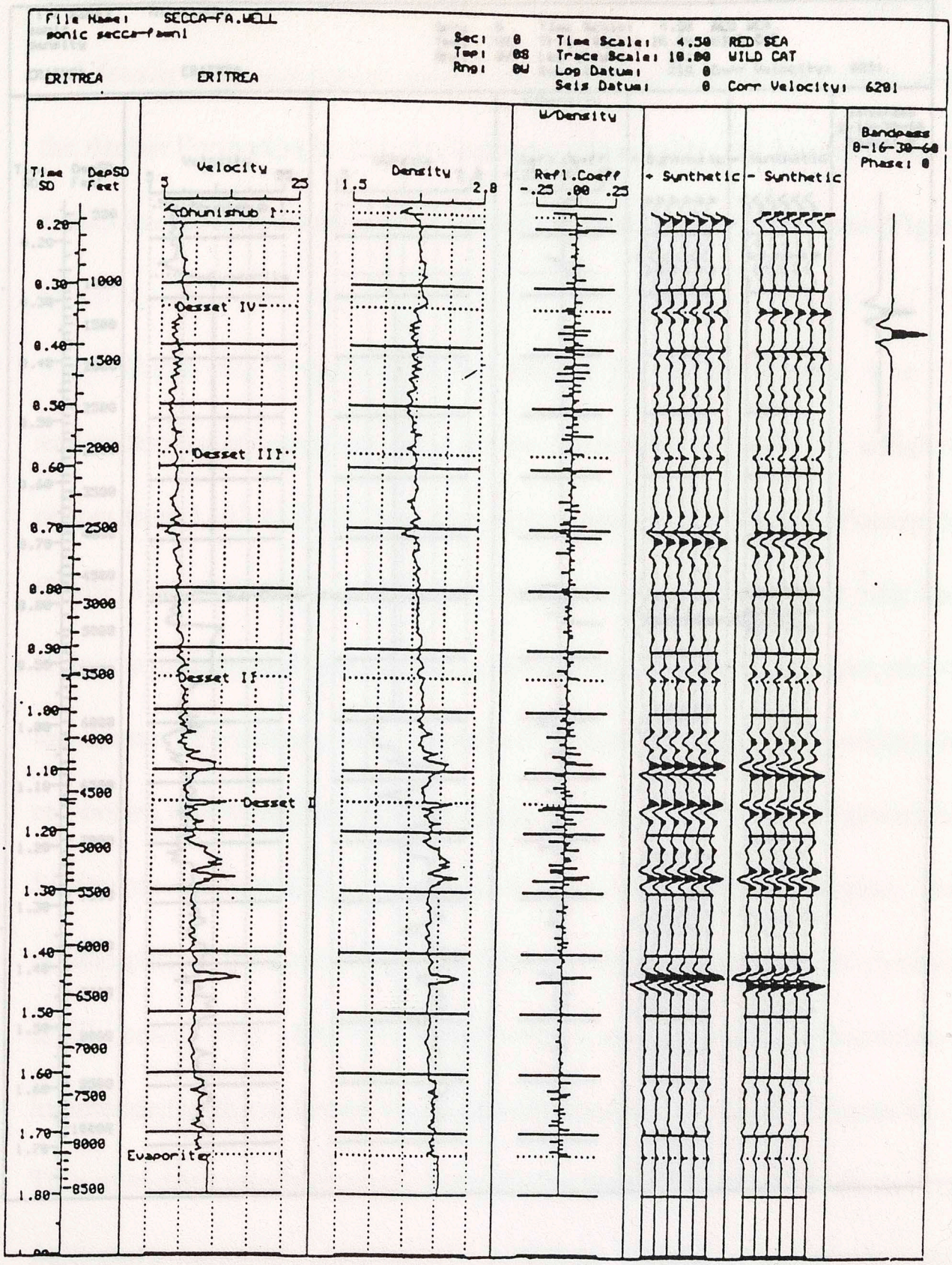

Figure 10. Synthetic seismogram for Secca Fawn-1 well.

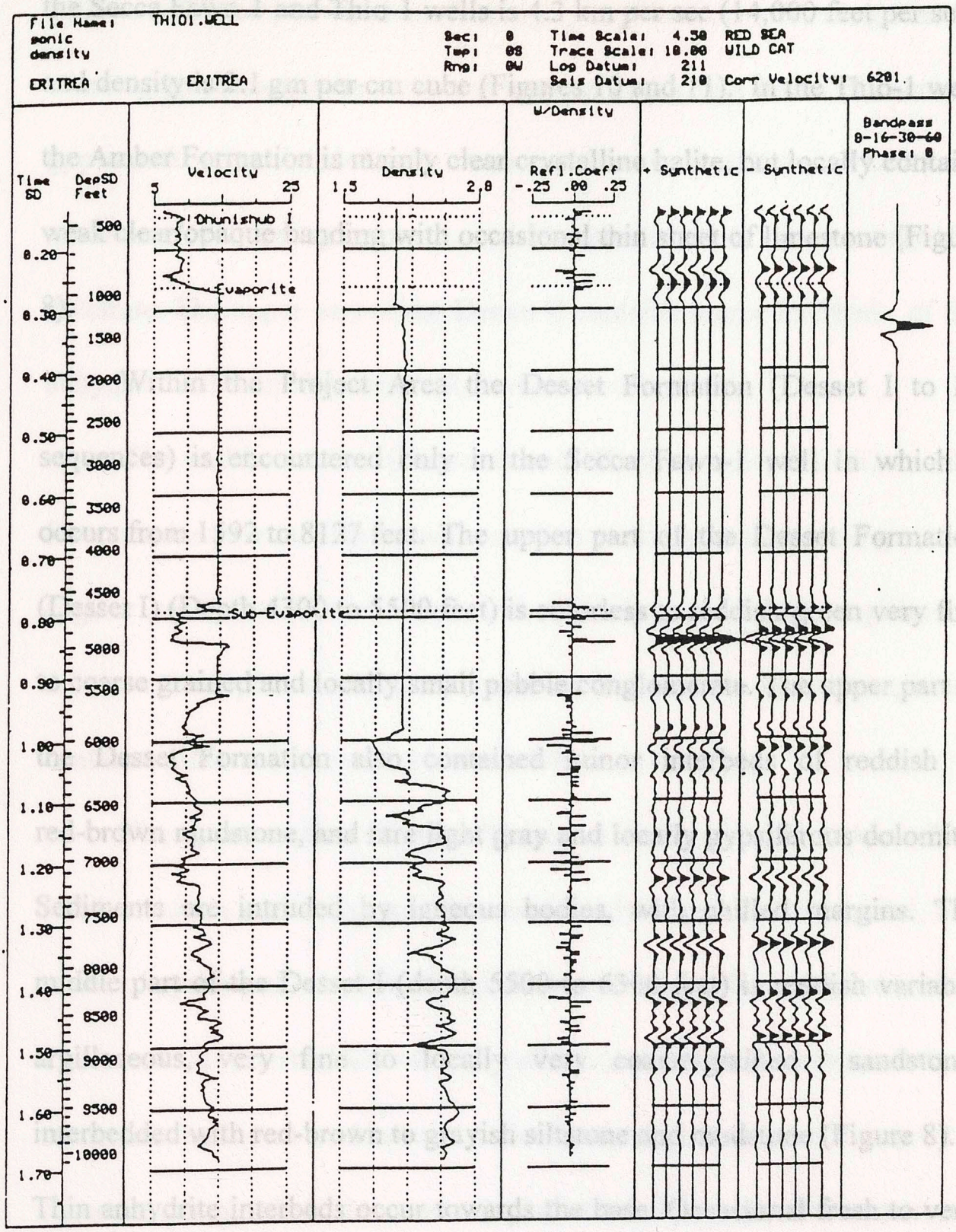

Figure 11. Synthetic seismogram for Thio-1 well.

the Secca Fawn-1 and Thio-1 wells is 4.3 km per sec (14,000 feet per sec), and density is 2.1 gm per cm cube (Figures 10 and 11). In the Thio-1 well, the Amber Formation is mainly clear crystalline halite, but locally contains weak clear/opaque banding with occasional thin sheet of limestone (Figure 8).

Within the Project Area the Desset Formation (Desset I to IV sequences) is encountered only in the Secca Fawn-1 well in which it occurs from 1592 to 8127 feet. The upper part of the Desset Formation (Desset I) (Depth 4300 to 5500 feet) is colorless to reddish-green very fine to coarse grained and locally small pebble conglomerate. The upper part of the Desset Formation also contained minor interbeds of reddish to red-brown mudstone, and rare light gray and locally gypsiferous dolomite. Sediments are intruded by igneous bodies, with chilled margins. The middle part of the Desset I (depth 5500 to 6300 feet) is reddish variably argillaceous, very fine to locally very coarse-grained sandstone, interbedded with red-brown to grayish siltstone and mudstone (Figure 8). Thin anhydrite interbeds occur towards the base. Occasional fresh to very fresh mafic intrusive consisting of plagioclase, feldspar, clino-pyroxen and ortho-pyroxen observed. The lower most part of this formation (depth

6300 to 8120 feet) is variable often highly argillaceous medium-grained to coarse-grained sandstone, with sub-angular clasts, and traces of chert and gypsum. It is interbedded with minor red-brown, variably silty and sandy mudstone containing gypsum, and medium to dark brown, anhydritic dolomite. The upper part of the Desset I) contains scarce interbeds of thin anhydrite and mafic intrusive (Robertson Group, 1991).

The middle section (Desset II and III) from a depth 2000 to 4300 feet contains pale reddish brown, very fine to coarse-grained and generally angular sand. It is interbedded with light brown variable argillaceous dolomite, amorphous anhydrite, and minor halite beds at the base, it also contains minor red-brown to black mudstone.

The upper section (Desset IV) from a depth of depth 1140 to 2000 feet is medium grained to granular, moderately to poorly sorted sand, with traces of pyrite and anhydrite. Detrital clasts include chert and mica schist. The sand is interbedded with locally abundant red-brown siltstone, mudstone and rare red-brown varicolored clay toward the top. The sequence as a whole is coarsening upward, however, the upper part contains less sand than the lower part (Robertson Group, 1991).

The Dhunishub Formation (Sequence V) is a carbonate unit, which overlies the Desset Formation (Desset IV) in the Secca Fawn-1 well and the Amber Formation (Intra-evaporite sequence) in the Thio-1 well (Figures 10 and 11). The base of the Dhunishub Formation is at 981 feet in Thio-1 well and 1150 feet in the Secca Fawn-1 well (Table 2b and Figures 10 and 11). The penetrated thickness in the Thio-1 well is 770 feet and the Secca fawn-1 well it is 1140 feet. The Dhunishub Formation in the Secca Fawn-1 well, is white to pale brown coquina, locally containing oolitic and reefal limestone that is commonly vuggy. It has calcareous matrix which is in part chalky, very fossiliferous. Porosity is good to excellent and intergranular, interfossil, and small vuggy. Minor thin clay beds are present. Usually the clay is gray to olive green, blue gray, rarely reddish, soft and non calcareous. In the Thio-1 well the Dhunishub is white poorly lithified grainstone/packstone at the top and it is underlain by thinly bedded red clay interbeded with anhydrite, gypsum and limestone.

III. 1.b. Synthetic Seismograms

With respect to the reflection seismic data available for study the Thio-1 borehole is located on Line 435E at shotpoint 8435, and the Secca Fawn borehole is on Line 710 at shotpoint 8717 (Figure 12). Sonic and



Figure 12

SOUTHWESTERN RED SEA (OFFSHORE ERITREA)

SHITPOINT LOCATION & THE TECTONIC PROVINCES

density logs from these two wells were loaded into the Mira (Landmark PC) synthetic program, to produce synthetic seismograms (Figures 10 and 11). The complete sonic log for the Thio-1 well was directly obtained was complete from the tapes in LIS format, but because the density log was incomplete portions were digitized from the paper copy. For Secca Fawn-1, a complete sonic log in LIS format was obtained from the tapes. Because no density log was available, a Gardner fit was obtained from the empirical relationship (Gardner, 1977).

$$\rho = 0.23 * V^{0.25} \qquad \text{eq III.1}$$

Where ρ = Density and V = velocity

The Mira program calculates the reflection coefficient (RC) for each horizon based on the difference in acoustic impedance between the layers.

$$RC = (\rho_2 V_2 - \rho_1 V_1)/(\rho_2 V_2 + \rho_1 V_1) \qquad \text{eq III.2 from Gregory (1977)}$$

Where RC = reflectivity, V_1 and V_2 are velocities of layer 1 and layer 2, and ρ_1 and ρ_2 are densities of layer 1 and layer 2 respectively.

The reflectivity profile for the well section is convolved with wavelet having the same frequency band width and phase as that of the seismic section.

III. 1.c. Refraction Seismic Profile

Refraction seismic surveys aimed at mapping the crust underlying the Red Sea were conducted in the late 1980's by Egloff et al. (1991). The particular refraction information incorporated in this thesis was obtained during the SONNE cruise OS 53 (Egloff et al., 1991). Refraction seismic was used to augment the reflection seismic in several fundamental ways. For example, McQuillin et al. (1984) has summarized its use as: 1) to map basement for reconnaissance purposes; 2) To map horizons extending beyond the depth range of the reflection method; 3) To provide control data points for reflection interpretation by providing both depth and velocity data, especially in areas where bore holes are sparse or absent; 4) To map horizons underlying complex geological structures such as salt domes, shale, salt diapirs, igneous intrusions and multiple thrust-faults in orogenic belts. For this study, point number 3, i.e. the velocity information, was the primary benefit for augmenting the reflection seismic.

The OS 53 refraction investigation (Egloff et al., 1991) centered on the western flank of offshore Sudan and the eastern flank of offshore Yemen, with onshore extensions in both Sudan and Yemen. However, the

location of one of the profile transects, Profile VI, fell exactly within the thesis area. Profile VI was therefore used to constrain the reflection seismic interpretation work. The profile was 100 km in length, and had 18 observation stations (OBS) at a 6 km spacing. The seismic energy was generated by 48 small explosive charges (25 kg) fired at a two km spacing and a large shot (150 kg) at the end of the profile (Egloff et al., 1991). Egloff et al (1991) computed all observation positions and shot points (shown in Figure 13, Figure 14 and Figure 15) and concluded in general that the crust is overlain by three to four km of sediment containing one km of evaporite.

Profile VI (Figure 15) is tied to two reflection seismic lines (Lines 1140 and 1160 (Figures 16 and 17) from the southwestern Red Sea study area. The matching was done by converting the two way time (twt) reflection section into depth using the relationship

$$D_i = \sum_{i=1}^{n} [\, V_i*(T_i-T_{(i-1)})/2] \qquad \text{eq III. 3}$$

where Di = depth to the ith section, Vi = interval velocity of ith section,

Ti = two way time of the ith section, and n = number of intervals.

Matching depth from refraction profile and twt from reflection seismic sections are given in (Table 3).

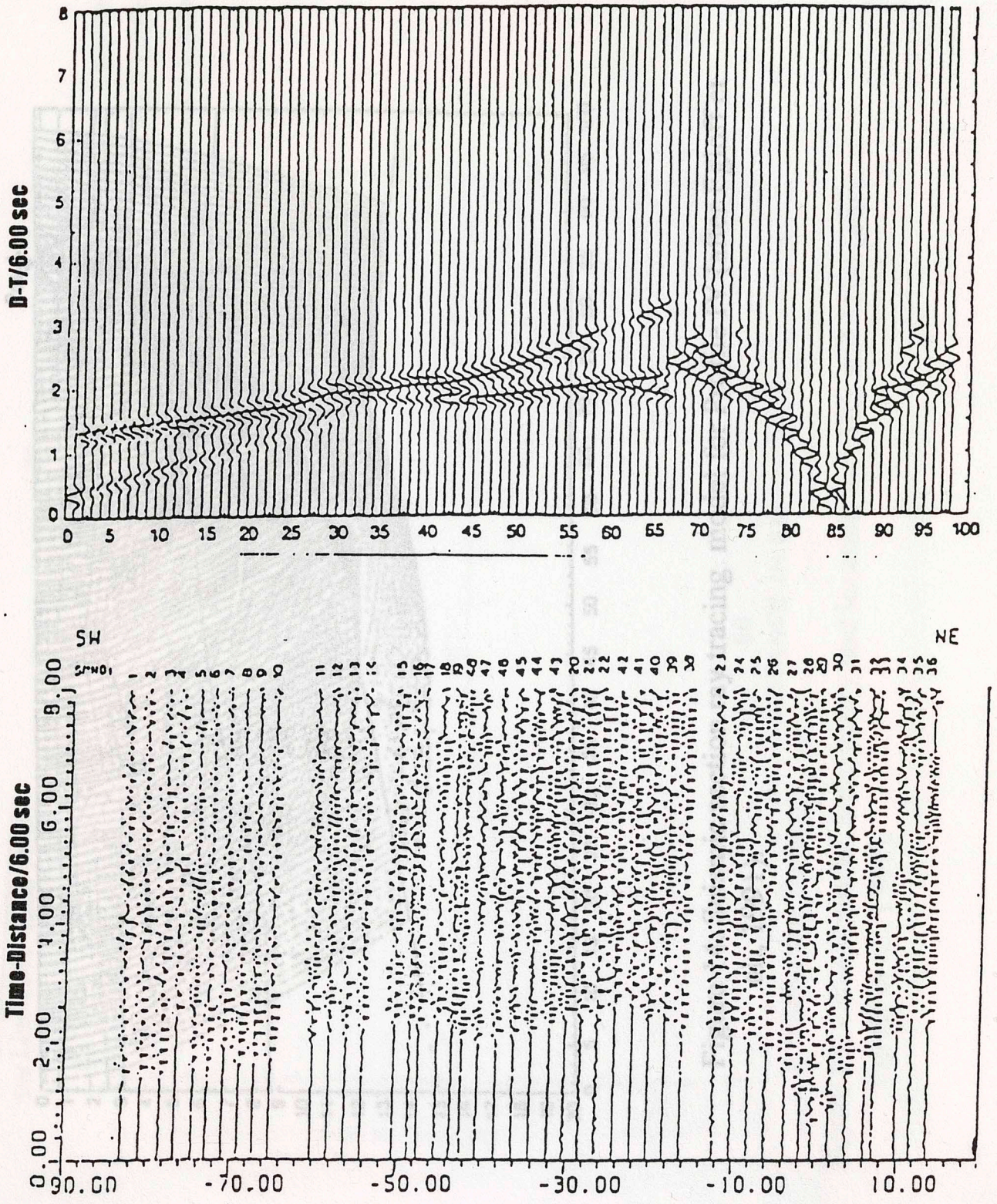

Figure 13. Synthetic seismogram (top) observed seismic section for profile VI (after Egloff et al., 1991).

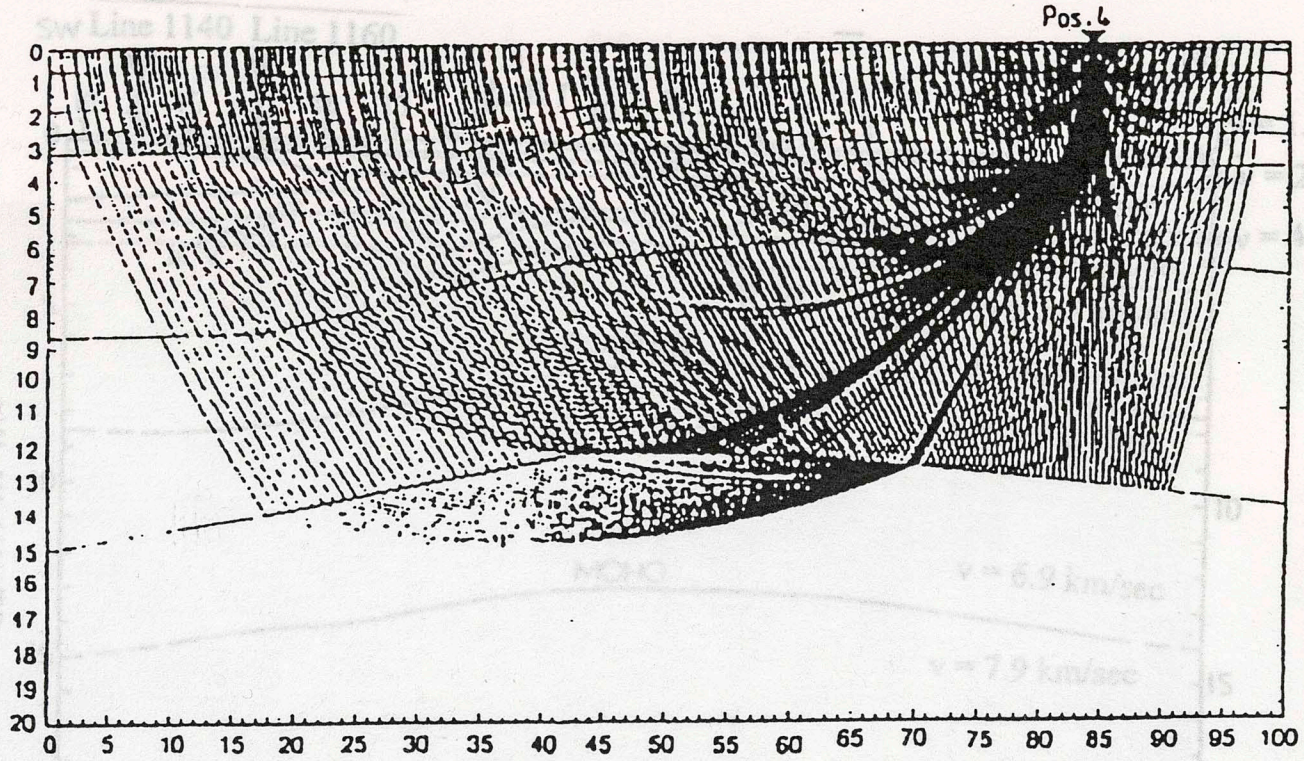

Figure 14. Seismic section ray tracing model for Profile IV (after Egloff et al., 1991).

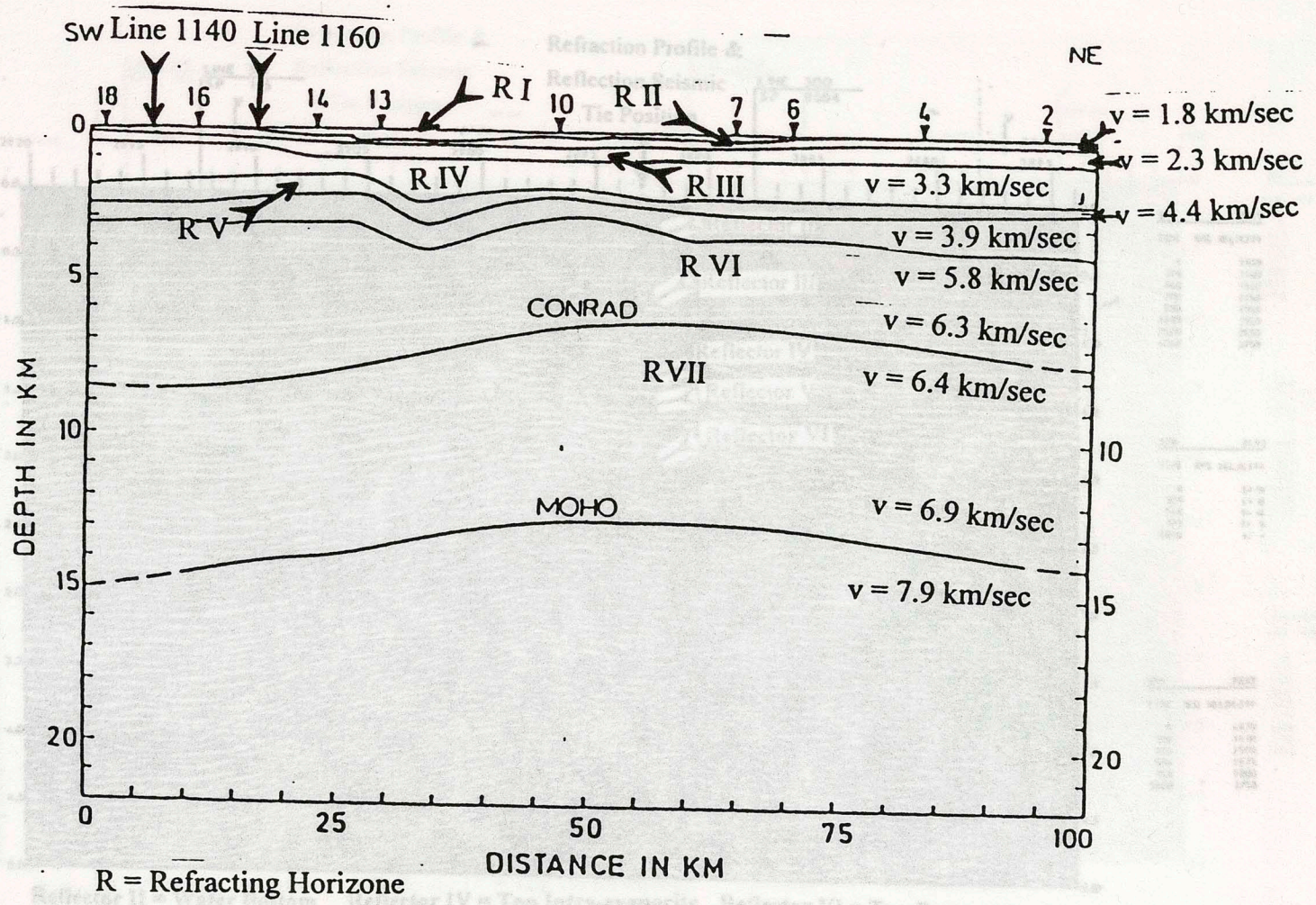

Figure 15. Crustal model, bathymetry and location for OBS and 1160 (after Egloff et al., 1991).

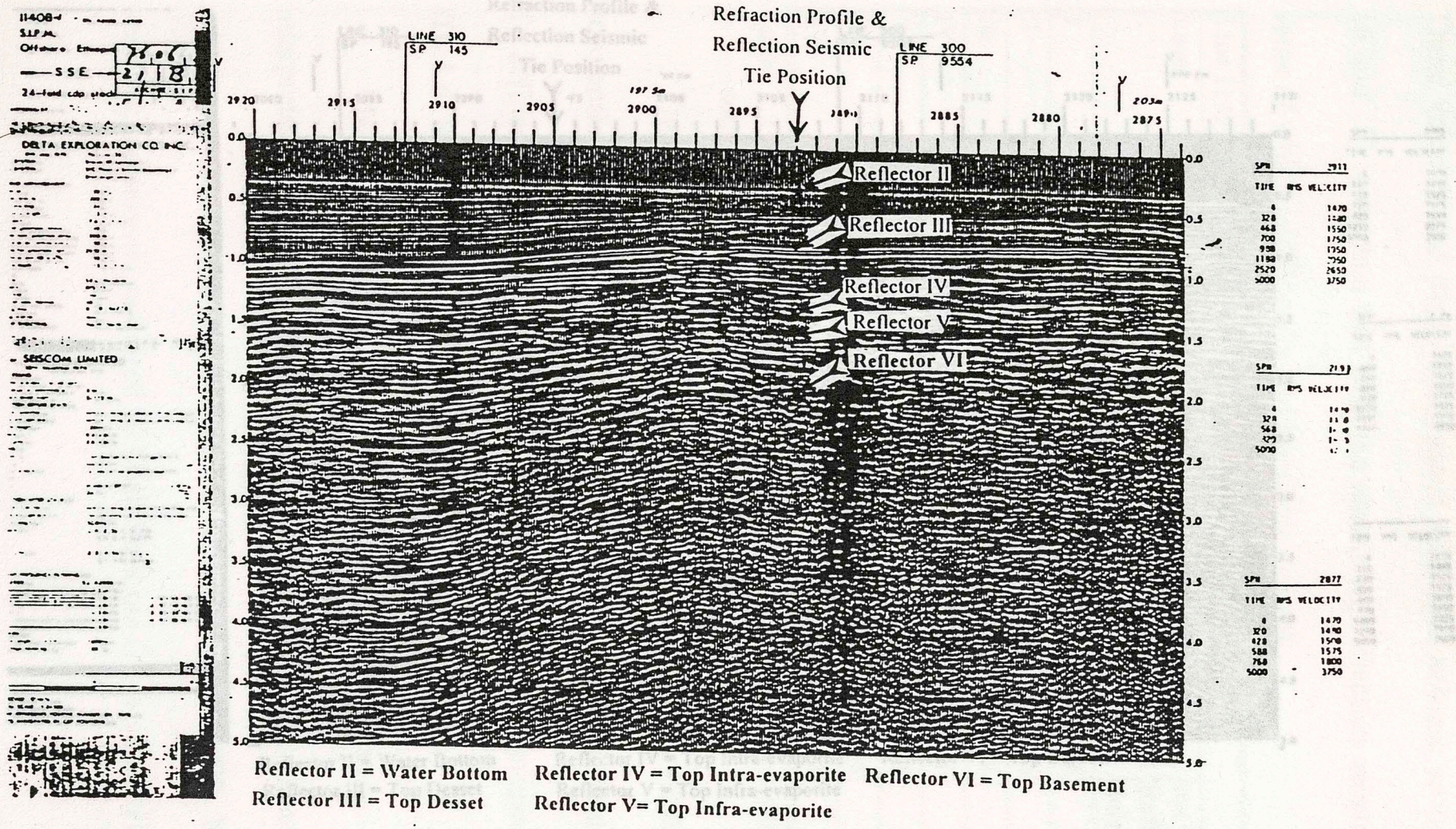

Figure 16. Line 1140 (twt) depth corelated to refraction Profile VI

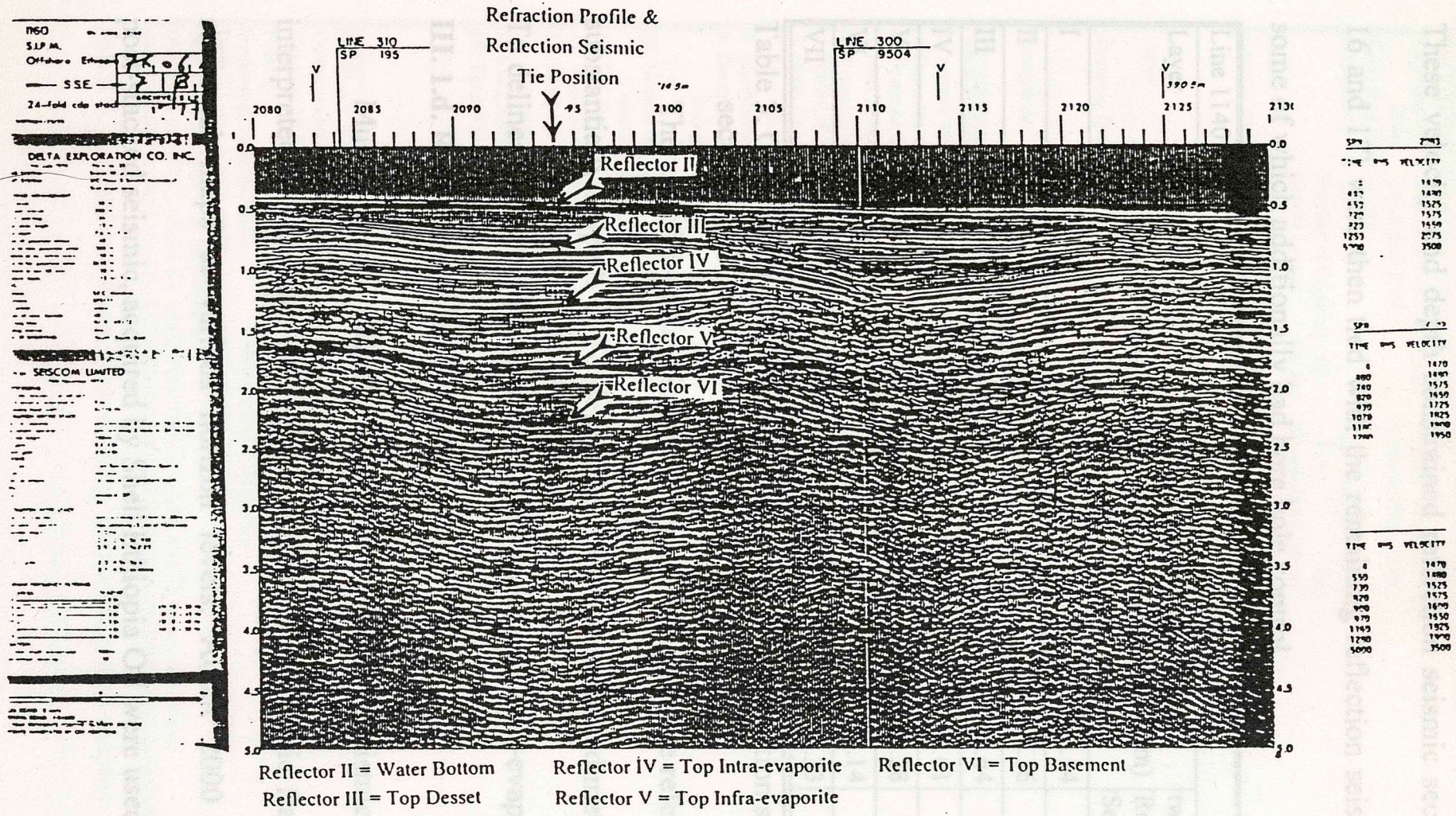

Figure 17. Line 1160 (twt) depth correlated to refraction Profile VI

These velocity and depth constrained reflection seismic sections (Figure 16 and 17) were then tied with the remaining reflection seismic sections, some of which additionally had bore hole control.

Line 1140			Line 1160	
Layer	Depth top Refractor (km)	twt from Reflection seismic (sec)	Depth from Refraction (km)	twt from Reflection Seismic (sec)
I	0	0	0.14	0.2
II	0.25	0.34	0.36	0.49
III	0.64	0.79	0.64	0.79
IV	1.79	1.33	1.61	1.49
V	2.55	1.55	2.28	1.84
VI	3.15	1.99	3.14	2.28
VII	8.61	4.63	8.33	4.95

Table 3. Correlation for refraction profile depth vs reflection seismic sections twt.

The use of the refraction profile in constraining the refection seismic substantially helped: 1) To define the Infra-evaporite sediment top and 2) To delineate the contact between the basement and Infra-evaporite section.

III. 1.d. Reflection Seismic Profiles

Multi-channel industry acquired reflection seismic data were interpreted to construct the regional seismic stratigraphic framework and structural maps at various horizon levels. About 2000 line km of post-stacked seismic, acquired by Shell Ethiopia Oil were used for

RECORDING PARAMETERS SHOT FOR SHELL

Recorded by :	Delta Exploration Co. Inc.	Vessel:	American Delta
Date:	December 1974	Direction Shot :	238
Recording Information:			
Instruments:	DFS-3	Tape Format:	SEG-A
	Number of Channels 62	B.P.I.	800
	Record Length 6.0 sec	Sample Rate	4 ms
Filters:	Low Cut Out	High Cut	62 Hz 18 DB/OCT
Energy Source	Air Gun Array	Shot Depth	7.5 m
	Gun Delay 51.2 ms	Volume	1222 CU. IN
	Pops/Shotpoint 4	Pressure	2000 PSI
	Shot Interval 50 m	Offset to Near Group	350 m
Cable:	Length 2400 m	Cable Depth	15m
	Leading Channel 48	Number of groups	48
Shooting Geometry:			
	Group Interval 50 m	Shot point Interval	200 m
	C.D.P. Interval 25m	Fold of Coverage	48
Navigation:	Primary C.S.l		
	Primary Antenna to Center of Guns 83.2 m		

PROCESSING PARAMETERS

Processed 48 Channel. 24 Fold CDP Stack to 5.0 Seconds

1. Demultiplex and Edit
2. Common Depth Point Gather 24 Fold
3. First Break Suppression Mute
4. Exponential Gain: 3 DB/SEC. 0.0 - 3.0 SEC
5. Spherical Divergence Correction Using Velocities from this Area
6. Static Correction Applied for Gun Delay -51 ms
7. Pre-DMO Velocities Picked every 5 km. from DIGICON'S VELFANS
8. Dip-Moveout Correction Using DIGCON'S "DIPCOGLX" (24 Fold)
9. Deconvolution Before Stack: 120 ms Operator + 32 ms Gap
   Design Gates : Near 0.7 - 3.0 Sec
   Far 2.5 - 4.0 Sec
10. Normal Moveout Correction:
    Velocity Picked Every 1 Km. From DIGON's VELFANS
11. F/K Demultiple Using DIGICON'S "ZMULT" (90% Primary Velocities)
12. NMO Stretch Suppression Mute
13. Static Correction Applied for Source and Streamer Depth + 12 ms
14. Common Depth Stack 24 Fold
15 Chequerboard Noise Attenuation
16. Time Variant Band Pass Filtering

Time (Secs):	Frequency (HZ) /	Slopes (DB/Cycle):
0.0	15 (3) -	65 (1)
1.0	8 (3) -	60 (1)
2.0	6 (3) -	50 (1)

DISPLAY PARAMETERS

Compression Wave Recorded as Negative Number on Tape
Negative Number Plotted as Trough (White)

Polarity	SEG Normal		
Horizontal Scale	1:25000	Vertical Scale	10 cm/Sec
Date	July 1989	BID Number	6855

Shot Point Annotated at Shot Position
Displayed on SEISCHROM II LASER PLOTTER: 300 DPI; 50% Overlap; 125 Micron

Table 4. Reflection seismic recording, processing and display parameters

interpretation. The acquisition, processing, and display parameters are given in Table 4.

III. 2. Stratigraphy

The geology of the southwestern Red Sea records a history of its Cenozoic tectonic evolution. In general basement rocks record pulses of migmatization and metamorphism antecedent to Cenozoic tectonism. The sediments in the region are mainly influenced by a combination of Cenozoic tectonic, halokinetic and eustatic factors. The column of sediments in this area has been subdivided into three major groups by previous workers (Beydoun, 1989; UNDP/World Bank, 1991) based upon their relationship with respect to a hypothesized single rifting event which occurred during the Miocene. These groups are simply: Pre-rift, Syn-rift, and Post-rift sequences (Figure 18). Part of the problem in describing the Red Sea stratigraphy using conventional nomenclature is that the strata have been grouped genetically. That is, they have been subdivided with respect to a singular uniform synchronous rifting event which this paper clearly shows is neither singular nor uniform nor directly correlated to stratigraphy. Therefore, there will be an unfortunate overlap between the tectonic terms: Pre-rift, Syn-rift and Post-rift strata of Beydoun (1989),

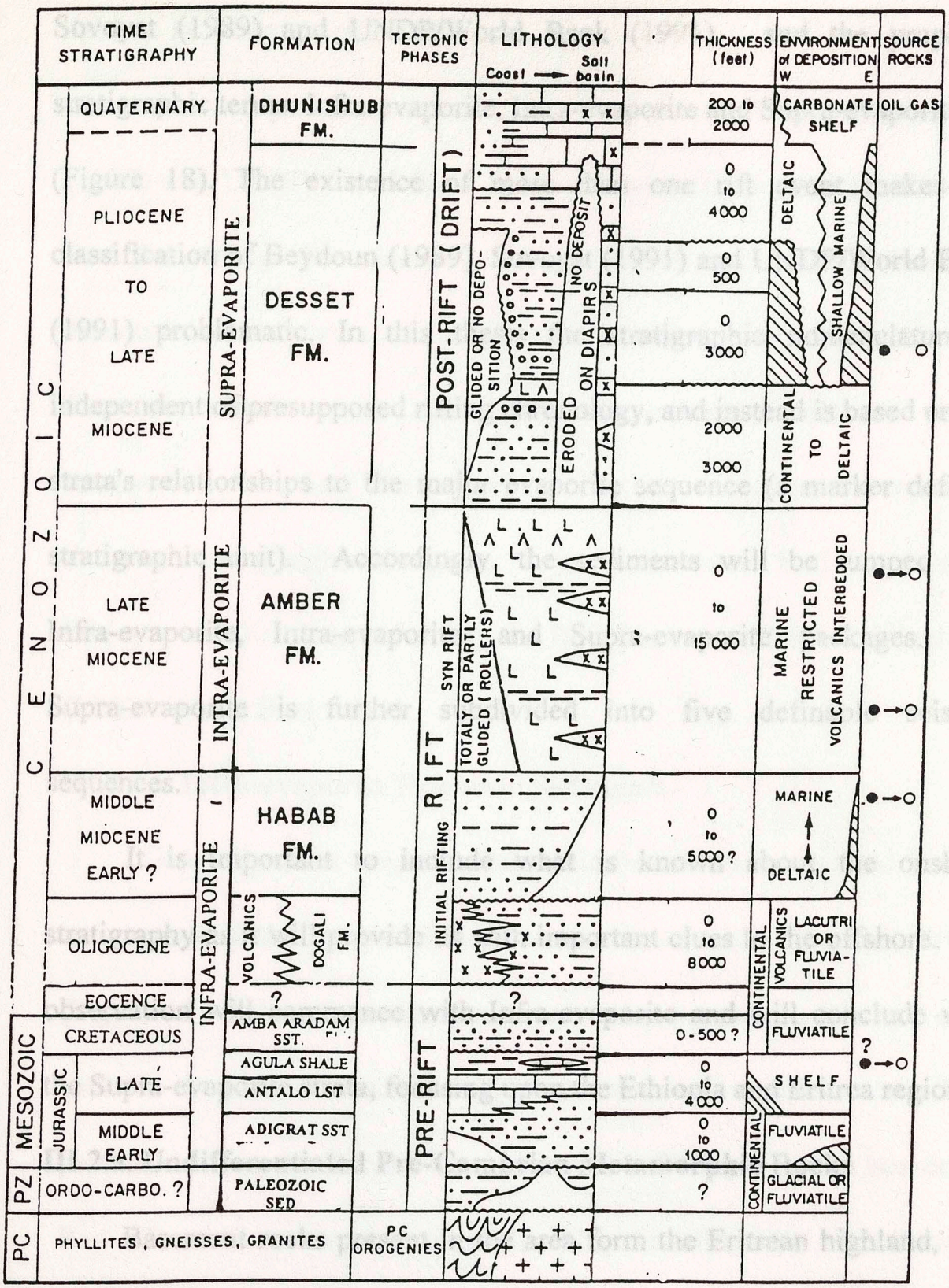

Figure 18. Generalized stratigraphic column for northern Ethiopia. (modified from Sovoyat et al., 1989).

Sovoyat (1989) and UNDP/World Bank (1991), and the proposed stratigraphic terms: Infra-evaporite, Intra-evaporite and Supra-evaporite (Figure 18). The existence of more than one rift event makes the classification of Beydoun (1989), Sovoyat (1991) and UNDP/World Bank (1991) problematic. In this thesis the stratigraphic nomenclature is independent of presupposed rifting chronology, and instead is based on the strata's relationships to the major evaporite sequence (a marker defined stratigraphic unit). Accordingly, the sediments will be lumped into Infra-evaporite, Intra-evaporite, and Supra-evaporite packages. The Supra-evaporite is further subdivided into five definable seismic sequences.

It is important to include what is known about the onshore stratigraphy as it will provide us with important clues to the offshore. Our observation will commence with Infra-evaporite and will conclude with the Supra-evaporite strata, focusing upon the Ethiopia and Eritrea region.

III.2.a. Undifferentiated Pre-Cambrian Metamorphic Rocks

Basement rocks present in the area form the Eritrean highland, and part of the Danakil Alps. They are composed of intermediate to low grade metamorphic rocks and deformed granites (Mohr, 1971).

III.2.b. Infra-evaporite Rocks

According to the previous works by Beydoun (1989), Sovoyat et al. (1989) and UNDP/World Bank (1991) these rocks predate the Cenozoic Red Sea rifting. The observed Infra-evaporite rocks include Paleozoic, Mesozoic sedimentary rocks and Cenozoic coastal plain rock onshore, and Cenozoic clastic rocks underlying the evaporite offshore in the southwestern Red Sea. The Infra-evaporite rocks are generally exposed in the neighboring highland regions of the southwestern Red Sea (northern Ethiopia and Eritrea), and along the Red Sea coast (Eritrea) (Figure 19) (UNDP/World Bank 1991) .

III.2.b.i. Infra-evaporite Paleozoic Sediments

Generally Infra-evaporite Paleozoic Sediments in the Red Sea area are exposed at the margin of the escarpment and within the Danakil Alps (Figure 15). Paleozoic sediments have not been penetrated in any of the wells in the project area. Overall, these rocks are exposed in the Tigrai province and in the Danakil Alps of northern Ethiopia which boarder the Red Sea. These rocks unconformably overlie the Pre-Cambrian metamorphic rocks. The rocks are of two kind: a) a tillite facies (Edaga Arbi Glacial), and b) a sandstone to micro-conglomerate (Enticho

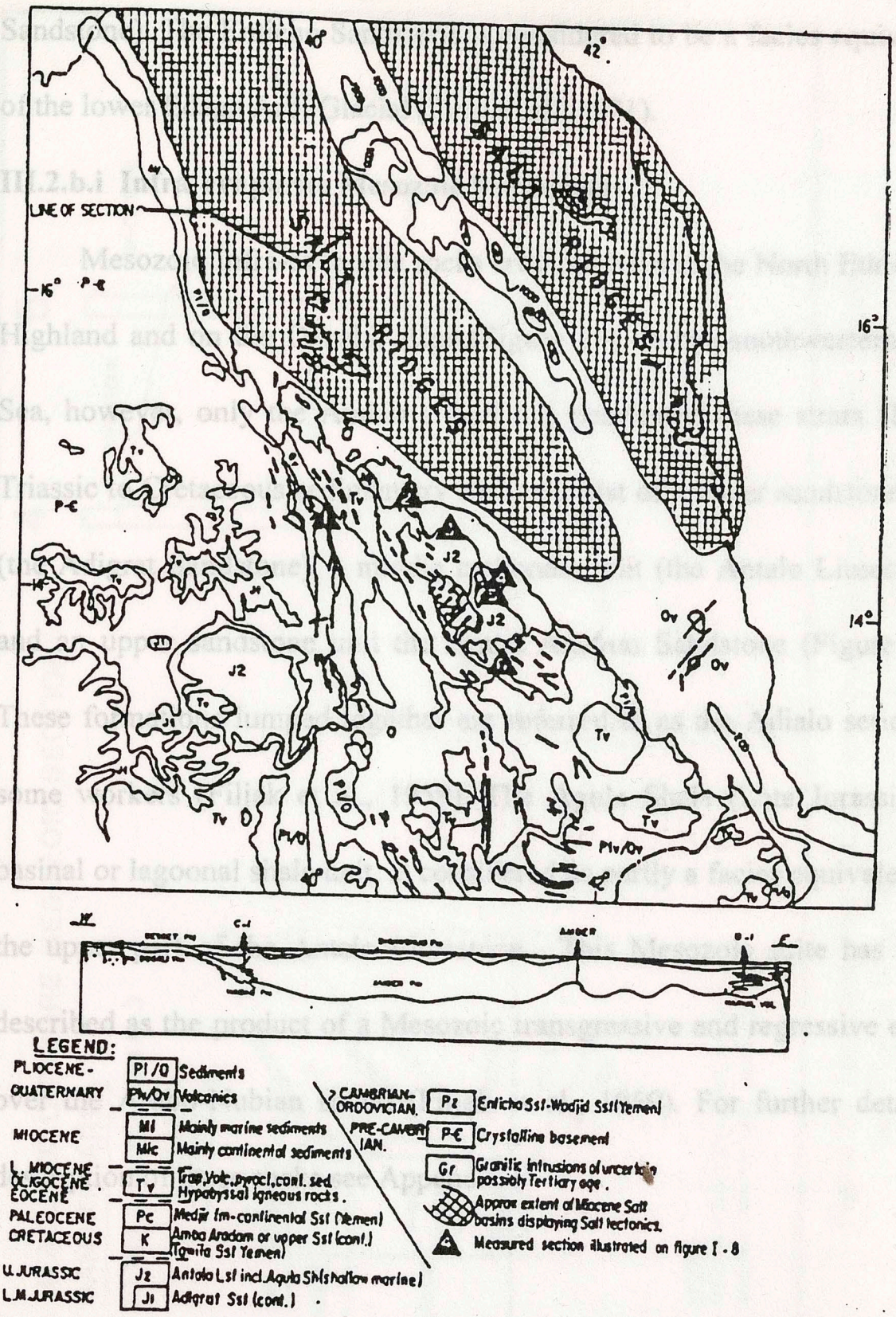

Figure 19. geologic map of northern Ethiopia, with offshore evaporite distribution of the Ethiopian Red Sea (modified from Hutchinson, 1972)

Sandstone). The Enticho Sandstone is considered to be a facies equivalent of the lower Edaga Arbi Glacial (Dow et al., 1971).

III.2.b.i Infra-evaporite Mesozoic Sediments

Mesozoic Infra-evaporite rocks crop out both in the North Ethiopian Highland and on the Danakil Alps (Figure 19). In the southwestern Red Sea, however, only the Amber-1 well has penetrated these strata. These Triassic to Cretaceous sedimentary rocks consist of a lower sandstone unit (the Adigrat Sandstone), a middle carbonate unit (the Antalo Limestone) and an upper sandstone unit the Amba Aradam Sandstone (Figure 20). These formations lumped together are referred to as the Adialo series by some workers (Filjak et al., 1959). The Agula Shale (Late Jurassic), a basinal or lagoonal shale unit, is considered as partly a facies equivalent of the upper part of the Antalo Limestone. This Mesozoic suite has been described as the product of a Mesozoic transgressive and regressive event over the Arabo-Nubian shield (Filjak et al., 1959). For further detailed description of these rocks see Appendix I

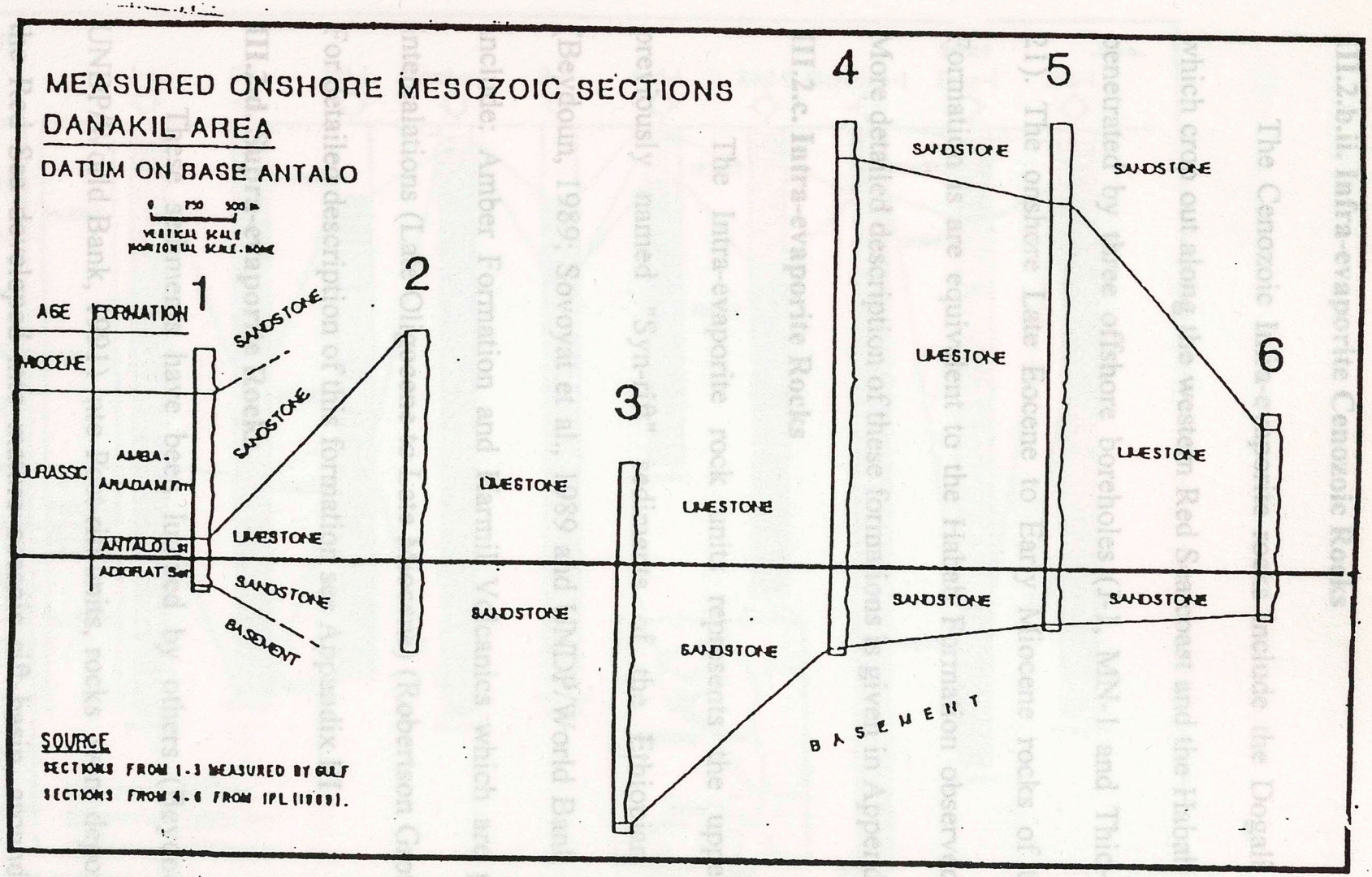

Figure 20. Measured Mesozoic sections from Danakil Area, North Ethiopia (see Figure 19 for location). (source IPL internal inter-office report, 1989 and Gulf Oil unpublished report).

III.2.b.ii. Infra-evaporite Cenozoic Rocks

The Cenozoic Infra-evaporite rocks include the Dogali Formation which crop out along the western Red Sea coast and the Habab Formation penetrated by three offshore boreholes (J-1, MN-1 and Thio-1) (Figure 21). The onshore Late Eocene to Early Miocene rocks of the Dogali Formation is are equivalent to the Habab Formation observed offshore. More detailed description of these formations is given in Appendix II

III.2.c. Intra-evaporite Rocks

The Intra-evaporite rock units represents the upper part of previously named "Syn-rift" sediments of the Ethiopian Red Sea (Beydoun, 1989; Sovoyat et al., 1989 and UNDP/World Bank 1991) and include: Amber Formation and Harmil Volcanics which are present as intercalations (Late Oligocene to Late Miocene) (Robertson Group, 1991). For detailed description of this formation see Appendix III

III.2.d. Supra-evaporite Rocks

These sediments have been lumped by others (Beydoun, 1989; UNDP/World Bank, 1991) into Post-rift units, rocks were deposited after the Red Sea developed into mature oceanic rift basin, around the Late Miocene to Pliocene. These sediments are Pliocene to Recent in age. In the

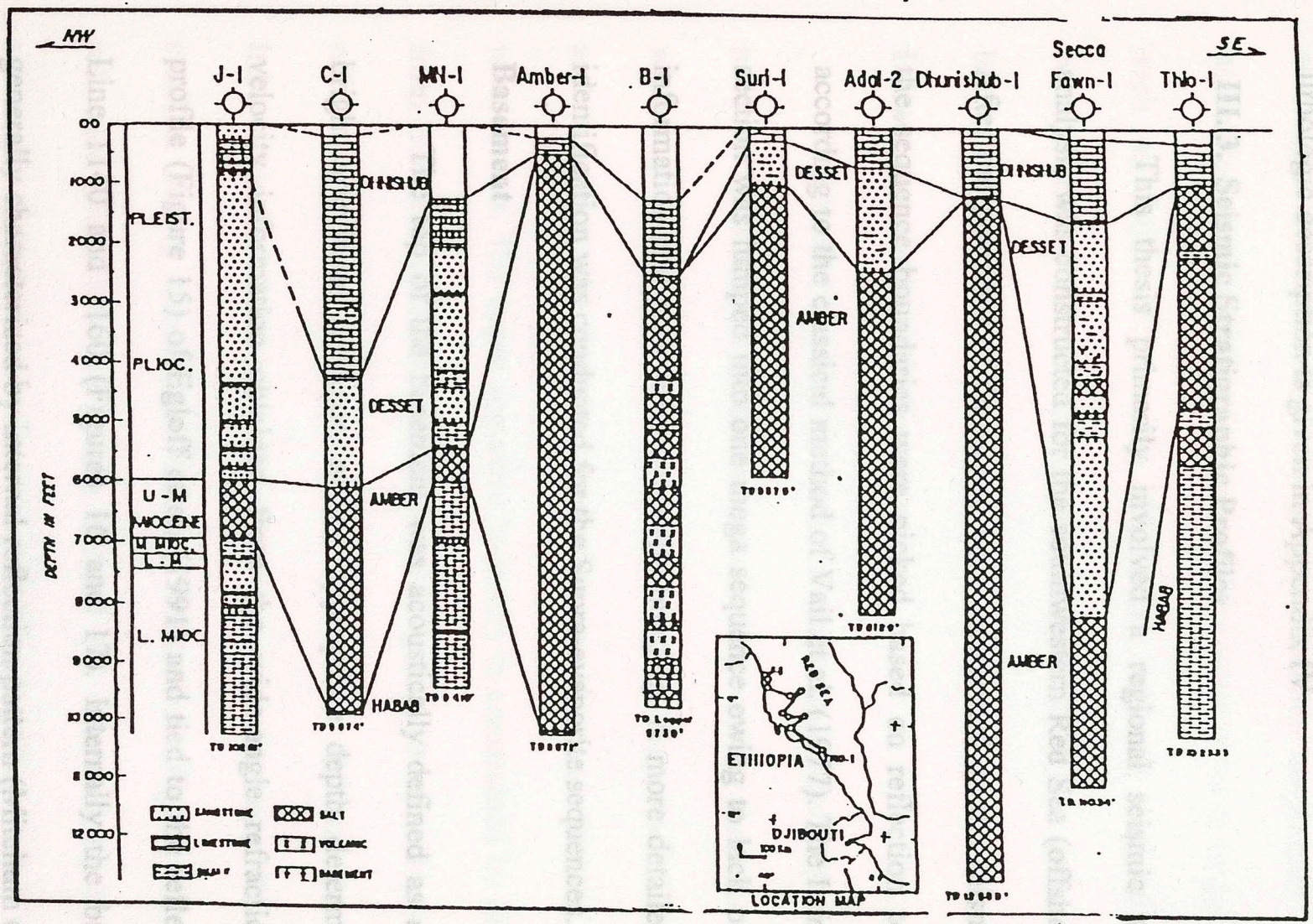

Figure 21. Condensed borehole lithologic column for Ethiopian Red Sea (for location of wells see Figure 2.) (source UNDP/World Bank, 1991).

offshore the Supra-evaporite is represented by the Desset and Dhunishub formations. Onshore, only the Desset Formation is represented. Detailed lithologic description is given in Appendix IV

III. 3. Seismic Stratigraphic Profiles

This thesis primarily involved a regional seismic stratigraphic analysis was constructed for the southwestern Red Sea (offshore Eritrea). After the positions of faults had been interpreted on the seismic sections the sequence boundaries were picked based on reflection terminations according to the classical method of Vail et al. (1977). The Infra-evaporite section was lumped into one mega sequence owing to lack of borehole information and poor Infra-evaporite imaging. A more detailed sequence identification was conducted for the Supra-evaporite sequences.

Basement

The top of the basement was acoustically defined as a generally bright amplitude reflector, at the appropriate depth determined from velocity information obtained from the wide-angle refraction seismic profile (Figure 15) of Egloff et al. (1991) and tied to the reflection lines Line 1140 and 1160 (Figures 16 and 17). Internally the basement is generally characterized by internal reflection pattern (Mitchum et al., 1977

and Roksandic`, 1978) varying from reflection free to chaotic. Strong reflection amplitudes are observed in the basement where the overlying sediments are characterized by strong reflection amplitudes. Structure associated seismic diffractions commonly occur close to major structures such as faults (Figure 22). However, chaotic internal reflection configurations with diffractions (Roksandic`, 1978) also occur within the basement beneath horst blocks.

Infra-evaporite Seismic Sequence

The basal boundary of the Infra-evaporite sequence (the basement reflector by definition) was interpreted using velocity data obtained from wide-angle refraction survey (velocity of Infra-evaporite 3.2 km per sec. and basement 4.4 km per sec) (Figure 15), and from reflection terminations. The upper sequence boundary is constrained by information from borehole synthetic seismograms (Figures 10 and 11), wide-angle refraction velocity data (velocity of evaporite 2.3 km per sec and Infra-evaporite 3.2 km per sec), and reflection terminations. This sequence exhibits strong continuous internal reflections (Figure 22). Internal reflection characters are poorly defined (or featureless) beneath the salt-swells and salt-domes. Simple layered parallel (Roksandic`, 1978)

Figure 22. Southern Red Sea Regional Seismic Transect (for location see Figure 12.)

reflections are common, and in some places reveal a layered reflection patterns with complex layered or cross layered (Roksandic`, 1978) reflection patterns (see Figure 22). Chaotic reflection configurations (Roksandic`, 1978) are also common in this sequence (see Figure 22).

Intra-evaporite Seismic Sequence

The Intra-evaporite sequence varies greatly in thickness as well as in internal reflection amplitude and configuration. The thickness variation in the evaporite sequence ranges from 0.0 sec. to 1.5 sec twt (Figure 22). The evaporite laps out proximal to the axial trough, leaving the axial trough covered only by younger Supra-evaporite sequences (Figure 22). The greatest thicknesses (up to 1.5 seconds twt) occur on the tops and flanks of horst blocks (see Figure 22) in the central part of the western flank. The reflection amplitude varies from strong to very weak (Figure 22). Strong reflection amplitudes in the Intra-evaporite sequence are observed around the basin margin and within grabens. In contrast, weak reflection amplitudes are observed mainly on the flanks and tops of horst blocks. Salt domes and salt swells above horst are internally characterized by weak reflection amplitude. Simple layered parallel reflection configurations are characterized by strong reflector amplitude (Figure 22). Regions exhibiting

weak reflection amplitude have clear to chaotic reflection configurations. In other areas this sequence shows internal reflection configurations of clear to chaotic-reflection configurations with diffraction (Figure 22).

Supra-evaporite Sequences

Seismic reflection images of the Supra-evaporite sequences are of better quality than images of the deeper noisier sequences. These sequence boundaries are tied to well logs and show excellent character correlation. Because only sparse well control is available the detailed seismic facies description and classification is based upon reflection seismic interpretation was conducted. Based on the well information the first four sequences from bottom upwards are siliciclastic, the top sequence is carbonate. The clastic Desset Formation was subdivided into four sequences, referred to as the Desset I to IV sequences. The carbonate Dhunishub Formation is referred to as the Dhunishub sequence (Figure 22).

The Desset I to IV sequences show strong reflection amplitude. Internal reflection configurations in these sequences are simple layered horizontal or oblique (Figure 22). Downlap towards the basin margin is common within these sequences. A basinward downlap against tilted

sediment raft dipping away from the basin is observed over the monoclinal ramp (Figure 22). Termination of high angle dip reflectors are very common, particularly around salt swells and salt domes. In some of the sections the sequences show vertical change in internal reflection amplitude. Convergent parallel reflectors downlapping against tilted sequences are observed (Figure 22). Overall, internal reflection is stronger in the lower sequences than in the top sequences. The lower sequences (Desset I, II and III) are highly compartmentalized and show significant erosional truncation. This erosional truncation is clearly marked by the reflection termination, particularly in Zones II and III of the area (Figure 12).

The Dhunishub sequence is bounded at the base by a regional unconformity and at the top by the sea floor bottom. This sequence exhibits strong reflection amplitudes, with a simple parallel reflection configuration. This sequence shows little variation in thickness reflection amplitude, and reflection configuration.

III.4. Structure

III. 4.a. Structural Styles from Seismic Sections

A seismic structural interpretation on nineteen dip and nine strike lines of the southern Red Sea (offshore Eritrea) reveals complex structural styles. The structures observed indicate the presence of both extensional and wrench faults. The Project Area can be divided into four discrete zones or structural provinces (Figure 12) based upon their differing structural styles.

The observed major structural zones are: axial trough (Zone I), en-echelon tilted block province (Zone II), symmetrical horsts and grabens province (Zone III) and the downwarped rift flank (Zone IV) (Figure 12). These zones exhibit different fault systems: basinward dipping step faults, en echelon tilted block faults, high-angle symmetrical block faults, rift-margin parallel step faults, counter regional faults, listric faults, halokinitic associated faults and wrench faults. For the purpose of expressing non listric fault plane dip, the following terminology will be employed. For those fault planes with dip angles exceeding 60^0: high-angle, for those fault planes with dip angles between 30^0 and 60^0:

moderate-angle, and for those fault planes with dip angles less than 30^0: low-angle.

Basinward Dipping Step Fault Systems

These faults are basinward dipping step forming parallel faults, with high-angle dips (Figure 22). They have significant vertical throw (up to 0.5 second twt) and form the escarpment of the axial trough. The faults penetrate the thin sediment veneer into the underlying oceanic crust. The sediments dip basinward and form a stair like succession.

En Echelon Tilted Block Fault Systems

The faults bounding these blocks dip basinward. The rotated blocks dip away from the basin (Figure 22). The faults have moderate to high angle dip angles, throws up to 0.7 seconds twt (average 0.5 seconds twt) and lateral displacement (offset Sepencer (1969)) up to 2.4 kms (1.5 miles) (Figure 22). Numerous secondary pocket basins have developed which are separated by the apexes of the tilted blocks. A wide spread erosional truncation that characteristically clips the apexes of the tilted blocks is observed. The lower section of these pocket basins is filled with sediments which on-lap the block. Blocks proximal to the flank of the axial trough show a general rise in topography.

High-angle Symmetrical Block Fault Systems

These fault blocks generally occur in the central part of the basin within Zone III (Figure 18). The faults exhibit large throw (up to 1.1 second twt), and moderate lateral displacement (offset) more than 500 meters (Figure 22). These structural styles form alternating horsts and grabens that are bounded by high-angle normal faults. Sediments layers are horizontal to sub-horizontal in dip. These high angle symmetrical block fault systems include the basement, the Infra-evaporite, the Intra-evaporite and the Supra-evaporite sequences, and thus post-date the initial mechanical extension during the first rifting peak.

Rift-margin Parallel Step Faults Systems

These parallel normal step faults border the symmetrical horsts and grabens Zone III and form a gentle basinward dipping monoclinal ramp in Zone IV. This structural style generally occurs on the flanks of the basin (Figure 22). The faults dip basinward at a high-angle. Throw is moderate to small (up to 0.1 seconds twt), and lateral displacement (offset) is small (about 200 meters). This structural system is interrupted by a horst block that marks a transition from the downwarped rift flank zone to the symmetric horsts and grabens zone. The step faults are commonly

restricted to the units underlying the evaporite sequence. Only rarely do these faults extend into the Supra-evaporite sequences.

Counter Regional Dipping Faults

An elongate counter regional fault system extends from the border horst block of the symmetric horsts and grabens zone into the downwarped rift flank zone (Figure 22). Generally these faults dip away (counter regionally) from the basin, have a high dip angle near the surface that flattens with depth and soles at the base of the evaporite sequence, not extending into the underlying Infra-evaporite sequences.

Basinward Dipping Listric Faults

These faults general occur over the downwarped rift flank zone (Zone IV) and commonly are associated with the mass withdrawal of the salt. These listric faults dip basinward with antithetic faults terminating against their major fault planes. The listric faults have a high dip angle at the top which flattens with depth. The flat fault plane extends for a considerable distance and a number of anastomosing listric faults are blind at the base. Some of these listric faults turn into salt welds in areas where the salt is squeezed out to the surrounding area (Figure 22).

High-Angle Fault Systems Associated with Halokinesis

High angle faults generally striking NW, associated with halokinesis occur within the Supra-evaporite sequences, specifically on top of salt swells and piercements (Figure 22). Displacement on these faults is largely controlled by the extent of salt movement. Substantial vertical (up to 0.5 second twt) as well as horizontal displacement along fault planes is observed in areas of extensive salt mobilization (halokinesis). The highest concentration of these fault systems are observed in the central part (Zone III) of the basin associated with the high-angle symmetrical block fault system.

III.4.b. Subsurface Structure

A series of subsurface structural maps for base of the evaporite the southwestern Red Sea were constructed for the top of the basement, top of the Infra-evaporite and the top Intra-evaporite. The maps cover an area of approximately 25000 sq. km, between 14^0 20' to $15^0$20' latitudes and $40^0$20' $42^0$00' longitudes. These maps are based on information from the interpreted reflection seismic. The contour values are in seconds twt.

Top Basement Structure

Structure on top of the basement (Figure 29) reveals the presence of structural zonation which can be divided into four distinct structural zones, based on the intensity of extensional tectonism and associated structural styles. From the axial trough to the flank of the basin, the four structural zones are Zone I, Zone II, Zone III and Zone IV (Figure 12).

Although, Zone I (Figure 12) structures are not shown on the structure map owing to the absence of continental crust basement, instead this zone is covered by volcanic new oceanic crust of 5 ma. However, as observed on seismic sections structures in Zone I are high-angled basinward dipping parallel step fault systems.

Zone II (Figure 12) is characterized by an en echelon tilted block fault system. These faults generally trend in the NW-SE direction, with associated major synthetic faults trending in a NNW-SSE direction. Minor associated antithetic faults dip outward from the basin (Figure 23). In this zone strata of tilted blocks dip away from the basin as is indicated by an increase in the contour values to the foot of the fault. This asymmetrical fault throw is marked by development of a series of half grabens.

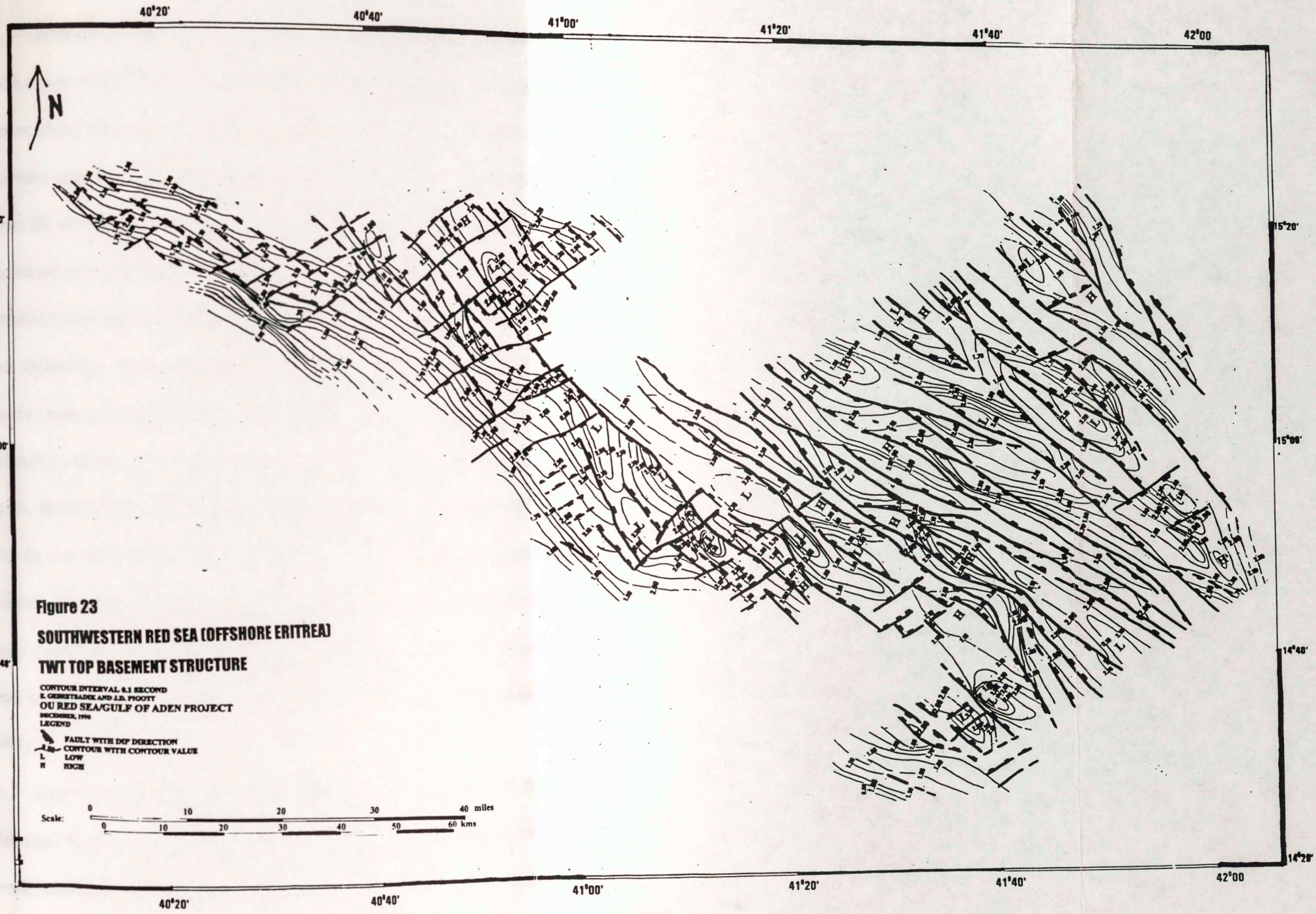

Figure 23

SOUTHWESTERN RED SEA (OFFSHORE ERITREA)

TWT TOP BASEMENT STRUCTURE

Zone III is represented by a number of parallel horsts and grabens with a general NW-SE trend. These horsts and grabens have a symmetrical throw along their bounding faults, and form a series of high-angle fault bounded sub-rifts, separated from each other by a series of horst blocks. Zone III, exhibits increasing structural complexity at a local scale. In this structural zone, the number of antithetic and synthetic faults increases. The antithetic and synthetic fault trends are complex in Zone III. The sub-rifts are segmented, and the geometry of the rift segments (Morley, 1995) varies widely within the area. The more common rift segment features geometry includes: rift-gap and rift-jump. Rift-gaps are dominant in the south, faulted rift-jumps (Morley, 1995) are common to the north (Figure 23). In the far North, extensive development of faulted rift-jumps has produced rhombic blocks (Figure 23). In the South individual sub-rifts show change in depth from very deep close to the foot of the bounding fault to shallow surface (flexural margin), forming strike ramps (Morley, 1995).

Zone IV fault systems mainly dip basinward and trend in a NW-SE direction. In this zone the blocks also dip basinward as highlighted by the gentle basinward increase in contour values (Figure 22). Secondary fault

systems are not observed. This zone forms a basinward dipping monoclinal ramp that shallows toward the basin flank. Because seismic coverage for this zone is missing in part, it is not mapped in its entirety.

Top Infra-evaporite Structure

Structural styles and features on the top of the Infra-evaporite generally parallel the structure of the underlying basement (Figure 24). However, the structural complexity observed in the basement decreases in the Infra-evaporite, some of the faults do not extend to the base of the evaporite and the magnitude of their displacement is less.

Structure on Top of Intra-evaporite

Structure on this horizon generally mimics the major underlying structural features yet filters out the older minor structures and some of the older major structures beneath (Figure 25). In Zone I, II, and III, most of these older structures are expressed. The structural trend (NW to SE) and styles exhibited are the same as that observed on the underlying horizons. There are local minor structural modifications are the result of halokinasis. The structures on top of the Intra-evaporite: high-angle fault systems associated with halokinesis, counter regional dipping fault systems and

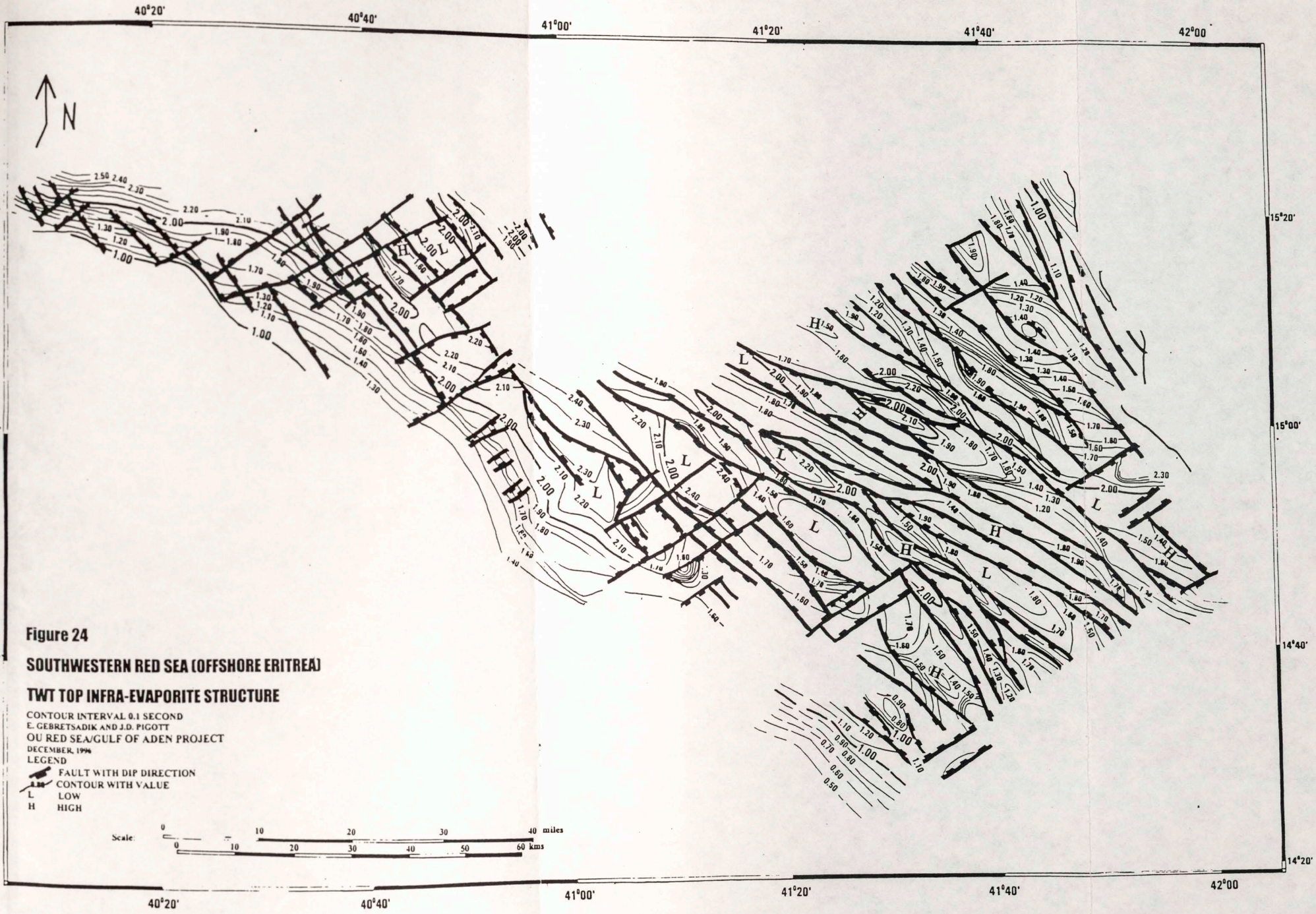

Figure 24

SOUTHWESTERN RED SEA (OFFSHORE ERITREA)

TWT TOP INFRA-EVAPORITE STRUCTURE

CONTOUR INTERVAL 0.1 SECOND
E. GEBRETSADIK AND J.D. PIGOTT
OU RED SEA/GULF OF ADEN PROJECT
DECEMBER, 1996
LEGEND
FAULT WITH DIP DIRECTION
CONTOUR WITH VALUE
L LOW
H HIGH

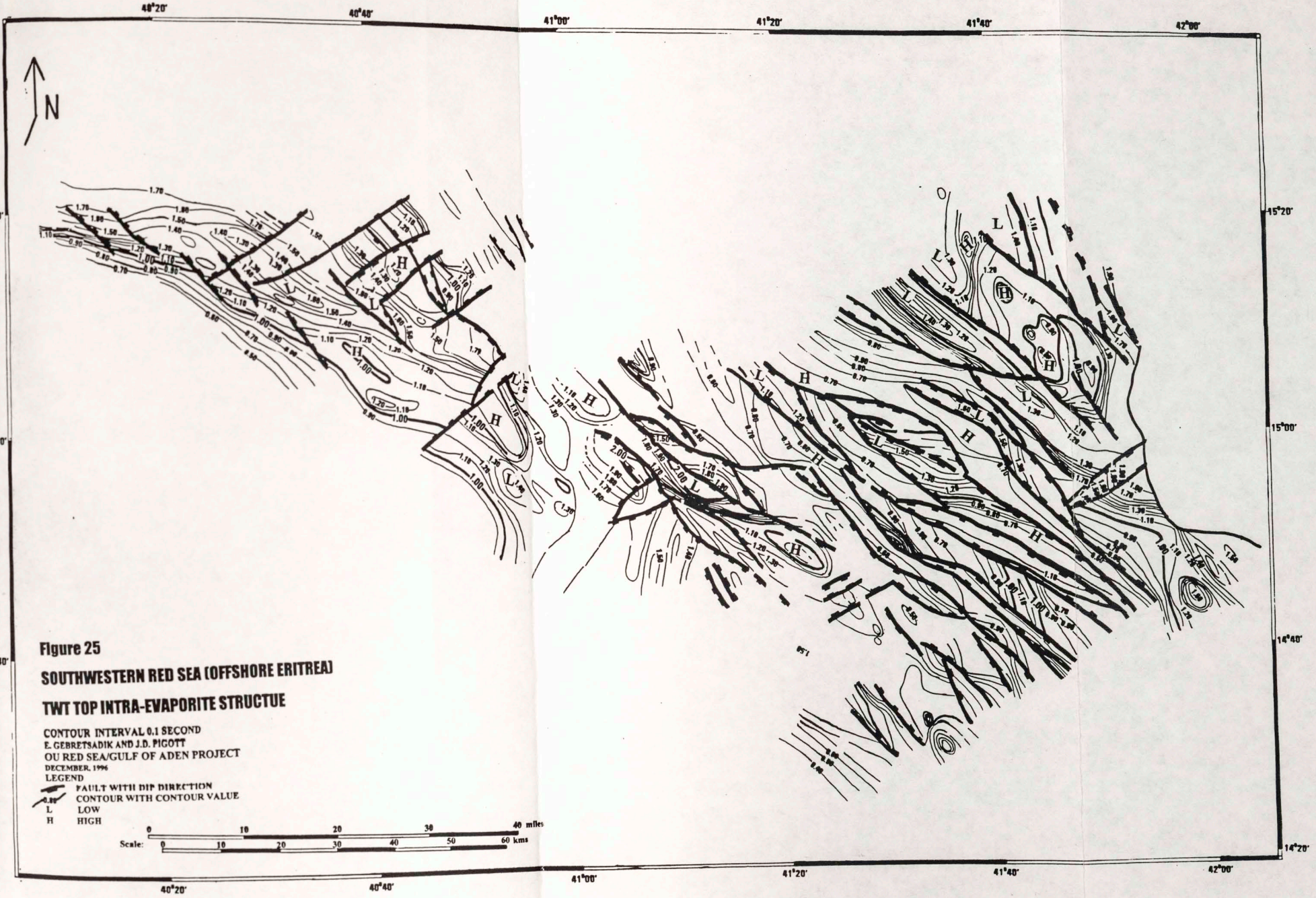

Figure 25

SOUTHWESTERN RED SEA (OFFSHORE ERITREA)

TWT TOP INTRA-EVAPORITE STRUCTUE

CONTOUR INTERVAL 0.1 SECOND
E. GEBRETSADIK AND J.D. PIGOTT
OU RED SEA/GULF OF ADEN PROJECT
DECEMBER, 1996
LEGEND
FAULT WITH DIP DIRECTION
CONTOUR WITH CONTOUR VALUE
L LOW
H HIGH



Figure 26

SOUTHWESTERN RED SEA (OFFSHORE ERITREA)

TWT INTRA-EVAPORITE ISOCHRON

CONTOUR INTERVAL 0.1 SECOND
E. GEBRETSADIK AND J.D. PIGOTT
DECEMBER, 1996
LEGEND
0.80 CONTOUR WITH CONTOUR VALUE

basinward dipping listric faults occur mainly in Zones III and IV (Figure 22 and 26), where salt mobilization was extensive.

III.5. Sequence Stratigraphy (Intra-evaporite Isochron)

The Intra-evaporite sediment thickness as measured vertically in time from multi-channel reflection seismic sections was contoured. The contour interval is 0.1 second, and the interval isochrons range from 0 to 1.3 seconds (Figure 22 and 27). The evaporite sediment distribution is considerably variable within the basin (Figure 27). The thickest evaporite accumulation occurs in the central structural zone (Zone III). The evaporite sediment sequence is absent in Zone I. Zone IV has its thickest evaporite section close to Zone III. However, the evaporite section is missing at the western margin of Zone IV (basin flank). Even within a single zone, evaporite thickness can vary. For example, a very thick (up to 1.3 seconds) section is observed on top of Infra-evaporite highs (Figure 22). In contrast, within Infra-evaporite grabens, the thickness is less (as low as 0.1 seconds). The evaporite thickness distribution also tends to follow the regional structural trend (NW-SE), with isolated thick evaporite islands, co-aligned in a well defined trend. The top Infra-evaporite structure significantly affected the Supra-evaporite sedimentation. Areas of thick

evaporite accumulation are characterized by thin Supra-evaporite sedimentation, and extensive erosional truncation of these sediments (Desset I to IV Sequences) indicates salt flowage contemporaneous with post-salt deposition. In contrast, areas of thin evaporite accumulation (salt withdrawal) are characterized by thick Supra-evaporite deposition (Figure 22).



Figure 27. a) Unprocessed condenced reflection seismic section of Line 435E. b) Magnified part of a.

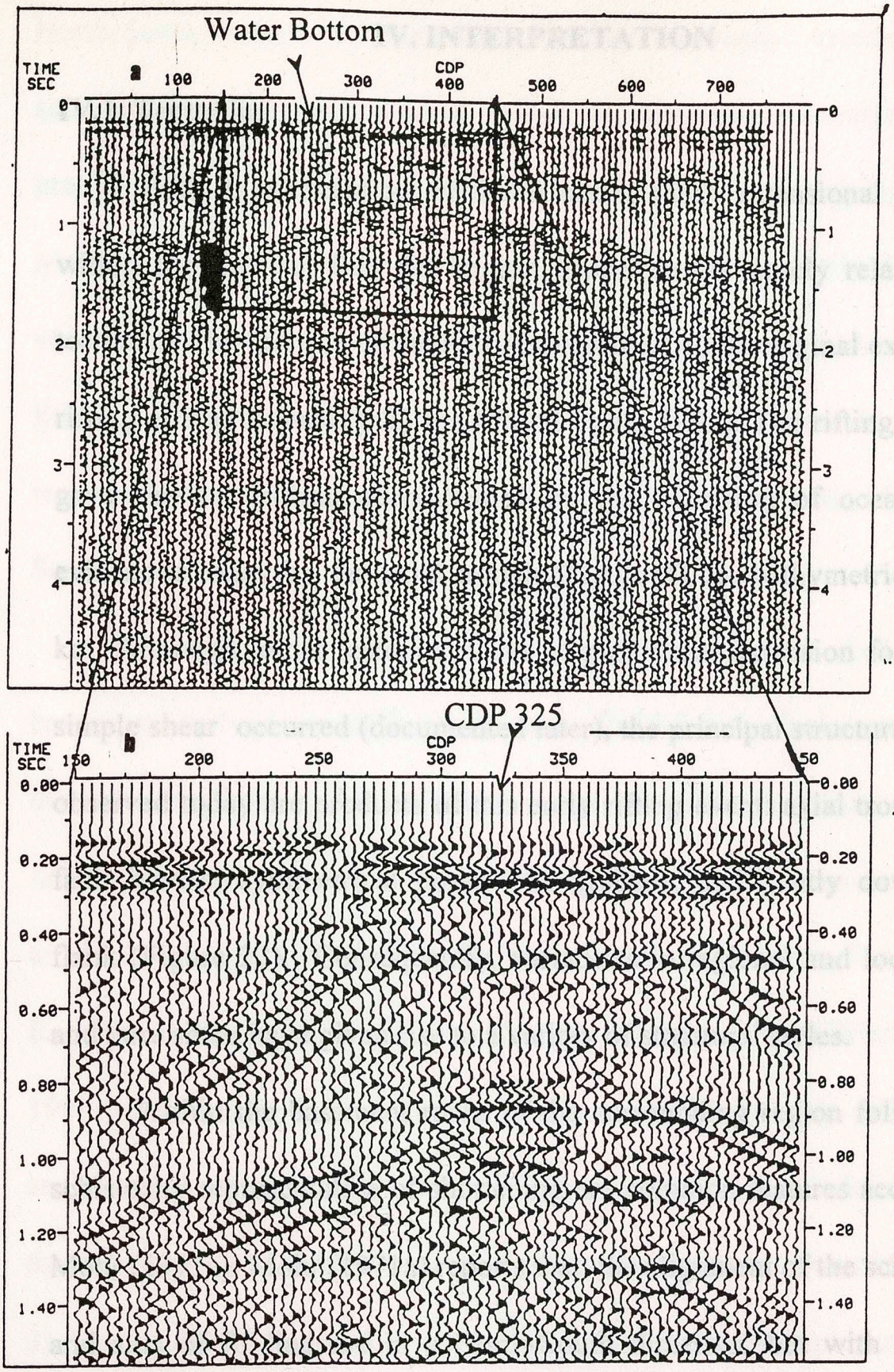

Figure 27. a) Unprocessed condenced reflection seismic section of Line 435E. b) Magnified part of a.

IV. INTERPRETATION

IV.1. Tectonics

With the exception of halokinesis, most extensional structures within the Eritrean Red Sea region appear to be closely related to rift tectonics. This portion of the Red Sea commenced its original extension or rifting at approximately 25 ma (Pigott et al., 1995). The rifting gradually gave rise to drifting accompanied by the extrusion of oceanic crust, evidenced today by the axial trough (Figure 3) the bathymetric low >. 2 km. Although, other tectonic pulses of pure shear extension followed by simple shear occurred (documented later), the principal structural features observed today are products of this early rifting event: axial trough, tilted fault blocks, symmetrical horsts and grabens, and gently downwarped flank (Figure 22). Consequently, variations in regional and local simple and pure shear have given rise to a variety of structural styles.

Within the basement rocks of the surrounding region foliation and schistosity representative of shortening are common features according to Mohr (1971a). Mohr (1971a) reports that the alignment of the schistosity and axis of folding are in a North-South direction, but with a marked clockwise divergence to northeast-southwest in Tigrai. In Eritrea, a broad

North-South trend folding has been recognized, together with superimposed isoclinal folding which is ubiquitous throughout the pre-Cambrian basement of Ethiopia (Mohr, 1971). The overlying marine Mesozoic rocks are sub-horizontal, and overlain conformably by Cenozoic volcanic rocks with only a minor unconformity in the highland regions of Ethiopia. Thus, the age of the foliation predates the Cretaceous and as such represents tectonism which occurred much before the opening of the Red Sea.

The predominant structural style of the offshore Red Sea is basement involved normal faulting, some of which these faults extend into the Infra-evaporite rocks. In addition, basinward dipping listric normal faults sole out into the base of the Miocene salt. These Cenozoic structures are faulted blocks which generally dip towards the western flank of the Red Sea. In the Gulf of Zula area of North Ethiopia (UNDP/World Bank, 1991), the deeply faulted graben forms a small sub-basin filled with sediments three to five kms thick (Behle et al., 1975) that is bounded on the east by a horst extending from the Buri Peninsula southwards (Figure 3). North of $15^{0}30'$ generally the regionally extensive fault planes tend to strike NNW parallel to the coast line. Faults south of this latitude strike

more westerly in a NW direction (Figure 3). Much of the change in the fault trend is inferred to have been caused by the block rotation of the Danakil Alps (Burek, 1974) that was caused by the opening of the Afar Depression (Burek, 1974). Fault trends within the Danakil Depression in the North have NNW trends (Figure 3). In the south the fault pattern is more complicated, and less oriented. The major strike directions in the southern part are NNW and NNE.

IV.2. Transfer zones

Transfer zones characterized by a change in the direction of major boundary faults (Morley 1995) are common. The Red Sea transfer zones encompass all the transfer zone types described by Morley (1995). The major rift boundary faults pass into conjugate convergent or divergent transfer zones (Figure 23). Synthetic (boundary faults facing each other) transfer zones are also common in the central zone (Zone III of Figure 23). Some transfer zones show significant overlap, while others lack overlap (Figure 23). Major strike slip faults are present which exhibit significant 24 kms (15 miles) lateral displacement. These strike slip faults commonly mark a zonal change in structural style. For example, the northern Zone III area which is characterized by rhombic blocks, changes

by transfer faults into Zone III which is dominated by rift-jump and rift-gaps (Figure 23). Minor cross strike faults become transfer zones, as they approach the axial trough.

IV.3. Fourier Division Wavelet Processing

Fourier division wavelet processing was conducted to refine and increase the frequency content of the reflection seismic, and to remove coherent and random noise components. The seismic wavelet analysis was carried out on scanned post-stacked line E435 the line with Thio-1 well situated at CDP 325 (SP 8431) Figure 28. A trace was extracted from this line at CDP 110 (between SP's 8458 and 57) for wavelet estimation. The time window selected for the extracted wavelet was between 100 ms to 250 ms (Figure 29a). The reason for selecting this time window was to include the wavelet generated by reflection at the water and sediment interface. Fourier division wavelet processing was performed under the assumption of minimum lateral variation. This reflection horizon was chosen to approximate this assumption, because the water and sea bottom (carbonate) interface was assumed to have constant acoustic properties. The reflection from this single horizon provides a wavelet which is a very close the product of the reflectivity and the source wavelet. Because of the

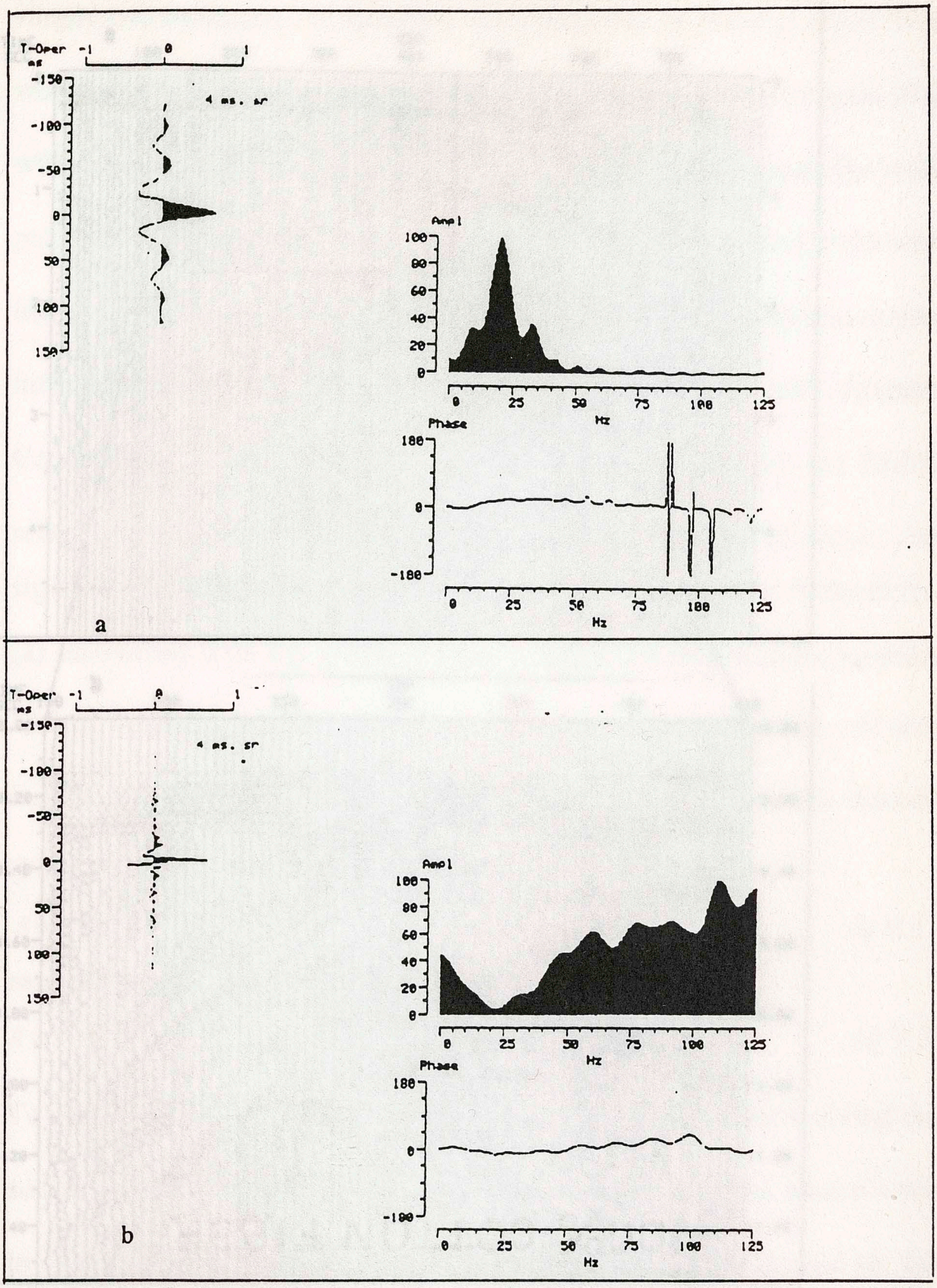

Figure 28. a) Zero-phase wavelet extracted from Line 435E at CDP 325. b) Forward fourier-division inverse wavelet of the zero-phase wavelet in 'a'.

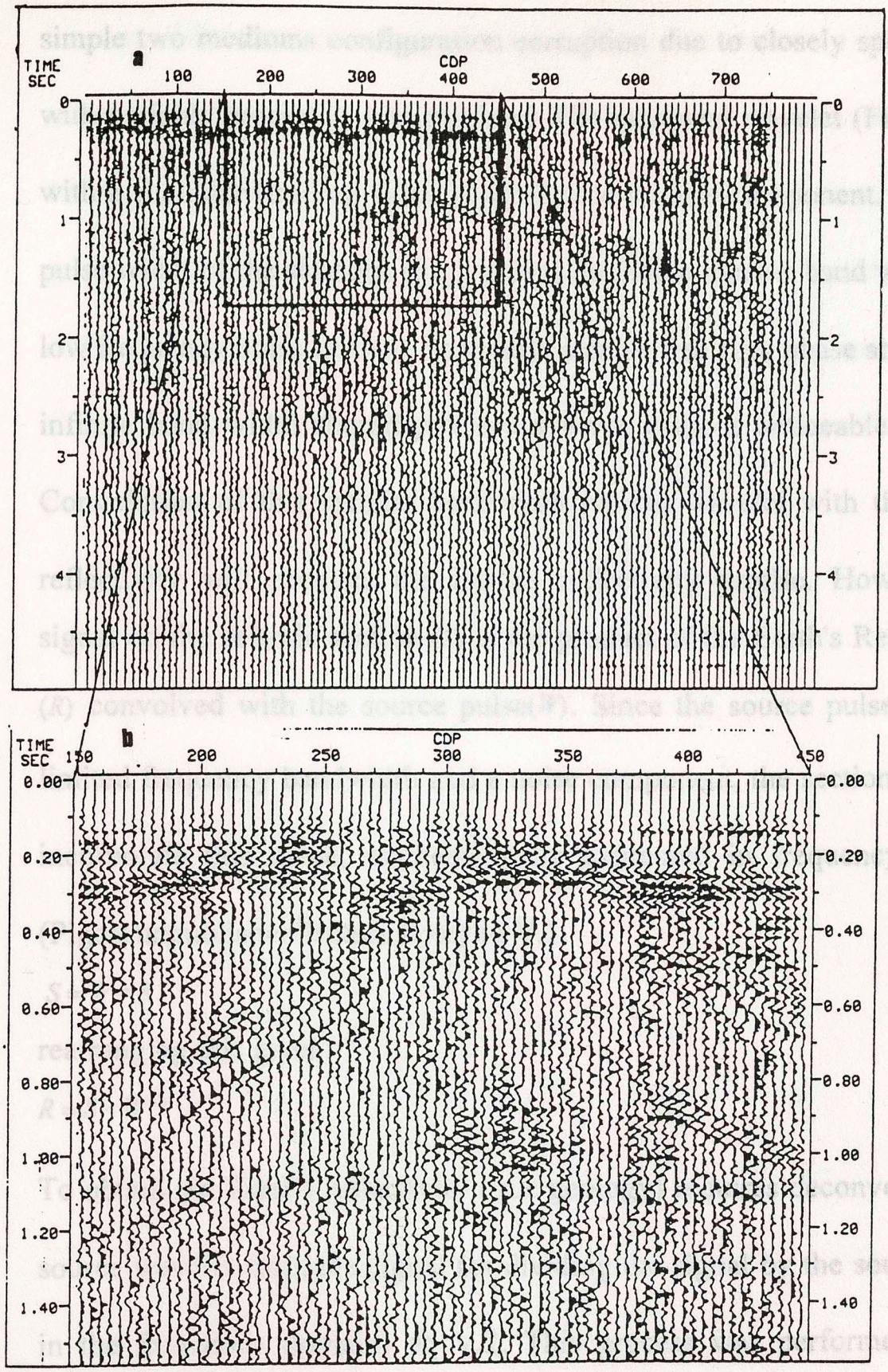

Figure 29. Forward fourier-divistion wavelet filtered seismic section of Line 435E. b) Magnified part of 'a'.

simple two mediums configuration corruption due to closely spaced beds with variable properties was minimal. The extracted wavelet (Figure 29a) with a shoulder (trailing sidelobs) indicated a noise component. The wide pulse width of the sidelobs (Figure 29a) implied a narrow band width with low frequency noise content. In theory, a noise free zero phase source with infinite band width should produce a wave without noticeable sidelobs. Convolution of this infinite bandwidth (spike) wavelet with the Earth's reflectivity will produce the Earth's reflectivity profile. However, the signal on the seismic section (S) is the product of the Earth's Reflectivity (R) convolved with the source pulse(W). Since the source pulse contains limited frequency bandwidth and a noise component, the section will also incorporate this noise, mathematically expressed in frequency domain (Pigott unpublished lecture note) eq V.1.

$$S = W * R \qquad \text{eq V.1}$$

rearranging this gives

$$R = S * W^{-1} \qquad \text{eq V.2}$$

To obtain the Earth's reflectivity (true geology) requires deconvolving the source wavelet from the signal (or dividing the signal by the source wave in the frequency domain) eq V.2. This process was performed on the scanned seismic line (Line 435E) using a Mira Landmark program. An

inverse of the extracted wavelet (Figure 29.a) was obtained (Figure 29.b), and the inverse wavelet was then convolved with the whole section (Figure 28.a and b). After convolution the filtered section of line 435E was generated (Figure 30a and b). These two sections, show the improvement in frequency content and bed resolution of the wavelet processed section. Coherency, observed in the unprocessed section is however reduced in the processed section.

IV.4. Seismic Attribute Analysis

Taner And Sheriff (1977) state that the analysis of a seismic trace as a component of an analytical signal permits the transformation to polar coordinates and the measurements of quantities called "reflection strength" and "instantaneous phase". These properties plus several other quantities derived from these, are termed attribute measurements. These attributes can be calculated by the formula from Taner And Sheriff (1977)

$g(t) = R(t)\cos\theta(t)$ the real Part eq IV.1

$h(t) = R(t)\sin\theta(t)$ the imaginary part eq IV.2

Solving for $R(t)$ and $\theta(t)$ will give

$$R(t) = \sqrt{(h(t)^2 + g(t)^2)} \quad \text{eq IV.3}$$

$$\theta(t) = \arctan h(t)/g(t) \quad \text{eq IV.4}$$

where $R(t)$ is the Reflection strength, and $\theta(t)$ is the phase angle.

An attribute measurement analysis of the fourier division wavelet processed seismic section Line 435E (Figure 29) was performed. A color display is given in (Figures 30 through 33). This line, about 20 km in length, has been compressed both vertically and horizontally to include the

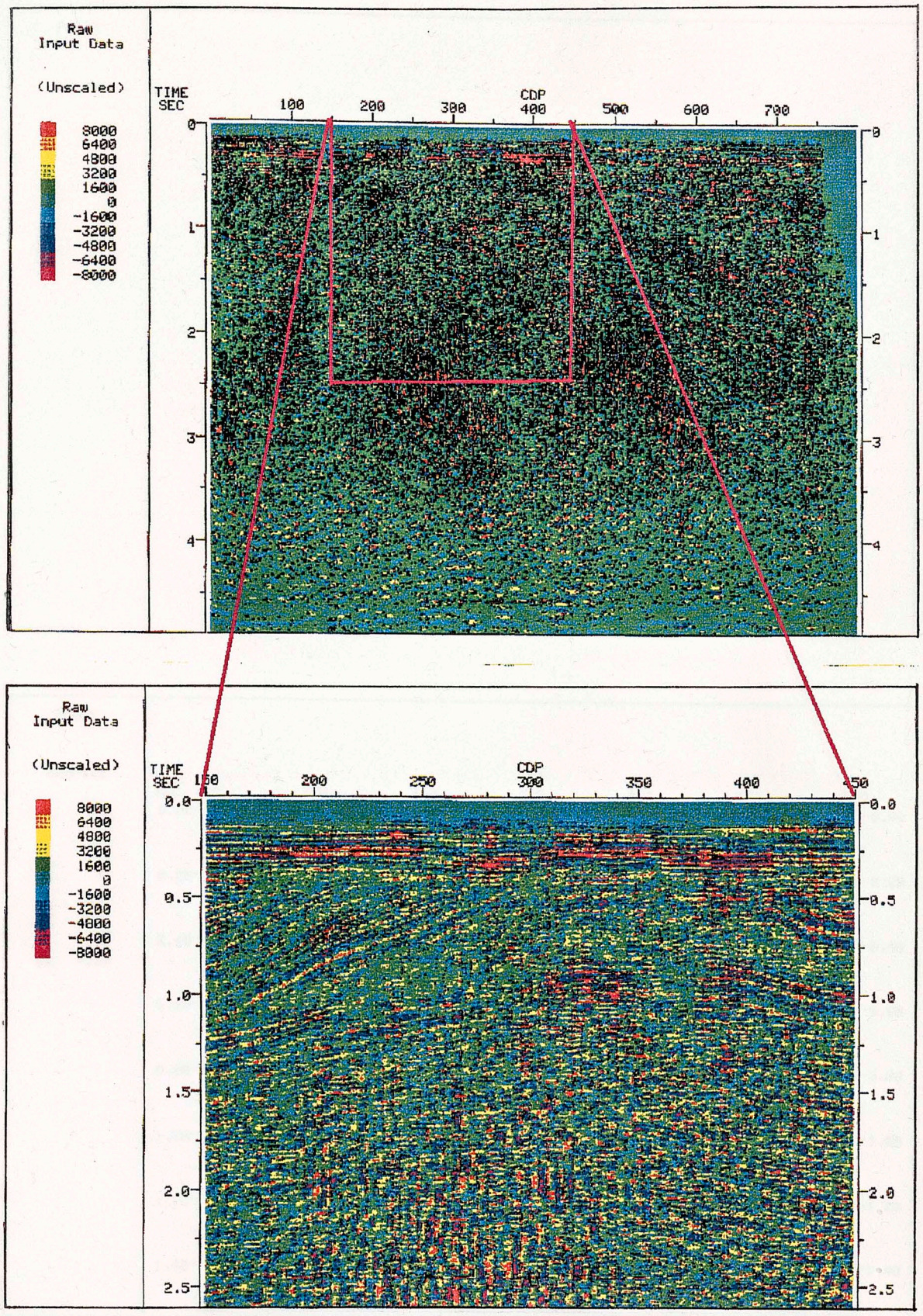

Figure 30. Seismic attribute display: color coded display of Line 435E b) Maginfied part of 'a'.

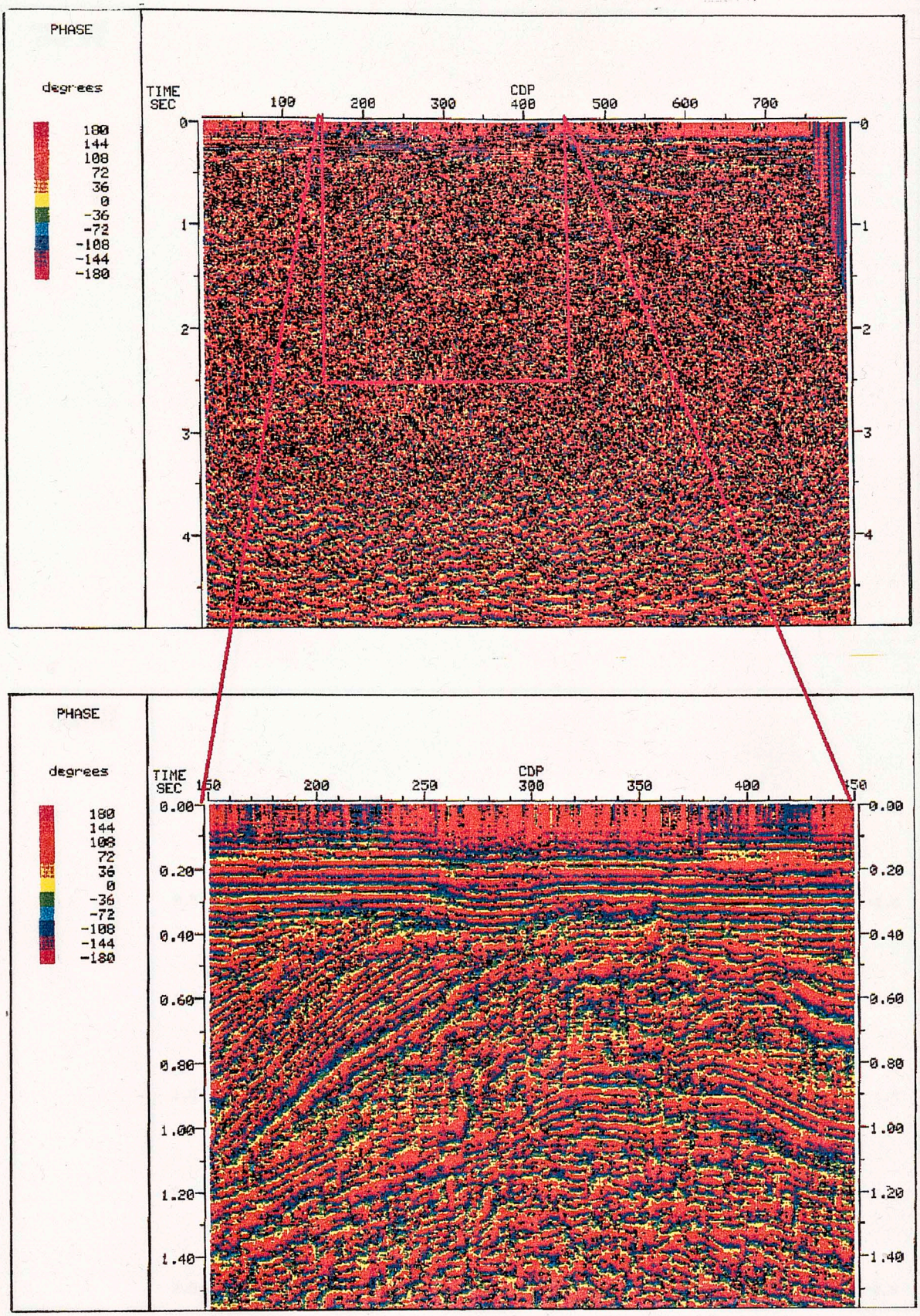

Figure 31. a) Seismic attribute display: instantaneous phase display of Line 435E. b) Magnified part of 'a'.

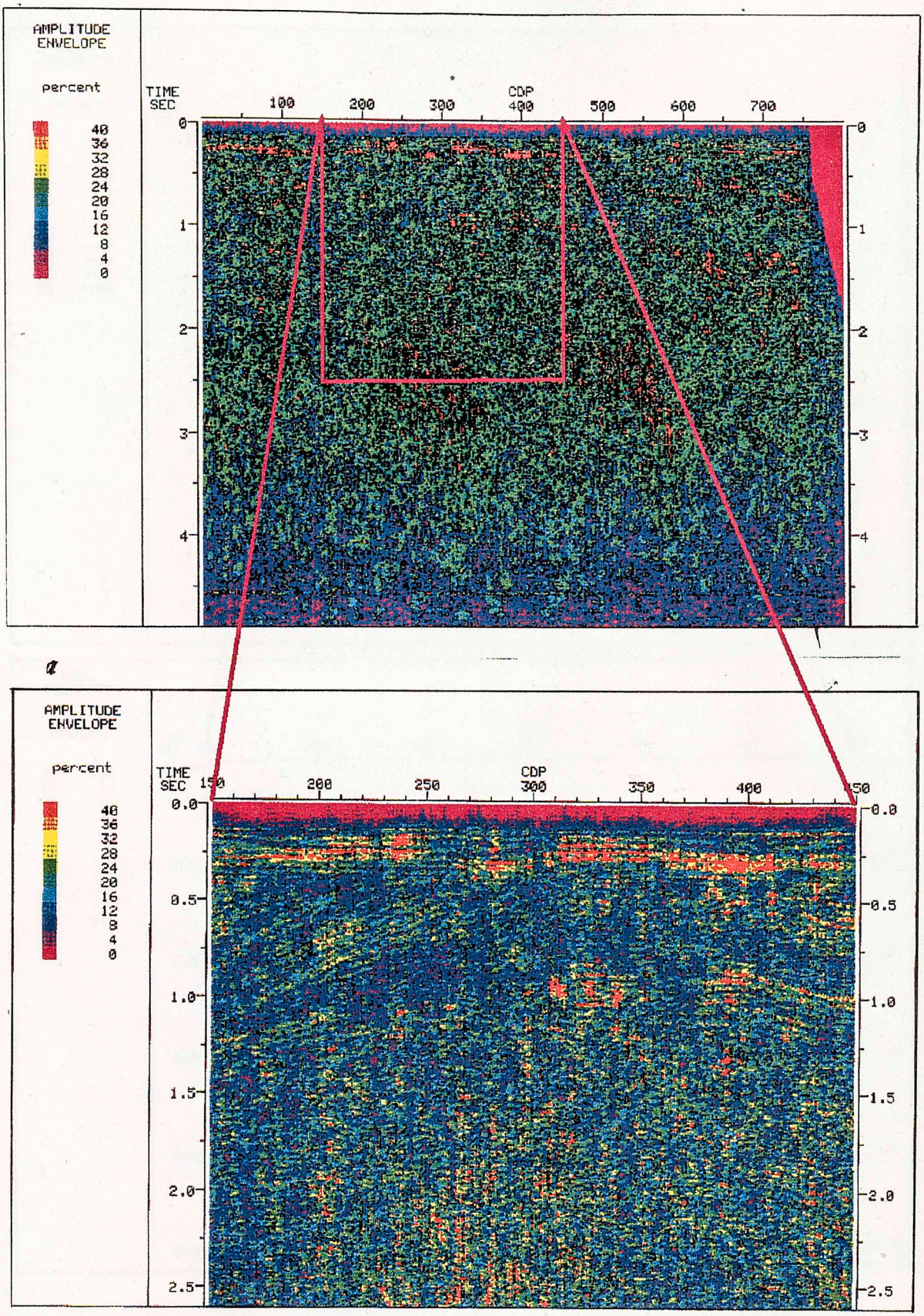

Figure 32. a) Seismic attribute display: amplitude strength (envelop) display of Line 435E. b) Magnified part of 'a'.

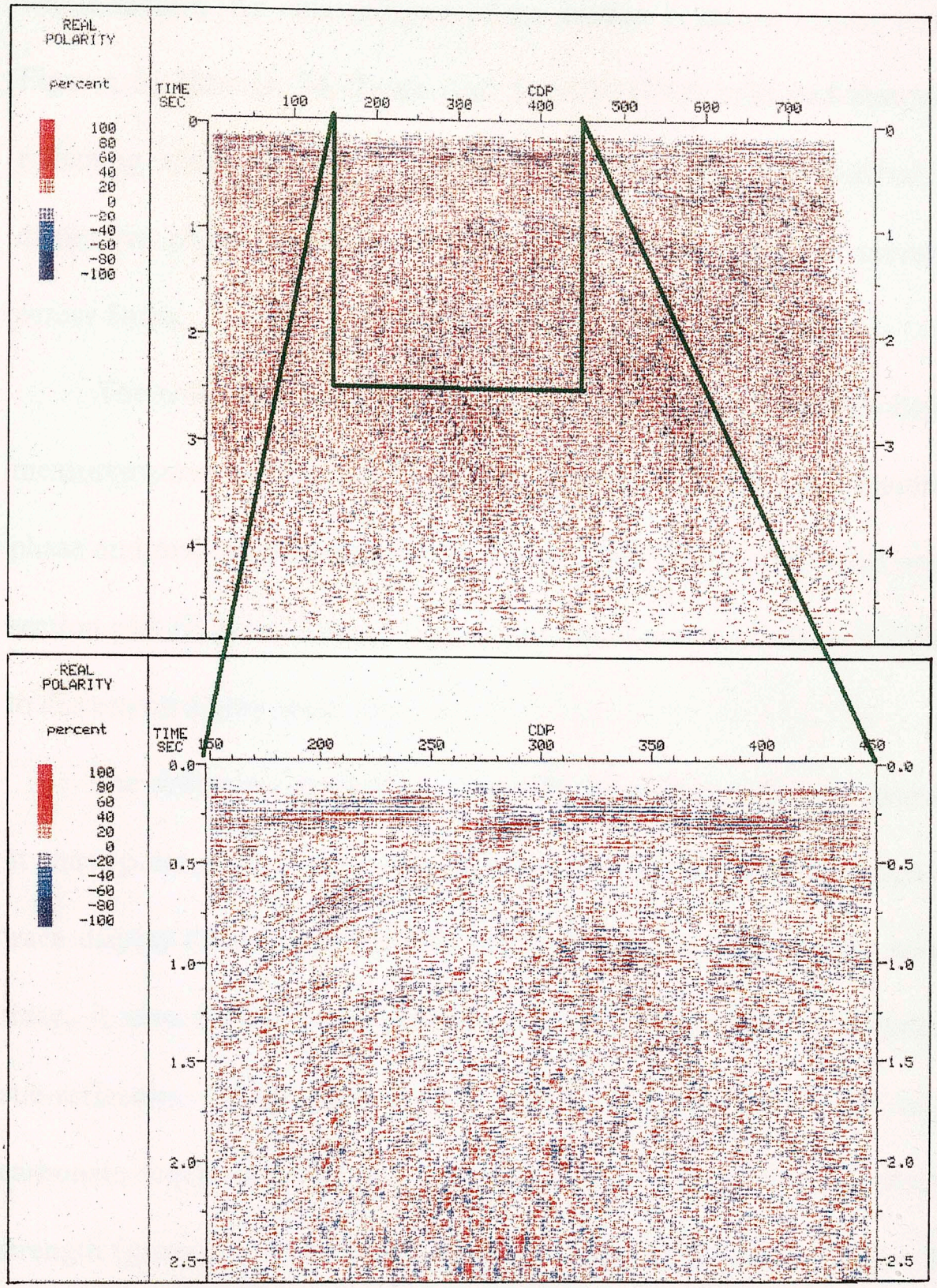

Figure 33. a) Seismic attribute display: real polarity display of Line 435E.
b) Magnified part of 'a'.

whole section. An enlarged part of the section is shown in part b of the Figures 31 through 34. Taner And Sheriff (1977) indicated that certain reflecting sequences, or depositional situations, are characterized by a distinctive phase waveform which can be used to assist in correlation across faults.

The color coded display of Line 435E shows four different attribute measurements: color coded seismic section, instantaneous amplitude, phase and real polarity (Figures 30 through 33). The color coded seismic section plot (Figure 30.a and b), brought out features which were difficult to discern on a gray scale plot.

The reflection strength of composite interfering reflectors measured at phase point gives a maximum value greater than the peak or trough on a trace display (Taner And Sheriff, 1977). Within an event on the seismic trace, it also indicates the composite reflection strength of interfering sub-reflectors (Taner And Sheriff, 1977). Massive beds such as the carbonate sequence at the top, show consistent strong internal reflection strength (green-red) over a long distance (close to 20 miles) (Figure 31.a and b). In contrast, reflection strength from composite reflectors (clastic sequence) varies much and can only be traced for a short distance (Figure

31a and b). The variation in reflection strength over short distances within the clastic sequence shows, local facies changes. The continuous strong reflection strength over long distance within the carbonate sequence, marks low lateral facies variation. The evaporite sequence internally has low reflection strength (purple - blue), and shows little variation. The underlying Infra-evaporite sequence shows a strong reflection strength, with significant lateral variation (Figure 31a and b).

The instantaneous phase plot (Figure 32a and b) illustrates the improvement in the ability to correlate horizontally persistent events such as unconformities (e.g. the top of truncated sequences). The boundary between the lower clastic sequence and the overlying massive carbonate sequence can be traced easily on the instantaneous-phase plot. The plot also assists in recognizing event terminations and top- and down-laps. Structures such as faults can easily be interpreted from the breaks seen on the continuous event of the top sequence at CDP 260 between 0.1 to 0.4 seconds.

A real polarity color display indicates the sign of the peak amplitude of the wave (Taner And Sheriff, 1977). The color intensity in both (-) and (+) indicate the amplitude strength. The blue in this case shows a negative

polarity, with high amplitude corresponding to a low acoustic impedance unit underlying a high impedance unit (Intra-evaporite on Infra-evaporite Sequence) (Figure 33.a and b).

IV.5. Crustal Stretching Analysis

Crustal stretching (Mackenzie et al., 1970,) values for the southwestern Red Sea were calculated according to the geometrical method described by Pigott (unpublished lecture notes) from the interpreted reflection seismic sections for line 520. Interpreted horizon boundary lengths were measured and used for the calculation after corrections for migration ($\beta = \arctan \sin \alpha$ (1) Pigott, 1995). The horizons used for this calculation are basement, Infra-evaporite, evaporite and Dhunishub tops. β values are calculated by dividing the stretched length (i.e. top Infra-evaporite length measured from the section excluding fault surface separation) by the original length (i.e. top basement length measured from the section excluding fault separation)

$$\beta stretching = l_1 / l_0 \qquad \text{eq IV.5}$$

where

β = is stretching value,

l_1 = stretched crust length, l_0 = original crust length.

Based on this calculation the various stretching values obtained for the southwestern Red Sea are tabulated in Table 5a and b. These data indicate stretching in the Red Sea occurred at different phases: at 25.2 ma, at 14.2 ma and at 5.2 ma. The region also exhibits variation in the amount of stretching Zone I, with maximum stretching (infinite) (Table 5a), where new crust was generated of new crust. Zone II shows the next maximum stretching a total 1.36, while the whole basin average is about 1.276. Maximum stretching occurred around 5 Ma (Table 5b), oceanic crust also formed at this time (Table 5a).

ZONE	Age (Ma)	β	Age (ma)	β	Age (ma)	β	Age (ma)	β
IV	25.2	1.01	14.2	1	5.2	1.01	0	1
III	25.2	1.01	14.2	1.02	5.2	1.09	0	1
II	25.2	1.01	14.2	1.1	5.2	1.25	0	1
I	25.2	1	14.2	1	5.2	Infinite	0	Infinite

Table 5a. Calculatedβ for southwestern Red Sea (offshore Eritrea Line 520)

Age	β	ZONE	*total*β
25.2	1.008	IV	1.02
14.2	1.036	III	1.11
5.2	1.171	II	1.36
0	1.041	I	Infinite

Table 5b. Calculated averageβ for southwestern Red Sea (Line 520) at each rifting episode and within each zone.

IV.6. Petroleum System

IV.6.a. Potential Source Rocks

The presence of oil seeps on land (Figure 2) and oil shows in exploration wells (Figure 2) in the southwestern Red Sea (offshore Eritrea) clearly indicates the presence of source rock capable of generating oil and/or gas. Very few samples from limited wells have been geochemically analyzed for source rock potential in the southwestern Red Sea. The results of these source rock evaluations could be considered as indications of source rocks petroleum. The limited geochemical work on the available samples by BEICIP (1985, 1991) identified some potential source horizons.

Infra-evaporite potential source rocks

These were only visually analyzed from hand specimens collected in the field (IPL 1989), and considered potential source rocks based on stratigraphic and lithologic correlation to the Madbi Formation of Yemen, and the Uarandab Formation of the southeast Ogaden basin, Ethiopia. The Infra-evaporite units includes Jurassic to Cretaceous organic rich shales and marls of the Antalo Limestone, Agula Shale and shale beds within the Habab Formation. The lower part of the Infra-evaporite sequence (the

Antalo Limestone and Agula Shale were not penetrated in the offshore southwestern Red Sea wells, thus their existence and maturation must be considered speculative. However, in the southern part of the southwestern Red Sea (offshore Eritrea) where the Intra-evaporite Sequence (Amber Formation) pinches out, the Infra-evaporite units occur at shallower depth. If the Infra-evaporite rocks are in fact organically rich like their correlative units the Urandab Formation of the Ogaden Basin (Ethiopia) and the Madbi Formation of Yemen, they would be good source rocks. Geochemical analysis of samples from the Habab Formation penetrated by three wells, was conducted by BEICIP (1991). In the J-1 well section an average total organic content of 1.30% was recorded for samples from 6920 and 8050 feet depth . The kerogen is dominated by Type II (oil and gas prone). In the Thio-1 well where a thick Habab Formation is penetrated, an average TOC value of 1.14% was reported (BEICIP, 1991), again with dominantly Type II kerogen. However, in the MN-1 well the organic content was lower and was Type IV (reworked kerogen type). The result of analyses by BEICIP (1985 and 1991) suggests that the most favorable source beds occurs in the upper part of the Habab Formation.

Intra-evaporite Sequence (Amber Formation) Source Potential

Within the Intra-evaporite Sequence (Amber Formation), which is regionally pervasive throughout the southwestern Red Sea, Eritrean offshore wells, only few samples were analyzed (two samples from the MN-1 well). The result of the TOC analysis for these two samples is 1.00% and 2.32% (BEICIP, 1991).

Moreover, a number of oil shows and a gas blow out in the C-1 well within and immediately below the evaporite sequence, suggest that source horizons within the Amber Formation may have generated oil and/or gas.

IV.6.b. Potential Reservoir Rocks

Potential reservoir rocks in the southwestern Red Sea (offshore Eritrea) include: Infra-evaporite Mesozoic sediments, Infra-evaporite Cenozoic rocks, and Supra-evaporite rocks.

Infra-evaporite Mesozoic Potential Reservoir Rocks

Potential reservoir rocks of Infra-evaporite Mesozoic rocks include: the Adigrat Sandstone, fractured and dolomitized sections of the Antalo Limestone, and beds of the Amba Aradam Sandstone. The thick (600 to 3000 feet onshore) (Figure 20) Adigrat Sandstone based upon hand specimen description (Gulf Oil 1972) shows good reservoir potential, but

its' existence in the offshore southwestern Red Sea has not been reported in any borehole. Onshore the middle part of the Antalo Limestone shows porosity development due to fracturing and dolomitization. Surface outcrop samples of the Amba Aradam Sandstone indicate the presence of a good porous lower part. The stratigraphic relationship of this potential reservoir to the underlying the Agula Shale, a potential source rock, make this formation a good prospect for receiving a petroleum charge.

Infra-evaporite Cenozoic Potential Reservoir Rocks

Infra-evaporite reservoir beds of Cenozoic age mainly occur within the Habab Formation. These reservoir sections include intercalations of sandstone beds with shales (Figure 9). The Habab Formation was penetrated by three wells (J-1, MN-1 and Thio-1). Porosity calculations from available sonic logs indicate the presence of porous horizons with porosity values that range from 14% to 22%. In the J-1 well sonic porosities in the interval 7800 to 7980 feet average 18%, and in the interval 8630 to 8750 feet average 22%. In Thio-1 well (Figure 9) for the same Habab Formation the sonic porosities yielded an average value of 14.5% for the interval 8000 to 8375 feet, and a value of 22% for the interval 8375 to 8575 feet. In the C-1 well the bottom sandstone interval

(possible Habab Formation?) (Robertson, 1991) has porosity values 18-23% (BEICIP, 1985). A gas blowout occurred from this interval (MOBIL 1969)

Supra-evaporite Cenozoic Potential Reservoirs

The Supra-evaporite Cenozoic potential reservoir rocks include the Desset Sequences (I to IV) (Desset Formation) and Dhunishub sequence (Formation). BEICIP (1985) reported sandstones with porosities ranging from 13 to 23%, from the Desset Formation in the Secca Fawn-1 well (Figure 8). Surface seeps around Dahlak Islands where thick carbonate rocks of the Dhunishub Formation crop out indicate reservoir potential for the zones with good to excellent intergranular, intra-fossil, and vugular porosities that range from 5 to 30 % (average > 20%) (Figures 8 and 9).

IV.6.c. Sealing Rocks

In the Eritrean Red Sea, there are numerous sealing horizons in the Infra-evaporite, Intra-evaporite and Supra-evaporite rocks. The shale horizons and evaporitic beds near the top of the Infra-evaporite (Habab Formation) are potential seals. The thick salt and evaporitic sections of the Intra-evaporite sequence (Amber Formation) should provide excellent

seals. Within the Supra-evaporite rocks shales, claystones and evaporitic horizons interbedded with the reservoir quality zones are potential seals.

IV.6.d. Traps

Trapping mechanisms in the Red Sea area are related to both structural and stratigraphic traps. The structural traps are related to block faulting and salt tectonics. Fault related traps include traps such as traps against fault plane, drapes over horst blocks (Figure 22). Halokinesis traps include turtle back anticlines, role over anticlines and drapes (Figure 22). Stratigraphic traps include unconformities, facies changes and porosity changes (Figure 22).

V. SUMMARY

The Red Sea has been used as a world-wide paradigm for rifting. Unfortunately, much of the examples of rifting which have been proposed are based less upon clearly imaged geophysical information than upon extrapolated inferences and imagination. As a result, there are a plethora of rifting hypotheses for this region.

Part of the image problem comes from the lack of available industry acquired reflection seismic and part is derived from what seismic is available from the thick evaporite which have masked much of the underlying detail. By taking refraction velocities and integrating this information with synthetic seismograms, this study correlated major seismic reflectors throughout the southwestern Red Sea (offshore Eritrea) and has made an introductory effort at unraveling the subsalt information. The effort was not wasted. Images and the three dimensional mapping which resulted allows now the definition and stratigraphic determination of the structural style. Surprisingly, although some structural symmetry is observed which many previous workers had proposed for rifting, substantial asymmetry is also evident. Altogether, the findings clearly suggest that the rifting in this portion of the Red Sea is not one event, but

is episodic, and that pure shear on a regional scale has been locally modified by simple shear. Salt mobilization has complicated the sedimentary overburdens drape upon the basement, but in so doing has lead to the possibility of several new hydrocarbon play concepts.

VI. CONCLUSIONS

The Red Sea is presently at an early passive margin and or late rift basin stage in its evolutionary development. To get to this stage, the Red Sea has passed through multiple episodes of rifting which have generated a complex structural and stratigraphic framework. The presence of thick acoustically heterogeneous evaporite sediments and their subsequent mobilization have complicated the geophysical mapping of the region, especially beneath the evaporite. Understanding of this complex rifting and sedimentation history of the southwestern Red Sea (offshore Eritrea) required an integrated geological and geophysical approach. Therefore, seismic stratigraphy which incorporated wide-angle-refraction seismic, borehole seismology and reflection seismic was used to analyze the structural stratigraphy of the southwestern Red Sea.

The use of this integrated approach allowed the delineation and mapping of the following mega seismic sequences: Basement, Infra-evaporite, Intra-evaporite and Supra-evaporite. The Supra-evaporite mega sequence was further subdivided into: Desset I, Desset II, Desset III, Desset IV and Dhunishub Sequences. In the Thio-1 borehole section the Desset I to IV Sequences (Desset Formation) are missing owing to erosion

over the salt mobilization accentuated horsts. However, to the North, in the Secca Fawn-1 borehole section, thick (6535 feet) deposits of the Desset I to IV Sequences were recorded (Robertson Group, 1991). This section shows only minor effects of salt tectonics.

The southwestern Red Sea can be subdivided into four parallel structural zones, beginning with the axial trough outward: Zone I (the axial trough), Zone II (the en echelon tilted block zone), Zone III (The symmetric horst and graben zone) and Zone IV (the downwarped rift flank), each with its distinct assemblage of structural elements. Zone I is characterized by basinward dipping step faults. Zone II is characterized by en echelon tilted block fault systems, salt mobilization and minor shear zones. Zone III is marked by high-angle symmetrical fault systems, extensive salt mobilization and wrench faulting. Zone IV exhibits gentle basin ward dip with parallel step-fault systems, counter regional dipping fault and basinward dipping listric faults.

Spatially, the measured cumulative stretching from the seismic sections is infinite in Zone I, major within Zone II ($\beta = 1.36$), moderate in Zone III ($\beta = 1.11$) and minimal at Zone IV($\beta = 1.02$).

Temporally, in the southwestern Red Sea at least three episodes of rifting were recognized. The first episode (25 ma) was basement involved pure shear (high-angle normal fault) capped by a wide spread unconformity. The second rifting episode (25 ma) was reactivation of older rift faults and the creation of new ones, with associated wrench faulting. The third rift episode (5 ma) was dominated by pure shear involving modification of evaporite blanket into swells in phase with underlying horst apexes.

Although many investigators have proposed singular unique rifting models for the Red Sea, this paper proposes instead for the southwestern Red Sea a multi-phased, crustal attenuation model which reconciles the observed episodic structural features of pure shear (high-angle faulting) on a regional scale with those of local transfer zones of simple shear.

Owing to the nature of the Red Sea basin formation, and presence of the various ingredients requisite for a petroleum system, the Eritrean Red Sea has demonstrable hydrocarbon potential.

REFERENCES

Abbate, E., Azzaroli, A., Bruni, P., Canuti, P., Fazzuoli, M., Sagari, M. and Tacconi, p., eds a geological map of Ethiopia and Somalia (1973), comment Firenz Consiglio Nazionale delle Ricerche, Italy: 25-32.

Aydin A. and Nur A., 1982. Evolution of pull apart basins and their scale independence. Tectonics vol. 1 No 1. 95-105 (in Compilation Foster N.H. and Beaumont E.A., 1991. Treaties of Petroleum Geology Reprint Series No. 10).

Behle, A., Makris, J., Baier, B. and Delbasis, N., 1975. Salt thickness near Dallol (Ethiopia) from seismic reflection measurements and gravity data. In: Pilger, A. and Rosler, A. (edit.), Afar Depression of Ethiopia. Stuttgart (Schweizerbart).

BEICIP, 1985. Petroleum Potential of Ethiopia (a report for Ministry of Mines and Energy of Ethiopia)

BEICIP, 1991. Petroleum potential of Red Sea Ethiopia. (report for UNDP/World Bank Red Sea Gulf of Aden HC Project)

Berhe, S.M., 1986. Geological and geochemical constraints on the evolution of Red Sea; Gulf of Aden and Afar Depression. J. Afr. Earth Sci., 5: 101-117.

Beydoun, Z.R. 1989, Hydrocarbon prospects of the Red Sea - Gulf of Aden; a review: Journal of Petroleum geology, v. 12, p. 125-144.

Beyth, M., 1972, Paleozoic-Mesozoic sedimentary basin of Mekele outlier, Northern Ethiopia. AAPG Bull., v. 56, 2426-2439.

----------. 1973, Correlation of Paleozoic-Mesozoic sediments in northern Yemen and Tigre, northern Ethiopia. A.A.P.G Bull., v. 57: 2440-2446.

Blanford, W.T., 1870, Observation on the geology and zoology of Abbyssinia, made during the progress of the British expedition to that country in 1867-1868: London, MacMillan, 487p.

Bohannon, R.G., 1989, Styles of extensional tectonism during rifting, Red Sea and Gulf of Aden: Journal of African Earth Sciences, v. 8, p. 589-602.

Brown, C. and Girdler, R.W., 1982, Structure of Red Sea: at 20^0N from gravity data and its implication for continental margins. Nature, 298: 51-53.

Burek, P.J., 1974, Palaomanetische Untersuchungen zum Danakil-Alpen-Problem und deren Bedeutung fur plattentektonische Problemeim Bereich der Danakil-Afar-Senke: Geotektonische Forschunggen, v.47, p. 54-93.

Burke, K. and Dewey, J.F., 1973, Plume-generated Triple Junctions: key indicators in applying plate tectonics to old rocks. J. Geol. 81, 406-433.

Burke, K. and Whiteman, A,J., 1973, Uplift, rifting and the breakup of Africa: In Implications of Continental Drift to the Earth Sciences, 2, Terling, D.H. and Runcorn, S.K., eds., London, Academic Press, 735-755.

Cochran, J.R. and Martinez, F., 1988, Evidence from the northern Red Sea on the transition from continental to oceanic rifting: Tectonophysics, 153:25-53.

Dainelli, G., 1943, Geologia dell'Africa orientalle. A. four volumes, R. Acc. d'Italia, Centro Studi per l'Africa Orientale Italia, Roma.

Dow, D.B., Beyth, M. and Hailu Tsegaye, 1971, Palaeozoic glacial rocks recently discovered in northern Ethiopia. Geol. Mag., 108: 53-59.

Engels, G.G. and Earl, J.P., 1966, Geological Report Amber No.1: Mobil Petroleum Ethiopia Inc. Asmara, 20p (unpublished).

Egloff, F., Rihm, R., Makris, J., Izzeldin, Y.A., Bobsien, M., Meier, K., Junge, P., Noman, T. and Warsi, W., 1991, Contrasting structural styles of the eastern and western margins of southern Red Sea: the 1988 SONNE experiment. In: J. Makris, P. Mohr and R. Rihm (editors), Red Sea: birth and Early History of a New Oceanic Basin. Tectonophysics, 198: 329-353.

Evans, A.L., 1988, Neogen tectonic and stratigraphic events in the Gulf Of Suez rift Area, Egypt: Tectonohpysics, 153: 235-247.

Filjak, R., Glumic, N. Zagarac, Z., 1959, Oil possibilities of the Red Sea region in Ethiopia, geological and geophysical exploration. Naftaplin, Enterprise for Exploration and Exploitation of Petroleum and Gas, Zagreb, 104p (unpublished).

Garfunkel, Z., 1988, Relation between continental rifting and uplifting, evidence from the Suez Rift and northern Red Sea: Tectonophysics, 150: 33-49.

Girdler, R.W., 1958, The relationship of the Red Sea to the East African Rift System. Q. J. Geol. Soc. London. 114: 79 - 105.

---------- 1967, Earth Satellite, terrestrial heat flow, mantle convection and the location of extensional and compressional features on the Earth's surface. Proc. Geol. Assoc. 78: 165- 178.

----------, 1970, A review of Red Sea heat flow. Philo. Trans. R. Soc. London, a267: 359-368.

----------, 1991, The case of oceanic crust beneath Red Sea. In J. Makris, P. Mohr and R. Rihm (editors) Red Sea: Birth and Early history of a New Oceanic Basin. Tectonophysics 198 441-466.

Girdler, R.W. and Darracott, B.W., 1972, African poles of rotation. Comments Earth Sci., 2: 131-138.

Girdler, R.W. and Styles, P., 1974, Two-stage Red Sea floor spreading. Nature, 247: 7-11.

Girdler, R.W. and Underwood, M., 1983, The evolution of early oceanic lithosphere in the southern Red Sea. Tectonophysics, 116: 95-108.

Gregory, A.R., 1977, Aspects of rock physics from laboratory and log data that are important to seismic interpretation, part 1. Fundamentals of stratigraphic interpretation of seismic data. In:

C.E. Payton (ed.), Seismic stratigraphy - Applications to hydrocarbon exploration. A.A.P.G. Mem. 26: 15-52

Hutchinson, R.W., and Engels, G.G., 1970, Tectonic significance of regional geology and evaporite lithofacies in southern Ethiopia: Philosophical Transactions of the Royal Society of London, Series A: Mathematical and Physical Science, v. 267, p. 313-329.

International Petroleum Limited, 1989, IPL Report (unpublished).

John J.W. Rogers, Mohamed E. Dabbagh, Brian M. Whiting and Sally a. Widman, 1989, Subsidence and origin of the Northern Red Sea and Gulf of Suez. Journal of African Earth Science. vol. 8, Nos' 2/3/4 pp. 617-629

Kazmin, V., 1975, Explanation of the geological map of Ethiopia: Ministry of Mines , Energy and Water Resources. Geological Survey of Ethiopia: Bulletin No.1: 1-14.

Kingstone, J., Olson, R.C. and Engels, G.G., 1970, Compilation geological Report, Mobil Esso Ethiopia concession. Mobil Petroleum Ethiopia Inc., Asmara, 50p (unpublished).

Lowell, J.D. and Genik, G.J., 1972, Sea floor spreading and structural evolution of Southern Red Sea . Am. Assoc. Pet. Geol. Bull., 56 (2): 247-259.

MacKay, S. and Dragoset, B., 1994, Imaging beneath a Gulf Coast salt-injection features case history. (The Society of Exploration Geophysists) The Leading Adge Aug. 1994 V. 13 No. 8. p 858-860.

Makris,J., Mohr, P., and Rihm, R., 1991, (editors) Red Sea: (abstract) Birth and Early history of a New Oceanic Basin. Tectonophysics, 198 275-278.

Makris J. and Rihm R., 1991, Shear controlled evolution of the Red Sea: pull apart model: In J. Makris, P. Mohr and R. Rihm (editors) Red Sea: Birth and Early history of a New Oceanic Basin. Tectonophysics 198 441-466.

Makris, J., Tsironidis, J. and Richter, H., 1991, Heat flow density distribution: In the Red Sea. in J. Makris, P. Mohr and R. Rihm (editors) Red Sea: Birth and Early history of a New Oceanic Basin. Tectonophysics 198: 383-393.

Martinez, F., and Cochran, J.R., 1988, Structure and Tectonics of the Northern Red Sea; catching a continental margin between rifting and drifting: Tectonophysics, v. 150, p. 1-32.

R., McQuillin, M., Bacon and W., Barclay, 1984, An Introduction to Seismic Interpretation: with contributions by R.E., Sheriff, R. Mc Evoy, R. Steel. Graham and Trotman, London (1984).

Merla, G., 1979. The Mesozoic of Ethiopia in ch. 4 of Merla, G., Abbatr, E., Azzaroli, A., Bruni, P., Canuti, P., Fazzouli, M., Sagri, M., and Tacconi, P., eds., A *Geologic Map of Ethiopia and Somalia (1973)*, Comments: Frenze, Consiglio Nazionale Delle Ricerche, Italy, p. 25-32.

Mitchum, Jr. M.R., Vail, P.R. and Thomson, S. III. 1977, Seismic stratigraphy and global changes in sea level, part 2: The depositional sequence as a basic unit for stratigraphic analysis. In: C.E. Payton (ed.), Seismic stratigraphy - Applications to hydrocarbon exploration. A.A.P.G. Mem. 26: 53-62.

Mohr, P., 1971a, Ethiopian Rift and plateaus: some volcanic petrochemical differences. J. Geophysics. Res., 76: 1967-1984.

Morley, C.K., 1995, Developments in the structural Geology of rifts over the last decade and their impact on hydrocarbon exploration. In: Lambiase, J.J. (ed.), 1995, Hydrocarbon Habitat in Rift Basins. Geological Society Special Publication no. 80, 1-32 pp.

Olson, R.C. and Engels, G.G., 1970, Geological summary Mobil/Esso Red Sea B-1: Mobil Petroleum Ethiopia Inc. (unpublished).

Pigott, J.D., 1995, Chapter 2: A seismic classification scheme for clastic shelf wedges (deltas). In: Michael, N. Oti and George, P., 1995. Geology of deltas (ed). A.A. Balkema/Rotterdam/Broohfield/1995. 17-29.

Pigott, J.D., Gebretsadik, E.S., Alahdal, A., 1995, Halokinetic associated crustal stretching in the southern Red Sea: New observation of the basement and sedimentary cover from refraction-constrained reflection seismic stratigraphy (Abstract to 12th International Confrence on Basement Tectonics '1995. Norman, Oklahoma)

Pilger, A. and Rosler, A., 1976, Temporal relationship in the tectonic evolution of the Afar Depression (Ethiopia) and the adjacent

Afro-Arabian rift systems. In: Pilger, A. and Rosler, A. (edit.), Afar between continental and oceanic rifting. Stuttgart (Schweizerbart).

Purser, B.H. and Hotzl, H., 1988, The sedimentary evolution of the Red Sea Rift; a comparison of northwest (Egyptian) and northeast (Saudi Arabian) margins: Tectonophysics, 153: 193-208.

Reiman, K. and Dielwart, J.E.A.M., 1977, Final well report Thio-1. Ethiopian Shell Petroleum Development Company (unpublished).

Robertson Group, 1991, Red Sea/Gulf of Aden Regional Hydrocarbon Study Project, The Ethiopian Red Sea, Biostratigraphy, Palaeo-environments, and Lithostratigraphy: Great Britain, Robertson Group.

Roksandic`, M.M., 1978, Seismic facies analysis concept, Geophysical Prospecting, v. 26, 383-398.

Taner, M.T., and Sheriff, R.E., 1977, Application of amplitude, frequency, and other attribute measurements to stratigraphic and hydrocarbon determination. In: C.E. Payton (ed.), Seismic stratigraphy - Applications to hydrocarbon exploration. A.A.P.G. Mem. 26: 301-327.

Sovoyat, E., Shiferaw, A, Balcha, T., 1989, Petroleum exploration in The Ethiopian Red Sea. Journal of Petroleum Geology. v. 12, No. 2. 187-204.

Spencer, E.W., 1969, Introduction to structure of the Earth. McGraw-Hill Book Company. New York St. Louis San Francisco London Sydney Toronto Mexico Panama. 597 pp.

Steckler, M.S., Berthelot, F., Lyberis, N. and Le Pichon,X., 1988, Subsidence in the Gulf of Suez,; implication for rifting and plate kinematics: Tctonophysics, 153: 249-270.

Triuliz, A.E. Von, 1898, Expedition S.M. schiff pola in das Roth Meer, nordlich Halfte. Wissenschaftliche. Ergebnisse. II Relative Schwerebestimmungen. Denkschr. K. Akad. Wiss. Math. Nat. Klassr, 65: 131-206.

----------, 1901, Expedition S.M. schiff pola in das Roth meer, nordlich Halfte. Wissenschaftliche. Ergebnisse. II Relative Schwerebestimmungen. Denkschr. K. Akad. Wiss. Math. Nat. Klassr, 69: 143-219.

UNDP/World Bank , 1991, The Ethiopian Red Sea petroleum geology and regional geophysical evaluation (a report to Minestry of Mines and Energy of Ethiopia)

Vail, P.R., Mitchum, Jr., R.M. and Thompson, S. III, Seismic stratigraphy and global changes in sea level, part 3: Relative changes of sea level from coastal onlap. In: C.E. Payton (ed.), Seismic stratigraphy - Applications to hydrocarbon exploration. A.A.P.G. Mem. 26: 53-62.

Vine, F.J., 1966, Spreading of ocean floor: New evidence. Science, 154: 1405-1415.

Voggenreiter, W. and Hotzl, H., 1989, Kinematic evolution of the southwestern Arabia continental margin: implications to origin of the Red Sea. Journal of African Earth Science. vol. 8: 565-587.

Wegener, A. 1929, The Origin of Continents and Oceans. Translated by Biram J., 1966. DOVER PUBLICATIONS, INC. NEW YORK, 246 pp.

Wernicke, B.P., 1985, Uniform-sense normal simple shear of the continental lithosphere: Canadian Journal of Earth Sciences, v. 22, p. 108-125.

Appendix I

Mesozoic Sediments

Adigrat Sandstone

The type section of the Adigrat Sandstone occurs in Adigrat, Tigrai Province, of northern Ethiopia, and was first observed by Blanford (1870). The formation also crops out Danakil Alps (Figure 19). The formation's thickness varies from 650 meters (Beyth, 1973 ; Marla, 1979) to 1605 meters (Figure 20) (Gulf Oil company report 1970) in the Danakil Depression area. The Adigrat Sandstone is a thick to thin bedded, often cross bedded, light colored brown to red quartzarenite. This sandstone has good porosity through out the section, except where cemented by diagenetic silica and/or calcite (Gulf Oil company report 1970). However, porosity enhancement through cement leaching is recorded in some places (Gulf oil comp report 1970). The age of the Adigrat Sandstone is poorly constrained owing to lack of fossils, with estimates ranging from Triassic to Middle Jurassic (Bathonian) (Robertson Group, 1991). Continental fluvio-deltaic to shallow marine depositional environments have been assigned to this formation (Robertson Group, 1991).

Antalo Limestone

Adjacent to the Red Sea area, the Antalo Limestone is exposed in the Mekele area of the Tigrai province and the Danakil Alps. Its measured thickness ranges between 300 meters (985 feet) to 900 meters (2950 feet) with thickness ranging up to maximum of 2400 meters (Figure 20) (7875 feet) (IPL, 1989). The Antalo Limestone represents coastal transgressive deposition, the contact of this limestone with the underlying Adigrat Sandstone being gradational. The base of the unit is dominantly terrigeneous sand, its middle section is marine fossiliferous wackestone, and its upper section is a micritic limestone. The upper micritic limestone has regularly spaced reddish brown calcareous sandstone lenses (Robertson Group, 1991). The age of this unit ranges from Upper Bathonian to Tithonian (IPL, 1989; Robertson Group, 1991). The depositional environment of the Antalo Limestone, inferred from micro-faunal and micro-floral fossil evidence is shallow to moderately deep marine.

Agula Shale

Similar to the Antalo Limestone the Agula Shale crops out both around Mekele and Antalo in the Tigrai province and on the Danakil Alps (Figure 19). The unit consist of laminated black shale, marlstone and

limestone with gypsum and minor sandstones. In the Danakil Alps this unit is represented by limestone intercalated with shale and gypsum (Hutchinson and Engels, 1970). The Agula Shale is coeval with the organic rich Urandab Shale of Ogaden basin of southeastern Ethiopia. The age for the Agula Shale is given as Late Jurassic (Marla et al., 1979). According to UNDP/World Bank (1991) report the Agula Shale has localized, pyritic shales, marl and claystone with brachiopod, which suggest a shallow marine deposition. In the Red Sea Amber-1 borehole has penetrated a slightly metamorphosed highly pyritic argillite and which was K-Ar dated as 36 +/-2 ma, and which has been named the Agula Shale (Lowell and Genik, 1972).

Amba Aradam Sandstone

The Amba Aradam Sandstone unconformably overlies both the Antalo Limestone and Agula Shale. This sandstone was first named and described by Shumburo (in Beyth, 1972). Formerly, it was known as the Upper Sandstone of northern Ethiopia (UNDP/World Bank, 1991). The formation is composed of white sandstones and conglomerates with clays. In the north the Amba Aradam Sandstone is a white to pink quartz feldspathic sandstone with interbedded red clay and siltstone. Owing to the

UNIVERSITY OF OKLAHOMA
LIBRARIES

absence of direct bio-stratigraphic evidence, the unit is inferred to be post-Late Jurassic. The Amba Aradam Sandstone is widely distributed throughout Ethiopia. The depositional environment as based upon its sedimentary facies characteristics is fluvial-lacustrine (Robertson Group, 1991).

Appendix II

Cenozoic Infra-evaporite Rocks

Dogali Formation

The name of the Dogali Formation is given to the lower most Cenozoic Infra-evaporite groups of rocks which crop out onshore on the western Red Sea (Filjak et al., 1959; Kazmin, 1975). In the offshore Red Sea; however, these clastic sediments, where penetrated by three wells and named the Habab Formation.

The Dogali Formation consists offshore of a variety of volcanics, volcanic conglomerates, sandstones, conglomerates, slightly calcareous shales, and infrequent carbonate beds (Filjak et al., 1959). Basaltic layers within this formation exhibit pillow structures with some layers spilittic, indicating sub-aqueous deposition in part (Kazmin, 1975). The age of this formation is poorly constrained. Olson and Engels (1970) carried out radiometric age dating of the volcanics in the upper part and suggested an early Miocene age. In contrast, BEICIP (1985) has suggested an Oligocene age for this unit. If an Oligocene age, this unit would be equivalent to that of the basinal Habab Formation. The depositional environments of this

unit range from continental clastics to marginal marine (Robertson Group, 1991).

The intercalated volcanic rocks within the onshore Dogali formation in the Danakil area are correlative to the offshore Harmil volcanic series interbedded within the Amber salt and observed in the B-1 well (Figure 20). Such a correlation indicates that a portion of the deep offshore basin salt is age equivalent to the onshore Dogali Formation.

Habab Formation

The offshore Habab Formation on the onshore region of the Red Sea is equivalent to the Dogali Formation. The Habab is penetrated offshore by three exploration boreholes (J-1, MN-1 and Thio-1). The thickest section of this unit penetrated is 1690 meters (5543 feet) (Figure 9). Lithologically and stratigraphically, this unit has been subdivided into three members: the Lower, Middle and Upper Habab Members.

The Lower Habab Member has been penetrated by J-1 and Thio-1 boreholes with a total thickness of 1267 meters (4158 feet) in Thio-1 borehole (Figure 9). Lithologically it is composed of clastics, which coarsen upward with interbeds of siltstones. The lower most part of this section contains reworked silici-clastic volcanic fragments. Rieman and

Dielwart (1977), proposed the source of the volcanics to be from the South. The Robertson Group (1991) has correlated this unit regionally to the Rudeis Formation the Gulf of Suez. The Lower Habab is the only sediment in the area to be assigned an Late Oligocene age (Robertson Group, 1991). The depositional environment is one of deep water turbidites with high fluxes of continental sediment (Robertson Group, 1991).

The Middle Habab Member is well represented in the Thio-1 borehole with thickness of 130 meters (425 feet). It consist of sandstones, thinly laminated and pyrite bearing shales, siltstones and minor volcanic fragments. This member has a low micro-fauna content. Its age as determined from its micro-faunal and nano-fossil assemblage, is Early Miocene (Robertson Group, 1991). The depositional environment of the Middle Habab as determined from the micro-fossil content, is moderately deep marine inner neretic (Robertson Group, 1991).

The Upper Habab Member forms the transition from the underlying clastics to the overlying lower evaporites of the Amber Formation. Regionally, this member is stratigraphically equivalent to that of the Belaym and Kareem Formations of the Gulf of Suez (Beydoun, 1989). The

age of the Upper Habab was determined by Robertson Group (1991) from the Thio-1 borehole to be Middle Miocene. The Upper Habab Member depositional environment ranges from middle neritic to outer neritic (Robertson Group, 1991)

Appendix III

The Amber Formation

The Amber Formation caps the Intra-evaporite (or Upper part of Syn-rift) rocks of southwestern Red Sea. This unit has been encountered in all wells drilled offshore Red Sea Eritrea. The Amber thickness ranges from 165 meters (540 feet) in J-1 up to more than 3050 meters (10000 feet) in its typical borehole (Amber-1) (Figure 21).

The Amber formation is generally uniform in its content: a thick section of salt with minor intercalations of anhydrite, shale, and volcanics. The Amber formation laps out laterally, leaving no evaporitic sequence to be found onshore in the northern Red Sea. However, in the Danakil Depression of the Afar region (Figure 3) of northern Ethiopia's interior, a thick evaporite section was reported by Makris and Ginzberg (1987). According to Behle et al, (1975) there is about 2.4 kms (1.4 miles) to 3.52 kms (2.2 miles) thick salt exists within Dallol area, south of the Denakil depression, within the Afar Depression (Figure 3). By contrast, within the Red Sea to the South (some 70 kms (44 miles) south of the Thio-1 well) the evaporite pinches out (Figure 15). The age given to this salt unit is varies widely. In the deeper part of the basin in the B-1 well the age has

been assigned to Eocene to Late Miocene (Olson and Engels, 1970). The Eocene age for the Amber Formation was determined from radiometric age dating of the interbedded Harmil Volcanic units. As such this age value equates this evaporite to the clastic Habab Formation and the Onshore Dogali Formation. The depositional environment for this evaporite formation is a restricted moderately deep marine environment with hypersaline condition (Robertson Group, 1991).

Appendix IV

Desset Formation

Offshore, the Desset Formation is penetrated by four deep nearshore wells: J-1, C-1, Mn-1 and Secca Fawn-1 (see Figure 2 for location and Figure 17 for the stratigraphic section). In the deep basinal wells (Dhunishub-1, Amber-1, B-1 and Thio-1) the Desset is absent due to none deposition. The lower part is characterized by abundant sandy beds containing numerous interbedded anhydritic stringers and infrequent salt beds. Thickness of this formation varies from well to well, with thickest sections observed from seismic sections within inter salt dome elongate basins. The thickest sections up to 1990 meters recorded in the Secca Fawn-1 Borehole. Age of this formation is Plio-Pleistocene. The depositional environment is generally shallow marine with relatively quiet conditions (Robertson Group, 1990). On the onshore Red Sea, the Desset Formation overlies the Dogali Formation and is represented by a clastic sequence (Robertson Group, 1991).

Dhunishub Formation

The Dhunishub is named after the type well the Dhunishub-1 (Olson and Engels, 1970). It is the youngest rock unit of offshore southwestern

Red Sea (Eritrea). It was first named the Jeded Formation (Engels and Earl, 1966) in the Amber-1 well section. They correlated this formation to the Shagara Formation of the northern Red Sea (Beydoun, 1989 and UNDP/World Ban, 1991). This unit is present in all wells drilled in the southwestern Red Sea (offshore Eritrea). However, its lithological thickness varies from nearshore to the deep basin.

In its type section (Engels and Earl, 1966), the Dhunishub contains gypsum associated with coral. Its contact with the underlying Desset Formation is conformable. However, in the deep basin wells it is observed to rest disconformably upon the Amber Formation, where the Desset Formation is missing from the section. The age of the Dhunishub Formation, according to Olson and Engels (1970a), is Pleistocene to Recent, but the Robertson Group (1991) has suggested an age of Pliocene to Recent. Its depositional environment as based on micro-fauna content is shallow marine, carbonate platform, within an inner neritic regime, (Robertson Group, 1991).

Figure 22

SOUTHERN RED SEA REGIONAL SEISMIC TRANSECT

PRELIMINARY INTERPRETATION BY:

ESHETU GEBRETSADIK AND DR. JOHN D. PIGOTT

OU RED SEA PROJECT

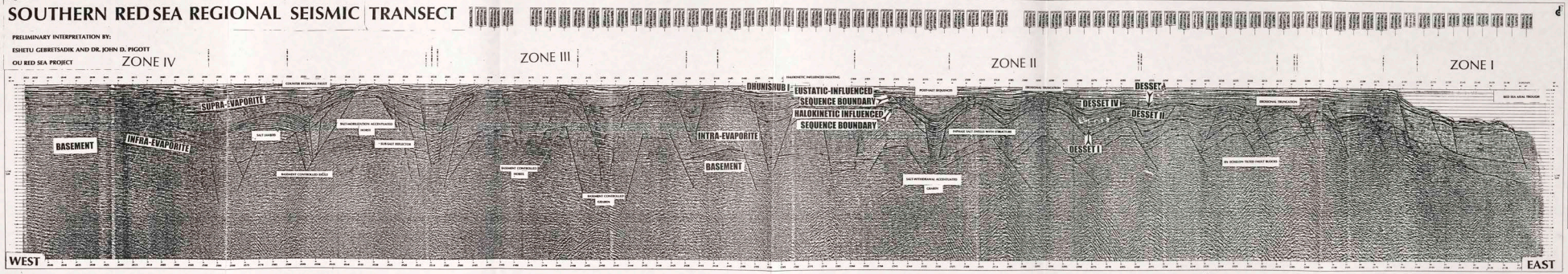

This volume is the property of the University of Oklahoma, but the literary rights of the author are a separate property and must be respected. Passages must not be copied or closely paraphrased without the previous written consent of the author. If the reader obtains any assistance from this volume, he must give proper credit in his own work.

I grant the University of Oklahoma Libraries permission to make a copy of my thesis upon the request of individuals or libraries. This permission is granted with the understanding that a copy will be provided for research purposes only, and that requestors will be informed of these restrictions.

NAME ESHETU GEBRETSADIK

DATE 27-1-97.

A library which borrows this thesis for use by its patrons is expected to secure the signature of each user.

This thesis by [redacted] has been used by the following persons, whose signatures attest their acceptance of the above restrictions.

NAME AND ADDRESS	DATE